

Confined Water for Catalysis: Thermodynamic Properties and Reaction Kinetics

Published as part of Chemical Reviews *special issue "Green Hydrogen"*.

Tao Wang,[†] Haldrian Iriawan,[†] Jiayu Peng,^{*} Reshma R. Rao,^{*} Botao Huang, Daniel Zheng, Davide Menga, Abhishek Aggarwal, Shuai Yuan, John Eom, Yirui Zhang, Kaylee McCormack, Yuriy Román-Leshkov, Jeffrey Grossman, and Yang Shao-Horn^{*}



Cite This: *Chem. Rev.* 2025, 125, 1420–1467



Read Online

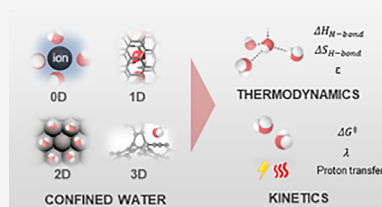
ACCESS |

Metrics & More

Article Recommendations

Supporting Information

ABSTRACT: Water is a salient component in catalytic systems and acts as a reactant, product and/or spectator species in the reaction. Confined water in distinct local environments can display significantly different behaviors from that of bulk water. Therefore, the wide-ranging chemistry of confined water can provide tremendous opportunities to tune the reaction kinetics. In this review, we focus on drawing the connection between confined water properties and reaction kinetics for heterogeneous (electro)catalysis. First, the properties of confined water are presented, where the enthalpy, entropy, and dielectric properties of water can be regulated by tuning the geometry and hydrophobicity of the cavities. Second, experimental and computational studies that investigate the interactions between water and inorganic materials, such as carbon nanotubes (1D confinement), charged metal or metal oxide surfaces (2D), zeolites and metal–organic frameworks (3D) and ions/solvent molecules (0D), are reviewed to demonstrate the opportunity to create confined water structures with unique H-bonding network properties. Third, the role of H-bonding structure and dynamics in governing the activation free energy, reorganization energy and pre-exponential factor for (electro)catalysis are discussed. We highlight emerging opportunities to enhance proton-coupled electron transfer by optimizing interfacial H-bond networks to regulate reaction kinetics for the decarbonization of chemicals and fuels.



CONTENTS

1. Introduction	1421
2. Thermodynamics of Confined Water	1423
2.1. Enthalpy and Entropy Changes from Confinement of Pure Water	1423
2.2. Structure and Thermodynamics of Water Solutions Containing Ions	1424
3. Water Structures and Properties under Confinement	1426
3.1. 1D Water Structures: Confinement of Water in Nanotubes	1426
3.2. 2D Water Structures: Water Networks at Solid Surfaces	1428
3.2.1. Water Monomers Confined by Metals/Metal Oxides	1429
3.2.2. H-Bonding Structures and Dynamics of 2D Water without Ions	1429
3.2.3. H-Bonding Structures and Dynamics of 2D Water in the Presence of Ions	1431
3.3. 3D Water: Water Clusters in MOFs and Zeolites	1433
3.3.1. Pure Water Adsorption Enthalpy within Cavities	1434

3.3.2. Characterization of H-Bonding Structures of Pure Water in Cavities

1435

3.4. Water Molecules Confined by High Concentration Ions and/or Solvents

1437

3.4.1. Water-in-Salt Electrolytes

1437

3.4.2. Water-in-Solvent Electrolytes

1439

4. Tuning Reaction Rates with Confined Water

1440

4.1. Tuning the Enthalpy and Entropy of Activation via Confined Water

1440

4.2. Tuning the Reorganization Process for Electrochemical Reaction Rates

1443

4.2.1. Relating the Reorganization Process to Reaction Kinetics via the Marcus Theory

1443

4.2.2. Characterization of Reorganization Dynamics of Water

1444

4.2.3. Reorganization Energy Trends for Electrochemical Reactions

1448

Received: April 11, 2024

Revised: January 10, 2025

Accepted: January 20, 2025

Published: February 4, 2025



4.3. Tuning Proton Kinetics via H-Bonds	1450
5. Conclusions	1453
Associated Content	1454
Supporting Information	1454
Author Information	1454
Corresponding Authors	1454
Authors	1454
Author Contributions	1454
Notes	1455
Biographies	1455
Acknowledgments	1456
References	1456

1. INTRODUCTION

Water is ubiquitous across Earth's biological, atmospheric, geological, and materials systems. Naturally, the properties of water under different conditions hold tremendous implications for understanding a wide range of chemistry. Studies of bulk water through diffraction,¹ spectroscopy² and simulations³ over decades show that the structure of water is key to the understanding of its properties and how it changes with different environments. The bulk structure of water near ambient pressure and temperature is identified commonly as tetrahedral coordination of five water molecules with an average of 3.5 hydrogen bonds (H-bonds) per water molecule.¹ However, the structure of water is dynamic in bulk. Pople first postulated that the structure of liquid water can be understood as having a distribution of H-bonds rather than a network of fixed H-bonds.⁴ The understanding of the structure of liquid water in the supercooled regime, i.e. above crystallization temperature during cooling, or amorphous ice, i.e. below the glass transition temperature during heating, has extended to include long-range network structures, often broadly categorized as either low-density water or high-density water,^{5,6} which can be modified through changes in temperature^{6,7} and pressure.⁵ For example, neutron diffraction has revealed that low-density liquid water with a hydrogen-bonded tetrahedral structure transforms to high-density liquid water with a broken hydrogen bond network when pressure increases at 268 K, showing structural resemblances to low-density and high density amorphous ices.⁵ Moreover, the liquid–liquid transition from high-density to low-density water induced by ultrafast heating in bulk supercooled water (before water crystallization) has been observed by femtosecond X-ray laser pulses.²² These bulk water structures highlight the opportunities to tune the H-bonding structure of water, which can alter its properties, including the diffusion of protons,^{8,9} dielectric function,¹⁰ H-bond dynamics,^{11,12} viscosity,^{13–15} and others.^{16,17}

Water in confinement can have different features compared to bulk water. First, the thermodynamic properties (e.g., H-bond enthalpy and entropy) of confined water can deviate from those of bulk water, which can correlate with structural changes (e.g., H–O–H bond length and bond angle) and change in proton activity (e.g., pK_a). For example, water in enzyme cavities exhibits different network structures from those of bulk,¹⁸ where water inside the binding pocket of a protein or water surrounding a ligand may be electrostatically stabilized on a polar molecular surface or geometrically strained by the shape of the cavity.¹⁸ In turn, the thermodynamic properties of confined water, including its enthalpy and entropy, dictate the Gibbs energy of activation

for the removal of waters from the binding site, leading to protein–ligand docking.¹⁹ Second, water confinement can influence the dynamics of the water network in terms of spatial reorientation and proton exchange. Confined water in inorganic cavities, such as zeolites^{20,21} and metal–organic frameworks (MOFs),^{22,23} resembles that in biological systems, where water molecules can interact strongly with hydrophilic sites such as OH moieties, hydrophobic sites such as defect-free pores and metal ions in cavities. The distribution, chemical nature and topography of hydrophilic/phobic sites in cavities dictate the water absorption isotherm,^{20,21} the structure of water networks (e.g., as measured by cluster size or the geodesic paths—the shortest unbroken H-bonded chains between any pairs of water—in the case of 1D extended H-bonding chain)^{20,21} and the fluctuation frequency.²⁴ Third, water confinement can alter their electronic properties such as local dielectric constants, where confinements can restrict the motions of water molecules, leading to suppressed local dielectric constant relative to bulk. Changes in the thermodynamics, network dynamics and electronic properties of water can be controlled such as via confinement in 1D (e.g., carbon nanotubes), 2D (solid surfaces), and 3D (zeolites and MOFs) structures and confinement by ions/solvent.

Beyond the effect of pore geometry and the water-cavity interaction, electrified interfaces can also significantly alter the properties of water. The classical mean-field theory fails to predict the behavior of molecules and chemical reactions that occurred there, since the specific water structure needs to be considered for simulating the interfacial electric field.²⁵ When a water solution contacts a surface, a potential difference between electrons on the surface (at the Fermi level) and the polar water molecules and ions drives electron transfer across the interface until the electron energy levels at the interface align up (equilibrium), leading to the formation of an electric double layer. Excess charge at the interface is screened electrostatically by the dipoles polar water molecules and ions in the solution. Potential of Zero Charge (PZC) is often measured to describe the interfacial structure and charge. PZC is defined as the potential with no excess charge on the interface, which is dependent on surface electronic and atomic structures and electrolyte compositions such as pH and ion concentration. Water dynamics, orientation of interfacial water, and its hydrogen bonding structure can be regulated by the surface charge^{26,27} and the resultant static electric field^{27,28} at metal and metal-oxide interfaces, which exists intrinsically at the PZC as well as extrinsically (i.e., at an applied potential relative to PZC, see Figure S1). The excess charge on the surface can attract water strongly and result in a higher density of interfacial water than that of bulk.^{29–31} The restricted dynamics at the interface lead to decreased dipole moment fluctuations and consequently a decrease in the static dielectric constant of interfacial water^{32,33} compared to that of bulk water, which can in turn affect physiochemical, transport, thermodynamic and kinetic properties such as the interface's double layer capacitance,³⁴ diffusivity of ion transport³³ and enthalpy and entropy of interfacial water.^{22,23,35} Moreover, the change in the dielectric constant of water under confinement can substantially alter the reorganization energy in charge transfer reactions at electrodes.^{33,36,37}

The properties of confined water can greatly influence reaction kinetics. First, by invoking the linear free energy relationship, the thermodynamics of confined water can influence the activation barrier of the relevant elementary

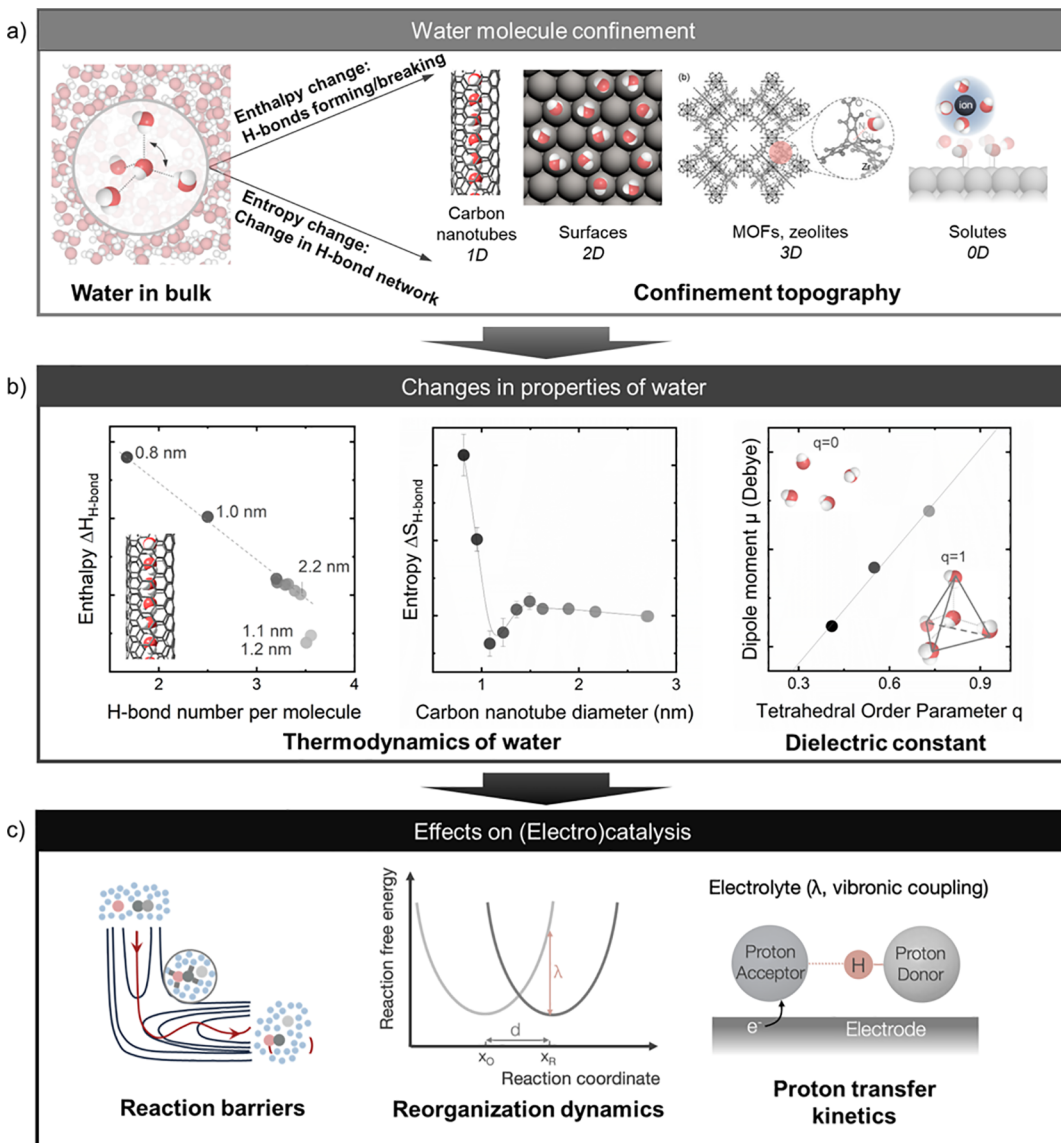


Figure 1. Overview of water under confinement for electrocatalytic applications. (a) Simplified overview of interactions that change the properties of water in hydrophilic and hydrophobic surface confinements,^{16,48–50} and representative schematics of water structure in confinement based on pore topography.^{8,51,52} (b) Thermodynamics (enthalpy^{35,53} and entropy^{35,53}) and dielectric constant changes⁵⁴ of water due to confinement. Adapted with permission from ref 35. Copyright 2011 National Academy of Sciences. (c) (Electro)catalytic reaction rates can be tuned via 1) altering the Gibbs free energy of activation by confined water surrounding the active site,³⁹ 2) changing the reorganization energy associated with the reorientation of solvent molecules along the reaction coordinate,³³ or 3) altering the proton transfer kinetics which can influence the pre-exponential term of the rate expression for proton-involved reactions.^{33,45}

reaction steps. For example, 1D short water chains that form within the subnanometer pores of zeolites lead to a lower entropy of reaction associated with the reorganization of water structure around the active site upon the formation of reaction intermediates, which outweighs the enthalpy penalty of disrupting this confined water structure.^{38–41} Such enthalpy–entropy compensation dictates the transition state free energies and hence rates of reaction such as in alkene epoxidation.^{38–41} Second, changes in the water dielectric constants due to confinement will change the local solution environment,²⁷ which will affect the reorganization process associated with electron transfer, as quantitatively described by Marcus theory. For example, In hydrogen evolution reaction (HER) and hydrogen oxidation reaction (HOR), the strength of the electric field at the interface at a given potential (relative to potential at zero charge, V_{pzc}), which can be influenced by pH

and electrolyte ions, dictates the energy required to reorient water molecules near the surface to accommodate the adsorption and desorption of a proton as a key step in hydrogen electrocatalysis.^{33,37} Moreover, as a water molecule carries a substantial magnitude of dipole moment, the specific structures of water under confinement can interact with the dipole moments of reaction intermediates (e.g., through H-bonding) and influence the elementary reaction step free energies and consequently the rates of reaction.^{28,42–44} Third, the dynamics of the water network as a result of confinement can affect the reaction kinetics,^{33,45} e.g. through changes in proton-tunneling probability which can affect the pre-exponential term. Therefore, the distinct features of confined water in local reaction environments provide an opportunity to regulate catalytic kinetics.

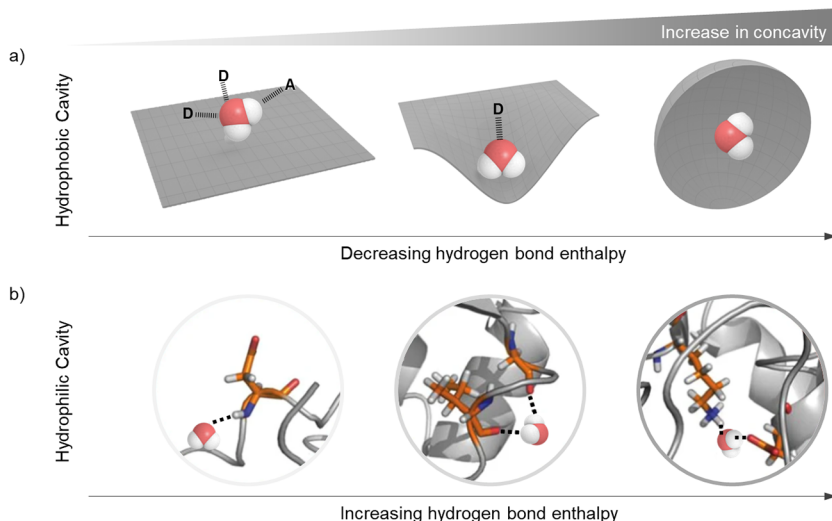


Figure 2. Water confinement in a hydrophobic and hydrophilic cavity. (a) Water in a hydrophobic cavity,⁴⁸ where the increase in the concavity of the cavity reduces the number of hydrogen bonds and hence the decreasing (more positive) hydrogen bond enthalpy of water and hydrophilic cavity. (b) Water in a hydrophilic cavity,⁵⁰ where the increase in the concavity leads to multiple hydrogen bond interactions between the water molecule and polar sites leading to higher (more negative) hydrogen bond enthalpy. Adapted from ref 50. Copyright 2017 open access article distributed under CC BY License 4.0.

In this review, we focus on the confinement of water by solid materials to understand the structure–property relationships of water at relevant interfaces for heterogeneous catalysis, with a special focus on electrocatalysis (Figure 1). The review is organized as follows. Section 2 describes how confinement affects changes in the enthalpy and entropy of pure water and water solutions containing ions. Section 3 analyzes the correlation between water structure under confinement and the thermodynamic properties of confined water, including enthalpy and entropy, as a function of the changes in geometry and hydrophilicity of cavities. Specifically, the hydrogen bonding networks formed in 1D structures (e.g., carbon nanotubes), 2D solid–liquid interfaces (e.g., metals and metal oxides), 3D structures (e.g., zeolites and MOFs) and 0D confinement (e.g., confined water around ions and solvent molecules) are discussed. Section 4 discusses the relationship between water under confinement and reaction kinetics. Since the unique structure of confined water results in different water enthalpy and entropy compared with bulk water, enhancing catalytic activities by tuning activation free energy with confined water in zeolites is discussed to illustrate opportunities for regulating catalytic kinetics by the local environment of water networks. The hydrogen bonding structure and dynamics can especially influence kinetic parameters (i.e., Gibbs energy of activation or reorganization energy and pre-exponential factor/tunneling probability) of charge transfer reactions, including electron transfer (ET), proton transfer (PT), and proton-coupled electron transfer (PCET), which are more sensitive to the solvent environment than other reactions due to the considerable energy required for solvent reorganization induced by charge separation, especially for polar solvents like water.^{46,47} Theoretical and experimental works are discussed, illustrating the promising opportunities in promoting the developments in electrocatalysts for the decarbonization of chemicals and fuels, e.g., the oxygen reduction reaction (ORR), CO₂ reduction reaction (CO₂RR), and nitrogen reduction reaction (NRR).

2. THERMODYNAMICS OF CONFINED WATER

2.1. Enthalpy and Entropy Changes from Confinement of Pure Water

Both the enthalpy and entropy of water molecules can be altered by confined environments.^{18,35,50} Different fields may define hydrogen (H-) bonding in different ways; for instance, H-bonds are formed and destroyed in the order of picoseconds⁵⁵ and thus are transient and dynamic in nature. Meanwhile, relatively stable H-bond characteristics, such as the bond length and bond strength,⁵⁶ exist. In this review, the definition of H-bond refers to a dipole–dipole interaction originating from a proton in one molecule and an electronegative atom in another, indicating average properties in lieu of transients. Moreover, hydrophobic/hydrophilic sites are defined based on the molecular-level classification of water monomer interaction enthalpy with a specific adsorption site, which would correlate with wetting/nonwetting on a homogeneous, microscopically flat surface, although the overall wetting properties of the system will also be dictated by surface roughness and surface heterogeneities (see Section 3.2). Different from bulk water with an average of 3.5 H-bonds,⁵⁷ steric restrictions in cavities can influence the number of H-bonds that can be formed.¹⁸ For example, in the case of water in a hydrophobic cavity, the interaction between water and the surface can be neglected, and the thermodynamics of water is dominated by the geometry of the cavity,¹⁸ where water confined in the hydrophobic cavity can have Gibbs free energy higher than that of bulk water. Increasing the degree of concavity decreases the number of H-bonds that can be formed between water molecules, resulting in a lower (less negative) enthalpy of the system compared to that of bulk water (Figure 2a).⁴⁸ On the contrary, in the case of hydrophilic surfaces, surface functional groups can interact strongly with water molecules, preferentially forming strong H-bonds with the cavity as opposed to neighboring water molecules. Such interaction can favor greater (more negative) H-bonding enthalpy compared to bulk water (Figure 2b).^{58,59} For instance, “trapping” free energy for water interacting with

protein surfaces, defined as the reversible work needed to transfer a water molecule from an infinite separation to a specific position and orientation near the protein complex,⁵⁰ is a key quantity influencing the ability of water molecules to reorientate and hence the dynamics of H-bond rearrangement ahead of a binding event in protein–protein interactions. The mobility of the water molecules and hence the speed of hydrogen bonding rearrangement depends on the number of H-bonds which the water can form with the protein complex.⁵⁰ Orientations in which water can form multiple H-bonds with the protein lower the “trapping” free energy relative to that of bulk water,⁵⁰ rendering the water more favorably trapped by the protein complex. In addition, the interaction between neighboring protein substrates can create an electrostatic field on the interfacial water, resulting in extra stabilization for water, in addition to the strong H-bonds.⁵⁰

The decrease in the Gibbs free energy induced by hydrophilic interactions is dominated commonly by negative enthalpy changes,^{60,61} where the entropic contribution is not large enough to compete with enthalpy changes.^{62,63} However, several recent works have observed that the entropy of water under confinement can play a critical role in reaction kinetics in cases where the specific structural footprints and alignment of the system components are required to drive the process (entropic origin), in lieu of H-bonds or electrostatic interactions of the high energy complex in the transition state (enthalpic origin, see Figure S2).^{19,64–66} For example, the entropic contribution of water confined in ribosomes exceeds the enthalpic contribution and dominates the kinetics of the peptide bond formation reaction^{19,65}—the ordered H-bonding networks of water which are preorganized around the active site by the presence of the ribosome decreases the solvent reorganization energy and accelerates the intrareactant proton shuttling during aminolysis of the P-site ester bond by the A-site α-amino group.⁶⁵

The entropy of water molecules consists of the different modes of motion (translational, rotational, vibrational) and electronic entropy. At normal temperatures, the electronic contribution to entropy is usually zero, as the electronic excitation (in the order of tens of eVs) far exceeds the thermal energy $k_B T$.⁶⁷ For water ($S^0 = 69.95 \text{ J mol}^{-1} \text{ K}^{-1}$ at $T = 298 \text{ K}$),⁶⁷ the configurational and rotational entropies dominate while the vibrational contribution to entropy is generally small due to the large vibrational frequencies of water, where for example the stretching frequencies of liquid water at $>3000 \text{ cm}^{-1}$ correspond to 0.37 eV or $14*k_B T_{298 \text{ K}}$. The proton exchange reaction in pure water (i.e., through water autoionization to form H_3O^+ and OH^-) will in principle contribute positively to the entropy due to the additional degree of freedom where the internal O–H bonds within each water molecule can break and form. However, its contribution might be small, as the dissociation of a randomly chosen water molecule to spontaneously form H_3O^+ and OH^- is an extremely rare event (every $\sim 10 \text{ h}$)⁶⁸ followed by the extremely fast recombination reaction (rate constant of $1.3 \times 10^{11} \text{ M}^{-1} \text{ s}^{-1}$ at room temperature for $\text{H}_3\text{O}^+ + \text{OH}^- \rightarrow 2\text{H}_2\text{O}$).⁶⁹ Therefore, we have invoked the traditional definition of bulk water entropy, where the entropy estimate via accounting for the different modes of motion from theory of $70.1 \text{ J K}^{-1} \text{ mol}^{-1}$ (incl. translational, rotational, vibrational as well as other motions such as librational and cratic motions) could accurately capture the experimental entropy of bulk water of $69.9 \text{ J K}^{-1} \text{ mol}^{-1}$.⁶⁷ The vibrational and rotational

components of water entropy are affected by the topography of cavities and the strength of the interaction between water and cavities^{18,35,70} since the motions of molecules under confinement are restricted,^{70,71} resulting in the decrease of translational and rotational degrees of freedom of the water molecules.⁷⁰ The density of states of water can be calculated following the quasi-harmonic approximation,^{62–64} which could give the entropies of translation (S_{trans}) and rotation (S_{rot}) as the following:

$$S_{trans} = k_B \ln \left(\left[\frac{24\pi k_e k_B T}{h^2} \right]^{3/2} \sigma_x \sigma_y \sigma_z \right) \quad (1)$$

$$S_{rot} = k_B \ln \left(\frac{8\pi^2 \sqrt{I_A I_B I_C}}{\sigma_s} \left[\frac{2\pi k_e k_B T}{h^2} \right]^{3/2} \right) \quad (2)$$

where k_B is Boltzmann’s constant, k_e is Euler’s constant, T is temperature, h is Planck’s constant, σ_x , σ_y , and σ_z are the principal root-mean-square fluctuations of the center of mass (COM) (i.e., mean-free path) of the molecule, σ_s is the symmetry number of the molecule, and I_A , I_B , and I_C are the ensemble averages of the principal moments of inertia. The restrictions resulting from the confinement would decrease the root-mean-square (rms) fluctuations (σ_x , σ_y , and σ_z) and the moments of inertia (I_A , I_B , and I_C) of water, which consequently decrease the entropies. In bulk water, the strong hydrogen bonding network which quenches the rotational and translational degrees of freedom leads to the lower entropy of liquid water ($69.95 \text{ J mol}^{-1} \text{ K}^{-1}$ at $T = 298 \text{ K}$) relative to that of gaseous water at room temperature and pressure ($S = 130 \text{ J mol}^{-1} \text{ K}^{-1}$, $T = 298 \text{ K}$, 1 bar), where the latter is calculated under ideal gas approximation.⁶⁷ When water is confined, the direction of change depends on the specific configurations relative to the tetrahedral H-bond network of bulk water, whose magnitude of change can be as high as $50 \text{ J mol}^{-1} \text{ K}^{-1}$ in the case of confinement by carbon nanotubes³⁵ (see Section 3.1.). Therefore, hydrophilic confinements, such as enzyme pockets, can regulate not only the enthalpy but also the entropy via spatial restriction and the strong interaction between the cavity and water, providing promising opportunities to regulate the thermodynamic properties of water networks in catalytic systems.⁷⁰

2.2. Structure and Thermodynamics of Water Solutions Containing Ions

Especially in an electrochemical cell, the electrolyte solutions contain ions which are solvated by water molecules and hence can alter the water structures in liquids. The electric field around ions can attract water molecules and increase the mean density of water in the hydration shell, exhibiting similar properties of water under high pressure.^{72,73} In addition, the effect of ions on local water structures has been found beyond the hydration shell, where ions can introduce distinct hydrogen bonding structures.⁷³ The concepts of water-structure making and water-structure breaking ions have been well established to describe the different effects of ions on the local water structure.^{74–78} Generally speaking, the water structure makers with high charge densities, such as Li^+ and Mg^{2+} , can create local water structures with more organized hydrogen bonds, while the water structure breaking ions, such as Cs^+ and Rb^+ , can create local structures with more disordered hydrogen bonds.

The detailed molecular interactions and structure of bulk water around structure-making and structure-breaking ions have been studied by X-ray and neutron diffraction, which can obtain the intermolecular pair correlation function $g(r)$ in the solution, giving the density probability of finding the center of an atom lying at a given distance (r) from the center of another atom. Therefore, the distance between cations and the oxygen atoms of water (R_{M-O}) has been measured with these methods.^{1,73} In bulk water, $g(r)$ measured by X-ray diffraction mainly comes from the O–O correlation and exhibits two peaks at 2.8 and 4.4 Å, suggesting the tetrahedral arrangements of water molecules, where the second peak (4.4 Å) is the signature of tetrahedral networks of water.¹ Water-structure making ions, such as Li^+ and Mg^{2+} , show shorter R_{M-O} and a lower water coordinate number (n) in the first hydration shell (Figure 3). Specifically, Li^+ has 4 water molecules in the first

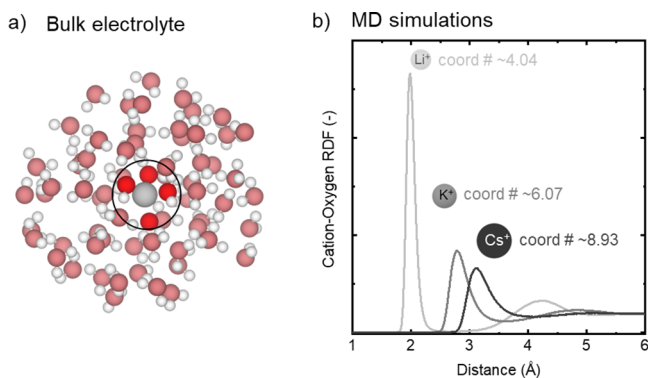


Figure 3. Influence of alkali metal cations on bulk water structure. (a) Water molecule orientation around an alkali metal cation, where the circled region denotes the first solvation shell. (b) Radial distribution function (RDF) between the cations and oxygen atoms from water molecules is shown in systems containing 10738 water molecules, 119 cations and 119 Cl ions in MD simulation, corresponding to 0.6 M chloride salts in water. The RDF is a form of pair correlation function, which indicates the probability of finding the center of an atom at a given distance (r) from the center of another atom, indicated as $g(r)$ in the text. The distance between cations and the oxygen atoms of water is shorter for water-structure making cations, which at the same time show lower water coordinate number. Vice versa for water-structure breaking ions.³⁷ Reproduced with permission from ref 37. Copyright 2021 American Chemical Society.

hydration shell and the R_{M-O} is around 1.9–2.1 Å.^{79,80} On the other hand, water-structure breaking ions such as Rb^+ and Cs^+ exhibit ~8 water molecules in the first hydration shell, and the R_{M-O} values of them are around 3 to 4 Å^{79–81} (Figure 3b). The summary of the coordination number and R_{M-O} values of different ions is listed in Table S1,⁷³ which shows that small cations interact more strongly with water molecules, resulting in shorter R_{M-O} and a more ordered water structure, while large cations can accommodate more water molecules in the first hydration shell but have larger R_{M-O} . Beyond the first hydration shell, the interaction between water in different layers has been studied by X-ray diffraction, which can measure the correlation between oxygen atoms, giving information about H-bonding networks of water molecules.^{82–84} Soper et al.^{81,85,86} have used neutron diffraction to show the second distance of the O–O coordination shift from 4.4 Å (bulk water) to ~4.0 Å in KX solutions ($X = \text{F}, \text{Cl}, \text{Br}$ or I) as the salt concentration increases from 0.7 to 2.7 M.^{81,86} Changing from K^+ to Na^+ , this distance

shifts to 3.4 Å in 3.3 M NaCl,⁸¹ indicating more structured H-bonding networks. The structure determination of water confined by ions studied by X-ray and neutron diffraction is always carried out in concentrated solutions (0.7–5.6 M) due to the sensitivity of these methods. The information on the long-range effect of cations and anions on water structures can be addressed by femtosecond second harmonic measurements to study the ions effect of nanoscopic water structures beyond three hydration shells in dilute solutions.⁸⁷ The ion-induced perturbations on nanoscopic structures of water are sensitive to ion concentration but independent of the chemical nature of ions,⁸⁷ where the orientational order of the H-bonding network increases evidently when the ion concentration is higher than 10 μM . Up to 1 mM, increasing orientational order on the nanoscale can further influence the macroscopic properties of water, and the collective hydrogen-bond interaction between the nanoscopic order domain induced by electrolytes decreases the surface tension of water.⁸⁷

Since ions alter the water structures in the hydration shell and beyond, the thermodynamic properties of the solutions change in response to the variation in the H-bonding structure induced by ions.⁷³ The distinct entropy of water under the confinement of ions has been extensively studied by Krestov,⁸⁸ Abraham,^{89,90} and Marcus,^{91–93} revealing the correlation between entropy changes and the water structure making and breaking ability of ions. There are several great reviews that have already summarized the different models for extracting the entropies considering the water structural effects of ions.^{73,91} We would only briefly introduce the latest model developed by Marcus in 1994, for illustrating the physical picture of ion regulating entropies.⁹² The hydration entropy of ions was denoted as $\Delta_{hydr}S^\infty$, describing the total entropy change in the hydration process, which includes effects of both the short-distance interaction in the hydration shell and the long distance interaction. In Marcus' model, the entropy change induced by the short-distance interaction can be further disintegrated into two parts, denoted as S_{nt} and S_{el} . S_{nt} represents the entropy change for creating a cavity for accommodating ions and the compression of water, which can be evaluated by the hydration of small neutral molecules and rare gas atoms with same radii of ions, giving the empirical equation as the following. The value of r is the radii of ions.

$$\Delta S_{nt} = -3 - 600(r/\text{nm}) \text{ J K}^{-1} \text{ mol}^{-1} \quad (3)$$

The second part, denoted as S_{el} , considers the contribution of the electrostatic interaction, which can be calculated using the Born model to give the equations as the following:

$$\Delta S_{el1} = (N_A e^2 / 8\pi\epsilon_0) \zeta^2 [\Delta r(r + \Delta r)^{-1}] \epsilon'^{-2} (\partial \epsilon' / \partial T)_P \quad (4)$$

$$\Delta S_{el2} = (N_A e^2 / 8\pi\epsilon_0) \zeta^2 (r + \Delta r)^{-1} \epsilon_r^{-2} (\partial \epsilon_r / \partial T)_P \quad (5)$$

The value of r is the radii of ions and Δr is the width of the hydration shell. Therefore, the S_{el1} pertains to the hydration shell and S_{el2} evaluates the entropy change induced by the electrostatic interaction outside the hydration shell. Assuming the infinitely large field in this model, the value of $\epsilon' = nD^2 = 1.776$, $(\partial \epsilon' / \partial T)_P = 2(\partial nD / \partial T)_P = -1 \times 10^{-4} \text{ K}^{-1}$ at 25 °C, and nD is the refractive index of water at the sodium D line.

Considering the effect of S_{nt} and S_{el} , the ΔS_{struc} can be deducted from $\Delta_{hydr}S^\infty$ as depicted in eq 6, which can be adopted as a descriptor for evaluating the effect of ions on the water H-bonding network. When ΔS_{struc} is negative, the ions

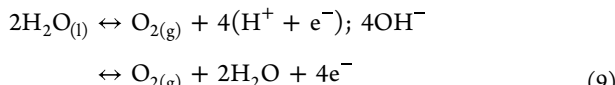
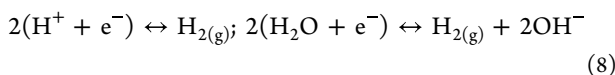
are considered as water structure maker, ordering the network structure outside the hydration shell. In contrast, the ions with positive ΔS_{struc} can disturb the network structure of water and are denoted as water structure breakers. ΔS_{struc} corresponds purely to the structural effect of the long-range network of water around the ions, which is dictated by factors including the ion's charge density, the coordination number and the structural implications from the screening of long-range electrostatics by water molecules.⁷³ The ΔS_{struc} values of different ions based on the Marcus treatment are listed in Table 1.

$$\Delta S_{struc} = \Delta_{hydr}S^\infty - [\Delta S_{nt} + \Delta S_{el1} + \Delta S_{el2}] \quad (6)$$

Table 1. Water Structural Entropy ΔS_{struc} /J K⁻¹ mol⁻¹. Values Obtained from Eq 6 According to Marcus Treatment⁹²

ion	Marcus ΔS_{struc}
Li ⁺	-52
Na ⁺	-14
K ⁺	47
Rb ⁺	52
Cs ⁺	68
Ag ⁺	-15
NH ₄ ⁺	5
Me ₄ N ⁺	41
Ca ²⁺	-59
La ³⁺	-113
F ⁻	-27
Cl ⁻	58
Br ⁻	81
I ⁻	117
NO ₃ ⁻	66
SCN ⁻	83
ClO ₄ ⁻	107
CO ₃ ²⁻	-52
SO ₄ ²⁻	8
PO ₄ ³⁻	-131

Altering the thermodynamics of water/ion via confinement can influence the thermodynamics of electrochemical reactions. The potential E for an electrochemical reaction is given by $E = -\frac{\Delta G}{nF}$ where ΔG is the standard Gibbs free energy of the reaction, n is the number of electrons transferred during the reaction, and F is Faraday's constant. In the case of water electrolysis (eq 7) which can be split into the cathodic and anodic half reactions undergoing H₂ evolution (HER) and O₂ evolution (OER) reactions, respectively (eq 8-9), the cell potential is 1.23 V at ambient conditions.

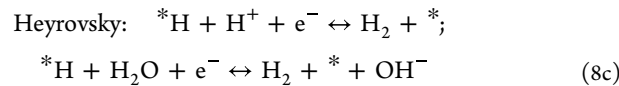
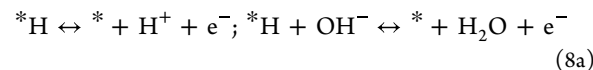


The free energy ΔG_r of the reaction can be tuned through the activity of the gaseous species (i.e., partial pressure) following $\Delta G_r = \Delta G^\circ + RT \ln \frac{p_{\text{H}_2}^2 p_{\text{O}_2}}{a_{\text{H}_2\text{O}}^2}$ having $p_{\text{H}_2}, p_{\text{O}_2}$ as the

partial pressure and $a_{\text{H}_2\text{O}}$ as the activity of the respective species. The activity of H₂O can influence the ΔG_r , which can be manifested in the changes in the enthalpy ΔH or entropy ΔS , which are direct functions of the formation enthalpy ΔH_f and entropy ΔS_f of water. Moreover, the standard potentials of HER and OER half reactions (eqs 8-9) can be tuned by the proton activity in the electrolyte. As such, the reaction free energy ΔG , and voltage E , is also a direct function of the thermodynamics of water (and protons for the half-cell potentials) which can be influenced by the confinement strategies.

The rates of reaction can be significantly (and more dramatically) influenced by the properties of confined water through changes in the Gibbs energy of activation and the pre-exponential factor (see Section 4), especially for reactions involving water and protons (H⁺). In electrochemical water-splitting the HER (at the cathode of water electrolysis) is commonly modeled through the Volmer (eq 8a), Tafel (eq 8b) or Heyrovsky (eq 8c) steps.

Volmer:



where H⁺, *, ${}^*\text{H}$ and e⁻ represent protons, catalytic active site, adsorbed hydrogen and electrons, respectively. As these elementary steps involve the transfer of protons and electrons to/from the catalyst active site, whose energetics and transfer rates will depend on the surrounding water molecules, the kinetics of the steps will be sensitive to the properties of water which can be tuned via confinement strategies. Therefore, assessing the potential connection between the water confinement thermodynamics and the kinetic parameters in catalytic systems is of primary interest in this review.

3. WATER STRUCTURES AND PROPERTIES UNDER CONFINEMENT

3.1. 1D Water Structures: Confinement of Water in Nanotubes

The thermodynamic properties of water filled in carbon nanotubes have been examined in nanotubes with different sizes and geometries.⁹⁴⁻⁹⁷ The thermodynamics of water in 1D confinement are dependent on geometric constraints, and more specifically the hydrogen bonding configuration which minimizes the free energy of water molecules under confinement. Diverse H-bonding structures of confined water have been observed in carbon nanotubes with different sizes and geometries. For example, the single-file arrangement of water molecules inside a single-walled carbon nanotube (CNT) (~ 0.8 nm) is illustrated in Figure 4a, where each water forms two H-bonds with its neighbors and is organized as a 1D water chain. With an increasing diameter of carbon nanotubes, more complex hydrogen bonding structures are observed in certain CNT geometries. As shown in Figure 4b, the exterior 4-fold-coordinated water molecules form a cylindrical "shell" near the nanotube wall of wider CNTs (1.4 nm). Meanwhile, interior water molecules (colored gray) form a one-dimensional chain

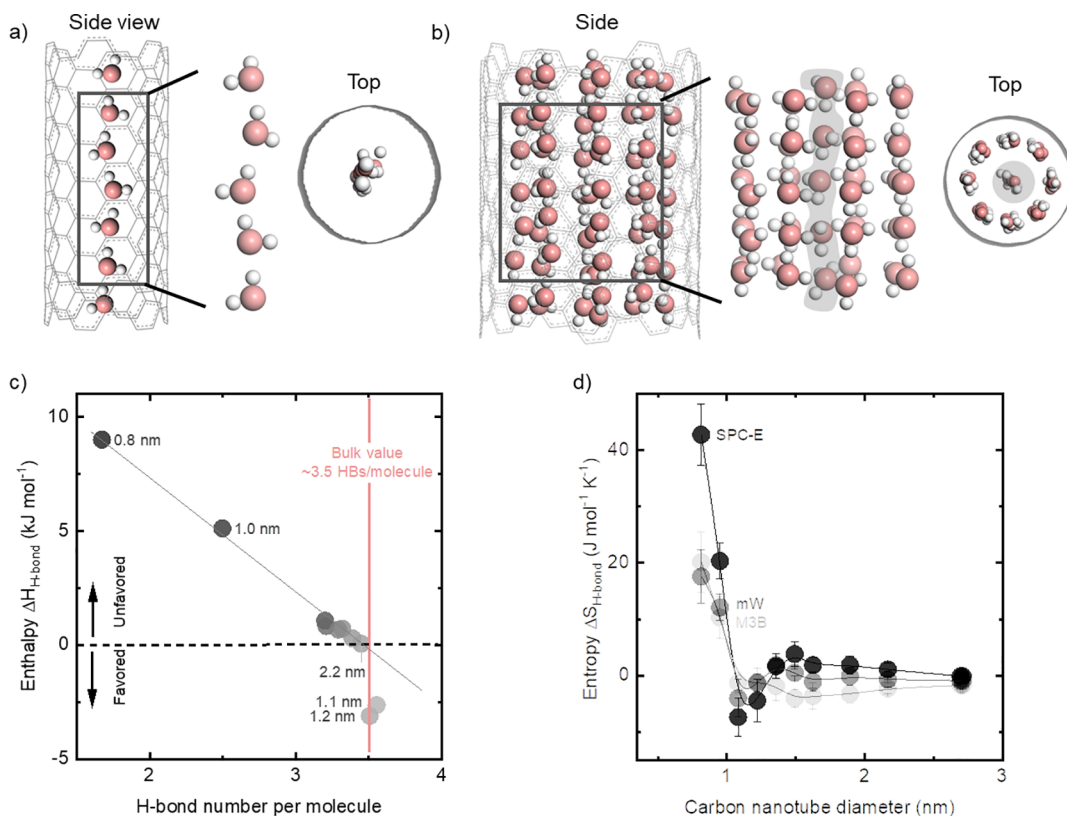


Figure 4. Hydrophobic confinement in carbon nanotubes. (a) A single file arrangement of water in CNTs (~ 0.8 nm).¹⁰⁰ (b) Exterior 4-fold coordinated water molecules with interior water molecules (highlighted in gray) forming a 1-dimensional chain in CNTs (~ 1.4 nm).¹⁰¹ (c) Correlation between the enthalpy and the number of hydrogen bonds formed per water molecule determined using molecular dynamics simulation. The number of hydrogen bonds decreases in the case of CNTs with diameters of 1 and 0.8 nm, resulting in unfavorable enthalpy. However, for tubes of 1.1 and 1.2 nm, water can form pentagonal or hexagonal ice-like structures, reducing the enthalpy.³⁵ (d) Entropy profiles for water in carbon nanotubes determined using molecular dynamics simulation at different levels of theory—simple point charge-extended (SPC-E), single particle (M3B), monotonic water (mW) models. The entropy gain for sub nm sized CNTs is due to increasing configurational entropy resulting from a loss of tetrahedral network of water molecules.³⁵ Panels (c) and (d) are adapted from ref 35. Copyright 2011 National Academy of Sciences.

along the tube axis (average coordination number 1.86) that retains fluidity down to as low as 50 K. The impact of such distinct structures of H-bonding networks on the enthalpy and entropy of water is shown in Figure 4c–d.³⁵ Generally, with decreasing size of the nanotubes, the number of hydrogen bonds decreases,^{18,98} where confinement results in an enthalpic penalty (Figure 4c).^{35,99} Within confined CNT diameters from 2.2 to 1.6 nm, the number of hydrogen bonds is similar to that of bulk water. Confinement of 1 nm is associated with water molecules losing an average of one hydrogen bond compared to bulk water whereas water molecules in confinement of 0.8 nm lose two hydrogen bonds per water molecule.³⁵ The decrease in H-bonds results in increased enthalpy along with diameter of carbon nanotubes from 0 to 9 kJ mol⁻¹, causing confined water chains in small carbon nanotubes to be enthalpy-unfavored. On the other hand, the cases of 1.1 and 1.2 nm deviate from the trend, where water can form ice-like stacked pentagons and hexagons in carbon nanotubes, respectively, and the number of H-bonding is increased to ~3.5.^{95,96} Consequently, ice-like rings of water can interact loosely via van der Waal's interactions with the walls, resulting in a decreased enthalpy of ~ 3 kJ mol⁻¹ relative to the bulk, which is thermodynamically favored.³⁵ Furthermore, the entropy of water within confinement can also be influenced significantly by the size and shape of the nanotubes (Figure 4d).³⁵ A lower entropy of 5 J mol⁻¹ K⁻¹ relative to bulk water

has been observed due to the rigid structure of pentagonal and hexagonal ice-like frameworks in the case of 1.1 and 1.2 nm confinement.³⁵ On the other hand, an entropy gain of ~ 50 J mol⁻¹ K⁻¹ can be obtained (~70% more than bulk water) due to more configurational entropy (translational and rotational) for subnanometer confinement relative to the tetrahedral arrangement in the bulk.⁹⁴ Therefore, water can be entropically stabilized but enthalpically penalized for subnanometer confinement, whereas water is enthalpically stabilized but entropically penalized within the cavity for confinement of ~ 1.1 – 1.2 nm of carbon nanotubes.^{35,95} This example shows that for noninteracting surfaces, enthalpy and entropy are influenced not only by the number of hydrogen bonds formed but also by the structure of the H-bond network that can be stabilized within the confinement.

The entropy of water correlates closely with dielectric properties since breaking the order of the H-bonding network suggested by increasing entropy, such as via increasing temperature, indicates the decreasing dipole moment of water (Figure 5).⁵⁴ The dipole moment dictates the static dielectric constant (ϵ_s) of water,¹⁰ which is around 80 for liquid water with an average dipole moment ~ 2.6 D, which is conventionally attributed to the ionic and molecular polarizations (Figure S3a).^{102–104} More recently, the origin of the dielectric response of water has been attributed to mechanisms of water dynamics, such as the migration of defects through the

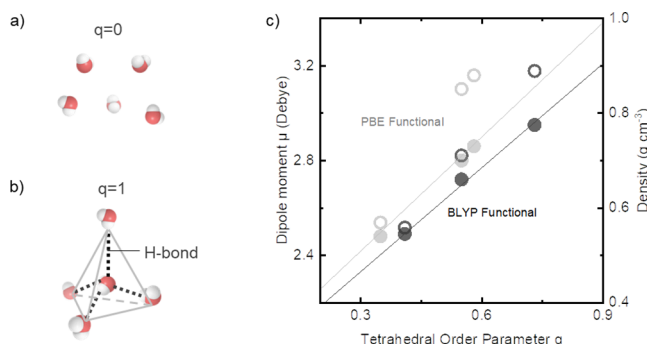


Figure 5. Dielectric constant of confined water. (a) Schematic of water arrangement at tetrahedral ordering parameter $q = 0$ and (b) at $q = 1$, where the parameter q closer to 1 represents a greater extent of tetrahedral ordering around a given molecule. (c) The average dipole moment (μ) (filled circles, left axis) and density of water (open circles, right axis) as a function of tetrahedral ordering parameter q of liquid water at $T = 323\text{ K} - 623\text{ K}$, examined using Monte Carlo simulations with Becke–Lee–Yang–Parr (BLYP) and Perdew–Burke–Ernzerhof (PBE) exchange correlation functionals. As temperature increases, the average dipole moment and tetrahedral order parameter decrease in part due to the decrease in density and also due to the disruption of the hydrogen bond network as the molecule possesses higher thermal energy to sample less energetically favorable configurations.⁵⁴ Panel c is created from the tabulated values in ref 54.

hydrogen-bond network¹⁰⁵ and the oscillatory-diffusion motion of protons related to the formation of short-lived H_3O^+ and OH^- ions from water molecules.¹⁰⁶ On the other hand, the optical dielectric constant of water is 1.8 (Figure S3b),¹⁰⁷ where only electrical polarization contributes to the dielectric properties and not the response to the dipole moment. The response of the static dielectric constant of water to common physical quantities such as temperature,¹⁰ density,¹⁰ electric field¹⁰⁸ and geometry of physical cavities has been studied^{109,110} (Figures S3–S4), where the latter two lead to a drastic decrease in the static dielectric constant. A

molecular dynamics study has shown that the dielectric constant of water at high electric fields decreases to around 20 in an electric field of $0.1\text{ V}\text{ \AA}^{-1}$ and to around 10 in the field of $0.3\text{ V}\text{ \AA}^{-1}$ (Figure S3d)¹⁰⁸ due to the polarization of water in the opposite direction to the external field.^{111–115} In carbon nanotubes, the confinement of water can decrease the static dielectric constant, as supported by MD simulations.¹⁰⁹ The dielectric constant of water in a spherical cavity can be calculated by estimating the mean square moment fluctuation ($\langle M^2 \rangle$), where M is the collective dipole moment of water molecules. For example, a nearly 50% decrease of the dielectric constant is observed when water is confined in a cavity of about 1.2 nm in diameter, reaching as low as 40 (Figure S4a).¹⁰⁹ In addition, MD simulations show that there is an oscillation of the density of water molecules near the walls, accompanied by the corresponding fluctuation in the dielectric constant as a function of distance from the wall, which increases evidently within $\sim 2\text{ \AA}$ of the walls (Figure S4b). The oscillation in the dielectric constant is attributed to an excluded volume effect. Near the walls, the average nearest neighbors of water increase from 5.2 to 6.2,¹⁰⁹ which leads to an increase in dipolar fluctuations and therefore a greater dielectric constant. This argument agrees with the fact that when water is instead confined by water vapor, i.e. no steric hindrance from the walls, no oscillation in the density or dielectric constant is observed (Figure S4c).¹¹⁰

3.2. 2D Water Structures: Water Networks at Solid Surfaces

Water at metal and metal oxide surfaces can serve as model systems to understand how the enthalpic properties of water are influenced by its interaction with the surface. As discussed for hydrophilic pockets of enzymes,⁵⁰ the H-bonding interaction between water and cavity can make the enthalpy more negative compared with bulk water. Although the H-bonding interaction between water and a metal surface is weak,¹¹⁶ the interaction accompanied by charge transfer from water to the surface manifests itself in a negative work function

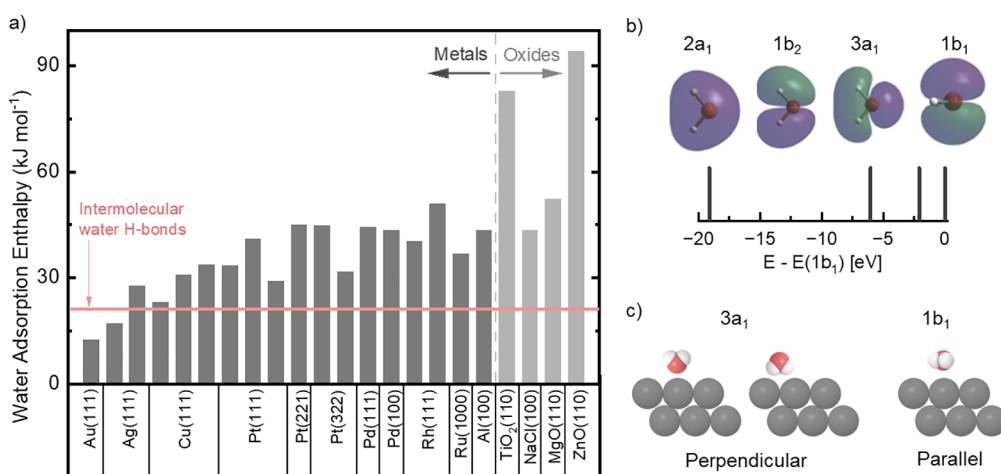


Figure 6. Water adsorption on surfaces. (a) DFT calculated adsorption enthalpies of water monomers on metal^{8,52,127} and metal-oxide^{52,129} surfaces are compared, which can be stronger than the H-bonding interaction between water molecules.^{123,139,140} The cohesive energy of water ($\sim 24\text{ kJ mol}^{-1}$) has been used as a measure of water–water interactions. In this plot, a higher value represents more favorable enthalpy. In contrast to metals with a distribution of weak (e.g., Au) to strong binding (e.g., Rh) surfaces, the calculated metal oxides in general show strong binding to water. The values are tabulated in Supporting Information, Table S2. (b) Molecular orbitals of water in the valence band and the corresponding energies relative to the highest occupied molecular orbital of water, 1b_1 .¹²³ Adapted with permission from ref 123. Copyright 2009 Elsevier. (c) Schematic of the impact of 3a_1 and 1b_1 orbital stabilization on the preferred orientations of water adsorption, leading to perpendicular (left) and parallel (right) configurations, respectively.

and decreases the enthalpy upon adsorption.¹¹⁶ Besides, the H-bonding structural changes at the surface will affect the enthalpy changes originated from the disruption/formation of hydrogen bonds, which should also be considered in the estimation of the enthalpy of 2D water.^{117,118} Commonly, the attractive/repulsive interaction between water and the surface should balance with the H-bonding formation between water molecules.^{117–123} Surfaces with weak water adsorption promote intact water networks with more H-bonds while strongly adsorbing surfaces to water can change water orientation in the H-bonding networks and results in less H-bonds.¹²⁴ Therefore, the enthalpy of 2D water could be estimated by considering water–surface interactions and water–water interactions, which will be contributed from the formation of metal–water bonds and H-bonds among water molecules. We note that liquid–gas interfaces are also of significant interest, as they can strongly influence the effective concentrations and reactivity of reactant gas molecules that drive heterogeneous processes in atmospheric and environmental chemistry.¹²⁵ However, they are beyond the scope of this review. Readers are referred to the excellent review by Björneholm et al.¹²⁶

3.2.1. Water Monomers Confined by Metals/Metal Oxides. The computed adsorption enthalpy of individual water molecules by density functional theory (DFT) for different metal/oxide surfaces, which can be used to evaluate the strength of interaction between water and surface, shows water binding on these surfaces is mostly greater (in magnitude) than interactions among water molecules ($\sim 24 \text{ kJ mol}^{-1}$), as shown in Figure 6a. The interactions between water and hydrophobic metal surfaces such as Au and Ag, are weak, with adsorption enthalpy 11–17 kJ mol^{-1} lower than that of H-bonds in bulk water.^{8,52} The metal surfaces such as Pt,^{51,127} Pd,¹²⁸ Ru⁵² and Rh⁵² exhibit higher adsorption enthalpy (30–55 kJ mol^{-1}), which is more hydrophilic considering the stronger interaction between metal and water compared to that among water molecules.^{51,52,127,128} The step sites with lower coordinator numbers, compared to low index facets such as (111), can further increase the adsorption enthalpy of water. In contrast to metals, metal oxides can have stronger binding to water (62–165 kJ mol^{-1}),^{129,130} which could be explained by how the surface electronic structure couples with water on the surface to dictate the binding strength, as determined by the spatial and energetic overlaps of the orbitals between water and the binding surface site.^{131–133} Molecular water has three occupied states in the valence band, noted as the 1b₂, 3a₁, and 1b₁ states (Figure 6b),^{116,134} where the energy of the 1b₂ state is the lowest, making it the least possible to be involved in the interaction with the surface. The 3a₁ (mostly localized on oxygen and hydrogen atoms) and 1b₁ (delocalized and parallel to the plane of the molecule) states exhibit similar energies and have higher probabilities of participating in the adsorption (Figure 6b). The relative stability of the 3a₁ and 1b₁ states on different surfaces dictates the adsorption geometry (Figure 6c),¹¹⁶ which has been investigated experimentally. For example, based on low energy diffraction (LEED), photoelectron spectroscopy and thermal desorption spectroscopy (TPD) studies, the 3a₁ state is stabilized on the Co surface, so the water molecules tend to adsorb in the perpendicular orientation (Figure 6c, left). On the other hand, Ru(0001) has been suggested to bind water through 1b₁ (Figure 6c, right),^{137,138} where the parallel orientation would be preferred. Unfortunately, the predom-

inant state of bonding cannot be identified easily by the photoemission spectrum for most metals, due to the relatively weak interaction and flexible adsorption configurations between water and metals.^{116,134} In contrast, the stronger adsorption enthalpy of metal oxides results in a more stable adsorption configuration than for metals, where the relative stability of the 3a₁ and 1b₁ states correlates well with the adsorption geometry on metal oxides. For instance, metal oxides such as SrTiO₃(100) and CuO(100) are shown to stabilize the 3a₁ state, having water adsorb on cation sites in a perpendicular configuration,^{131,133} where the greater energy shift of the 3a₁ state correlates with the larger strength of adsorption bonding between water and the surface.¹³³

Additionally, wettability on single crystal surfaces can, to an extent, be useful in classifying water–surface interactions. The lower measured contact angle (θ) indicates stronger wetting of the surface by water, which can be described by the Young's equation $\gamma_{SG} = \gamma_{SL} + \gamma_{LG} \cos(\theta)$, where γ_{SG} , γ_{SL} , and γ_{LG} are surface tensions of solid–gas, solid–liquid and liquid–gas, respectively, and γ_{SL} can be correlated with the Gibbs free energy of adsorption of liquid molecules on a solid surface.^{141,142} On closed-packed single crystal surfaces, metals such as Au(111) can have a larger contact angle, consistent with their weak water adsorption enthalpy $\sim 11 \text{ kJ mol}^{-1}$, although the specific experimental values remain highly discrepant (between $\theta_{\text{Au}(111)} = 0\text{--}93^\circ$),¹⁴³ likely owing to surface cleanliness issues and the specific experimental conditions. In comparison, lower contact angles have been measured for hydrophilic surfaces such as Cu(111) ($\theta_{\text{Cu}(111)} \sim 75\text{--}86^\circ$),¹⁴⁴ Ru(0001) and TiO₂ ($\theta_{\text{TiO}_2(110)} < 74^\circ$),¹⁴⁵ where dissociation of water molecules can occur. Unfortunately, inconsistencies in contact angle measurements on many surfaces are observed, highlighting experimental challenges in correlating the surface adsorption free energy of water with wetting angles,^{143,146} even for microscopically flat surfaces like single-crystal surfaces. Moreover, wetting angles can be influenced significantly by surface morphologies, roughness, and surface heterogeneities such as grain boundaries. For example, the wetting properties on microscopically rough surfaces (with nanometer-scale and micron-scale roughness) can be governed by surface roughness and wetting parameters beyond surface energy as described by the Wenzel (homogeneous wetting) or Cassie–Baxter (heterogeneous wetting) model,^{147,148} where the latter gives the apparent contact angle θ^* of a liquid droplet on n surface components, each having an areal fraction Φ_i and solid–gas ($\gamma_{i,SG}$) and solid–liquid ($\gamma_{i,SL}$) surface tensions, via the relation $\gamma_{LG} \cos(\theta^*) = \sum_{i=1}^n \Phi_i (\gamma_{i,SG} - \gamma_{i,SL})$.^{147,148} Therefore, the surface roughness and heterogeneities will influence the apparent contact angle through their influence on Φ_i , $\gamma_{i,SG}$ and $\gamma_{i,SL}$, where the term $\sum_{i=1}^n \Phi_i (\gamma_{i,SG} - \gamma_{i,SL})$ can be collectively dubbed as the overall roughness and heterogeneity factor. Surface wettability via macroscopic texture/patterning strategies is beyond the scope of the review, but readers are referred to previous comprehensive reviews.^{149,150} Therefore, the wetting properties of high-surface-area electrodes with rough surfaces for practical electrochemical processes are influenced by surface morphological features and voltage and adsorption thermodynamics of gas and liquid species, which requires further studies.

3.2.2. H-Bonding Structures and Dynamics of 2D Water without Ions. Beyond the water monomer binding on surfaces, the collective interaction among water molecules on the surface leads to surface-dependent H-bonding structures.

Scanning tunneling microscopy (STM) and atomic force microscopy (AFM) complemented by density functional theory (DFT) or molecular dynamics simulations (MD) have been used to identify the formation and behavior of 2D water structures on different surfaces.^{126,151} On hydrophobic metal surfaces such as Ag, Cu, and Au (111), with adsorption energy comparable to or weaker than the H-bond of water (Figure 6a),^{123,139,152} water forms intact clusters rather than wetting the surface (Figure 7a–b),^{117–123,153} in the form of

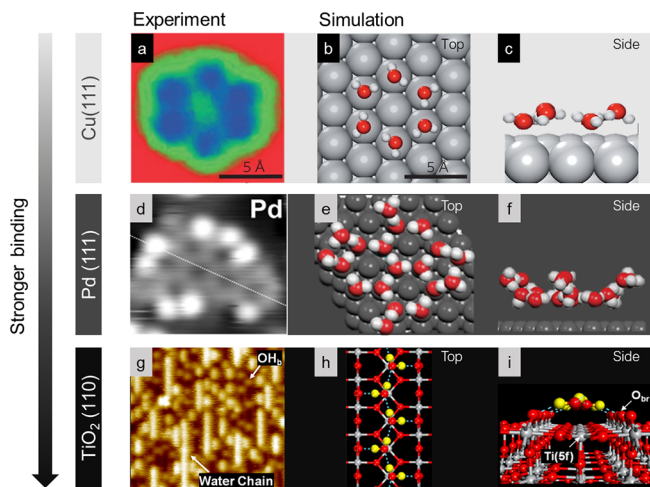


Figure 7. H-bonding networks on metals and metal oxide surfaces. (a) Experimental Scanning Tunneling Microscopy (STM) and (b, c) calculated water hexamer on Cu(111) with weak H₂O–metal interaction, showing a planar water hexamer.¹⁵⁸ Panels a, b and c are adapted from ref 158. Copyright 2012 Springer Nature. (d) Experimental STM and (e, f) calculated water structure on Pd(111) with strong H₂O–metal interaction, where water molecules are pulled in closer to the surface.¹¹⁸ Panels d, e and f are adapted from ref 118. Copyright 2009 American Chemical Society. (g) Experimental STM of water molecules on TiO₂(110) at an initial coverage of 0.5 ML, where bridging hydroxyl species (OH_b) are observed, as a result of water dissociation on oxygen vacancy or stepped sites. Moreover, a water chain network is formed only in one direction, as indicated by vertical streaks, in contrast to the two-dimensional water layers on metal surfaces.¹⁶² (h, i) Simulated water network structure for TiO₂(110), where, the 1-dimensional water chains are formed owing to the presence of bridging oxygens (O_b) which are a H-bond acceptor and act as guiding walls in one direction.¹⁶² Panels g, h and i are adapted from ref 162. Copyright 2013 American Chemical Society.

hexamers by balancing the competition between the H₂O–H₂O bonding and H₂O–surface interactions. The water network above the surface resides on a plane (Figure 7c) as the interaction of water with the surface is weak. In contrast, stronger H₂O–metal interactions such as on Pd(111) (Figure 7d–f) and Ru(0001) compared to Ag, Cu and Au can pull oxygen or hydrogen from H₂O down to the surface,¹⁵³ breaking the order of planar hexamer water clusters with smaller number of intermolecular H-bonds.¹¹⁸ The hexamer of water can be observed on the (111) facet of metals because the structure of the hexamer in the ice-like layer can fit the close-packed structure of most metals.¹⁵⁴ However, when the metal–metal bond extends to 3.5 Å in Pb(111), which is 22% larger than Au(111), water molecules organize into water dimers in chain-like structures, as revealed by ab initio MD simulations.^{151,155} Apart from (111) facets, the water structure

on Cu(110) can form 1D structures consisting of face-sharing pentagons.^{156,157} A direct comparison of (110) facets of Ni, Cu, Pd and Ag enables comparison of the interfacial water structure when the separation of the closed packed metal rows increases from 3.5 to 4.2 Å. Similar to Cu (110), Ni (110) with a smaller metal lattice parameter stabilizes the pentagon chains, whereas for Ag (110) with the largest lattice constant among the metals compared, hexagons are preferred over pentagons.¹⁵⁸ Therefore, the H-bonding structure of water confined to the surface is dominated by both the adsorption energy and the local geometry of surfaces. Although the water arrangement on the surface has been extensively studied via observing oxygen atoms of water by STM, directly observing protons and revealing the comprehensive picture of interfacial H-bonds is still a great challenge. To address this problem, Jiang et al. have developed high-resolution STM¹⁵⁹ and AFM¹⁶⁰ methods that are capable of acquiring submolecular images of molecular orbitals and hydrogen atoms of water. Four different types of water clusters that are composed of tetramers of water have been observed at 77 K on NaCl (001), where the tetramer building blocks are connected by some individual water molecules perpendicular to the surface.^{160,161} The water tetramers on NaCl (001) at 5 K and the proton tunneling can be accelerated by pushing Cl[−] on the STM tip closer to the surface. When the proton is transferred, the water tetramers are transformed from a clockwise state to an anticlockwise state, and the switching rate was measured by extracting the current versus time trace, which exhibited 2 orders of magnitude increment when the Cl[−] ion approached the surface. This STM study performed at cryogenic temperatures (5–20 K) has their kinetics not dominated by thermal fluctuations. Such a study reveals the concerted proton tunneling in the water network, revealing the dynamics of interfacial H-bonds.¹⁶³

Compared to metals, the interaction between water and metal oxides is much stronger. Water can dissociate at metal oxide surfaces due to the presence of coordinatively unsaturated metal cation sites and form a range of different surface structures from monomers, dimers, trimers, tetramers to 1D and 2D chains.¹⁶⁴ On the most well-studied TiO₂ (110) surface, water dissociation is prominent at oxygen vacancy sites and step edges,¹⁶⁵ forming bridging hydroxyls (OH_b) according to experimental STM measurement and DFT computation, as shown in Figure 7g–i. However, the structure of water at the interface can still be controversial, with the energetics for molecular adsorption and dissociative adsorption, forming *OH groups on the Ti site, with *H bound to the neighboring bridging oxygen site, being very similar.¹⁶⁵ Interestingly, as the coverage of water increases, the molecules tend to form 1D chains along the Ti rows (Figure 7g–h),^{162,166,167} as opposed to the 2D network in metal surfaces (Figure 7a, d), owing to the bridging oxygens which act as guiding walls on either side of the water 1-D chains.¹⁶² Water dissociation is found to be much more prominent in the case at oxygen vacancy sites and step edges.¹⁶⁵ In contrast to TiO₂(110) where water dissociation is prominent at oxygen vacancy and step sites, STM and DFT studies of the anatase TiO₂ (101) polymorph have shown that water binds as an intact molecule with a binding energy of 730 meV, with the charge rearrangement at the interface influencing the binding energy of subsequent water molecules.¹⁶⁸ On rutile RuO₂ (110) surfaces, water dimers were found to dissociate to form alternating *OH and *H₂O groups on the coordinatively unsaturated sites with *H being bound to alternate bridging

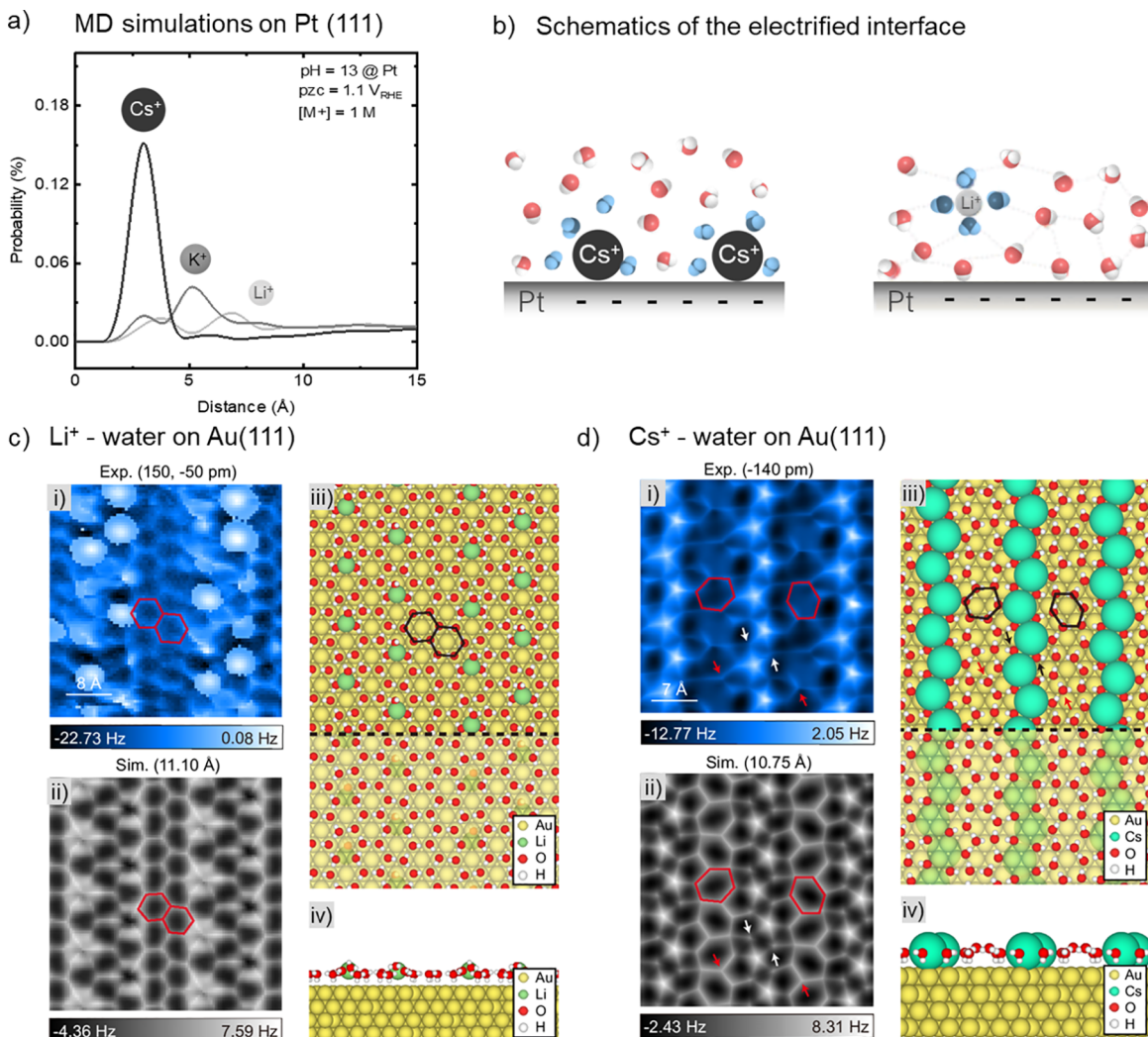


Figure 8. Influence of alkali metal cations on interfacial water structure. (a) Z-axis probability distribution function (ZDF) of the surface cation in classical MD simulation of Pt(111) at pH = 13 at 0 V_{RHE} , 1.1 V lower than PZC, where the unit cells contain 2293 water molecules, 42 cations, and 42 Cl^- anions, corresponding to 1 M cation in water.³⁷ With larger cations (Cs^+), surface water is removed due to strong ion-surface interaction. In contrast, a stable interfacial water layer is observed at the interface in the presence of smaller cations (Li^+).³⁷ Reproduced with permission from ref 37. Copyright 2021 American Chemical Society (b) Schematic of different water structures around alkali metal cations (Cs^+ vs Li^+) at the interface. (c) Structure of 2D Li^+ -water layer on Au(111), probed by constant-height AFM force-mapping (i) and simulated AFM (ii), where the hexagonal water network is indicated in red. The corresponding 2D structural model of Li on Au(111) via DFT is shown in panels (iii) and (iv) for top and side views, respectively. (d) Structure of 2D Cs^+ -water layer on Au(111) probed by the constant-height AFM force-mapping (i) and simulated AFM (ii). Two types of water orientation are observed; bridging and flat-lying water molecules are indicated in white and red arrows, respectively. The red distorted hexagon on Cs^+ shows the disturbance of the interfacial water network. The corresponding 2D structural model of Cs^+ on Au(111) via DFT is shown in panels (iii) and (iv) for top and side views, respectively. Panels (c) and (d) Adapted with permission by the authors of ref 172. Copyright 2024 open access article distributed under CC BY-NC-ND License 4.0.

oxygen atoms.¹⁶⁸ Similar to the case of metals, the surface orientation of metal oxides such as rutile TiO_2 ¹⁶⁹ and RuO_2 ¹⁷⁰ has been shown to significantly influence its interaction with water. For example, on RuO_2 surfaces, the degree of water dissociation was found to be highest on the (101) surface, followed by the (110), (001) and (100), which could be attributed, at least in part, to the arrangement of surface Ru and O sites and the degree of hydrogen bonding interactions that they could enable.¹⁷⁰ Although the STM and AFM studies provide revealing information about the H-bonding of surface-confined water, most of them are carried out under low temperatures, which differ from practical catalytic and electrocatalytic systems. Advances in ambient pressure X-ray

photoelectron spectroscopy can bridge this temperature and pressure gap.

3.2.3. H-Bonding Structures and Dynamics of 2d Water in the Presence of Ions. In an electrochemical system where ions are present alongside water molecules, the water solvation environment and network structure in the bulk electrolyte depends on the structure-making and breaking ability of the ions (see Section 2.2). When water and ions contact an electrode surface, the structures of the 2D water at the electrified interface are also strongly cation-dependent. Under a negative applied bias (relative to the PZC), cations along with their water solvation are attracted to the surface, resulting in a local effective concentration which could reach ~80 times or higher than the bulk concentrations.¹⁷¹ Based on

classical MD simulations on a Pt(111), a larger cation such as Cs^+ is present closer to the electrified interface as a result of partial desolvation of water molecules around structure-breaking ions (Figure 8a), as evidenced by the first peak center location in the Z-axis probability distribution (2.8 Å) being smaller than the second O–O coordination (around 4 Å) (Figure 8b). In contrast, smaller cations such as Li^+ , which have higher charge densities and thus bind solvating water molecules more strongly, can retain their solvation shell as they assemble >3 Å from the surface (Figure 8a–b).³⁷ These observations from MD simulations are consistent with the scanning tunneling microscopy and noncontact atomic force microscopy characterization of ion-specific water structures on a charged Au(111) surface (Figure 8c–d).¹⁷² In that work, the cation-water structures were grown on the Au(111) surface by depositing alkali metal atoms at room temperature, followed by dosing of water molecules at ~ 120 K. The difference in the Fermi levels between Au(111) and alkali metal atoms drives electron transfer from the alkali metal to the Au(111) surface, rendering the Au(111) and alkali metal atoms negatively and positively charged, respectively, hence emulating an electrified interface in the presence of a reducing bias. Based on the fabricated model system, which possesses an ion concentration of ~ 10 M (corresponding to a bulk concentration of ~ 0.1 M), the atomic structures of the cation water networks were found to be distinctly different between Li^+ and Cs^+ . With Li^+ , the water molecules were able to lift the cations from the substrate, forming an ordered hexagonal network structure¹⁷² (Figure 8c), pointing to the water-making property of Li^+ in maintaining its rigid H-bonding network structure¹⁷² and overcoming the substrate–alkali metal interaction. In the case of Cs^+ and K^+ , these structure-breaking cations adsorb on the substrate and disrupt the interfacial H-bonding network of water (Figure 8d),¹⁷² where two types of water orientation (i.e., bridging and flat-lying water molecules) are observed, and the distorted hexagon on Cs^+ shows the disturbance of the interfacial water network (Figure 8d). We note that the STM/AFM experiments were performed under vacuum and at low temperature, but the relative differences in the structures may have relevance in the electrified interface at ambient conditions. It is interesting to note the rather similar behavior of ion segregation can be found at the water–vapor interface: small anions are more depleted at the air–water interface due to the lack of polarizable solvents outside the water to favor the retention of its solvation), while large polarizable halide anions are less depleted or even enriched for Iodide at the water–air interface.¹⁷³ The differences in the solvation structure at electrified interfaces have been found to be an important factor in reaction kinetics, which will be discussed in Section 4.

To be able to measure water under truly operando electrochemical conditions (i.e., water in the presence of ions, catalyst surface and applied potential), spectroscopic experiments have been used to measure the orientations of surface-confined water molecules at room temperature for electrochemical systems to elucidate water orientation changes in response to the applied biases. Surface-enhanced infrared absorption spectroscopy (SEIRAS) has been adopted to study the water structure on the Au(111) electrode by Ataka et al.,¹⁷⁴ which reveals that the structure of interfacial water is distinct from that of bulk and highly dependent on the applied potential. When the potential is lower than the potential of zero charge (PZC, 0.3 V on Au), water molecules form weak H-bonds between each other, and hydrogen atoms tend to

approach the surface (oxygen-up orientation). On the other hand, water can form strongly hydrogen-bonded ice-like structure when the potential of Au is slightly higher than the PZC, and the oxygen of water approaches the surface (oxygen-down orientation) under this condition.¹⁷⁴ However, the H-bonding will break apart with increasing potential, since the specific adsorption of perchlorate ions occurs at higher potential. Similar potential-dependent reorientation has been observed on Pt by SEIRAS; the weakly hydrogen-bonded oxygen-up orientation appears at potentials lower than the PZC, while water can form a strongly hydrogen-bonded ice-like layer at potentials higher than the PZC.¹⁷⁵ Besides, the orientation of water molecules has also been studied on gold electrodes under bias using X-ray absorption spectroscopy,¹⁷⁶ where four different types of water orientations are identified, including no hydrogen bond donor (ND), a single hydrogen bond donation (SD^{\parallel}) parallel to the electrode, a single hydrogen bond donation (SD^{\perp}) perpendicular to the electrode, and double hydrogen bond donation (DD) as shown in Figure 9a. The pre-edge peak (535 eV) of water

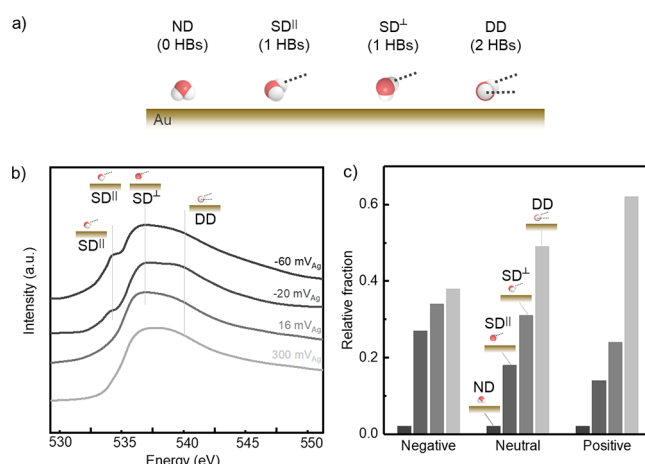


Figure 9. Water reorientation at electric double layer. (a) Schematic presentation of different water orientations on the surface. The no hydrogen donor (ND), single hydrogen bond donation parallel (SD^{\parallel}) to the surface and perpendicular (SD^{\perp}) to the surface, and double hydrogen bond donation (DD) can form 0, 1, and 2 hydrogen bonds with adjacent water molecules, respectively. (b) XAS spectroscopic measurements of water–solid interfaces on gold electrodes under ambient conditions as a function of applied potential bias.¹⁷⁶ The increase in the pre-edge peak at 535 eV at more negative bias is assigned to SD^{\parallel} water molecules according to AIMD simulations.¹⁷⁶ (c) The distribution of water orientation at different charge states of Au surface based on the corresponding AIMD simulations,¹⁷⁶ where a negatively charged surface enhances the SD at the expense of DD populations, disrupting the hydrogen bond network on the surface. Reproduced with permission from ref 176. Copyright 2014 AAAS.

grows with more negative potentials (Figure 9b–c), which comes from an increase in SD^{\parallel} water molecules as confirmed by ab initio molecular dynamics (AIMD) simulations. In addition, in situ Raman spectroscopy associated with AIMD has revealed the potential-dependent adsorption geometry at negative biases, revealing that water is parallel to Au(111) at 0 to -1.0 V (SD^{\parallel}). With decreasing potential, water rotates and one hydrogen approaches the surface at -1.3 to -1.8 V (SD^{\perp}), and both hydrogens of water approach the surface at -1.8 to -2.0 V (ND).¹⁷⁷

Using sum-frequency vibrational spectroscopy (SFVS), Ostroverkhov et al. have probed the OH stretching vibration at the water–quartz interface as a function of bulk pH from 1.5 to 11.5.¹⁷⁸ From the imaginary component of phase-sensitive SFVS measurements, the researchers have decomposed the interfacial water signal with the signs of the signals detailing the orientation of the water molecule polarization. Negative signal indicates that the water molecules are oriented with the oxygen toward the surface, and positive signal originates from water molecules with hydrogen oriented toward the surface (Figure S5). All three peaks become more positive with increasing bulk pH, as is expected from the quartz surface deprotonating ($\text{SiOH} \rightarrow \text{SiO}^- + \text{H}^+$) and water molecules preferring to orient their hydrogen toward the surface (Figure S5). On the other hand, there is a significant measure of liquid-like water molecules that are oriented with the hydrogen toward the surface even at pH 1.5, where the quartz surface should be protonated. The signal can be attributed to the presence of heterogeneous protonation sites on the quartz surface even under acidic conditions, where a significant number of surface sites remain deprotonated. An independent study using second harmonic imaging of a glass microcapillary–water interface provides support to this analysis.¹⁷⁹ From spatially resolved Second Harmonic Generation (SHG) intensity maps at different pH, the authors have confirmed significant spatial heterogeneity in the local deprotonation rate at the silica–water interface ($\text{pK}_{\text{a},\text{s}}$ 2.3–10.7). It should be noted that quartz, sapphire, hematite, and titania are well-studied hydrophilic substrates for confinement, and we refer the readers to discussion of this behavior elsewhere.^{173,180–182} While these studies provide detailed information on the H-bonding structure and orientation of interfacial water, they also present a clear need to relate the interfacial water structure to properties of interest for catalysis.

The presence of water has been shown to regulate both the adsorption configuration and binding energy of intermediates. For instance, CO is an essential reaction intermediate for organic oxidations¹⁸³ and the CO_2 reduction reaction (CO₂RR).¹⁸⁴ Ogasawara and co-workers have found the adsorbed water on Pt (111) can move part of adsorbed CO from atop sites to bridge sites, as revealed by Infrared Reflection Absorption Spectroscopy (IRAS).¹⁸⁵ The site-shifting effect of coadsorbed water is more significant on Rh (111) and Ni (100), where atop CO is shifted to 3-fold hollow sites on Rh (111)^{186,187} and 4-fold hollow sites on Ni (100),^{188,189} respectively. The attractive interactions between adsorbed water and CO have also been reported. On Pt (111), the decreasing of the infrared intensity of CO and red-shifted frequency have been observed by infrared adsorption spectroscopy when water coadsorbed, which indicates the attractive interaction between atop CO and H_2O .¹⁹⁰ Similar phenomena have been observed on Ni (100)^{151,155} and Ru (0001).^{138,191} The red shift of $\nu(\text{CO})$ on Pt (111) has been further confirmed by Sum-Frequency Generation (SFG) experiments.¹⁹² Rupprechter and co-workers have proposed that the charge transfer from water to the surface enhances the interaction between Pt and CO and consequently causes the red shift of $\nu(\text{CO})$.¹⁹² Therefore, the attractive interaction between water and CO is mediated by the electronic effect of the metal surface. Moreover, the coadsorption of water has been found to stabilize molecular oxygen (O_2) and adsorbed OH, which are essential intermediates for tuning activity for the ORR.¹¹⁶ Molecular oxygen has been found to induce the

dissociation of water to form a stable *OH H-bonding network, and $(\sqrt{3} \times \sqrt{3})\text{R}30^\circ$ OH and $c(3 \times 3)$ OH patterns are observed on Pt(111).¹⁹³ Therefore, the studies in UHV reveal the important role of interfacial water in tuning the adsorption behavior of intermediates for important catalytic processes (e.g., *CO for CO₂RR and *O₂ and *OH for ORR), suggesting it is necessary to consider the solvation effect of water for predicting the thermodynamics of heterogeneous catalysis and electrocatalysis. One or two water bilayers^{194,195} or full solvation with several bilayer structures^{196,197} have been incorporated in recent DFT studies for predicting the onset potential of ORR and kinetics of CO₂RR. The solvation of intermediates through hydrogen bonding in the explicit model can play an essential role for stabilizing *OH, which can reduce the enthalpy of the system and predict more precise onset potential compared with experimental data, while the implicit model underestimates the value. The explicit solvation model points out the essential role of interfacial H-bonding structure dictating surface thermodynamics. For the electrocatalytic processes such as ORR and CO₂RR, which pertain to the linear free energy relationship, the changes in thermodynamic adsorbate binding energy may influence the reaction barrier and provide insight into enhancing catalytic activities; we will discuss the kinetic details in Section 4.

Overall, while consistent molecular-level clarity of water monomer adsorption (all the way up to water layers) on flat metal surfaces has been achieved (see the seminal reviews by Björneholm et al.¹²⁶ and Carrasco et al.¹⁵⁸), the picture is relatively unclear for metal oxide surfaces where the existence of multiple unique atomic sites can give rise to more complicated binding configurations. More importantly, water adsorption geometries and the network structures under (electro)catalytic conditions are not completely understood. For example, uncertainties remain regarding (1) potential/surface charge on clean surfaces without adsorbates,¹⁷⁷ (2) interaction of interfacial water with surface adsorbates (this is particularly a very “hot” area for CO₂ reduction on copper surfaces,¹⁹⁸ and (3) electrical double layer structure in the presence of cations at interfaces.¹⁹⁹ Moreover, how the understanding of well-defined surfaces translates into nanostructures (where multiple facets and surface decorations such as terraces, kinks and steps) is still unclear but can be expected to have a significant influence. Surface-sensitive techniques such as surface-enhanced Infrared³³ and Raman¹⁷⁷ Spectroscopy, nonlinear optical techniques such as sum frequency generation,²⁰⁰ surface diffraction²⁰¹ and imaging techniques (i.e., scanning probe microscopy²⁰²) can help elucidate the nanoscale structure: some of these techniques have been discussed in Sections 3.2.2 and 3.2.3. However, all these techniques are low-throughput and require near-perfect samples. Advancements in experimental techniques will be needed to improve our understanding of interfacial water structure especially at nanostructure interfaces under (electro)-catalytic conditions.

3.3. 3D Water: Water Clusters in MOFs and Zeolites

Microporous materials with their tunable structures and chemistries are well-known to confine water,^{203,204} offering a rich design space to alter water interactions. For example, the pores of MOFs and zeolites can influence the hydrogen bonding networks of water, and both the physical size and chemical characteristics of the pores (e.g., hydrophobicity) in

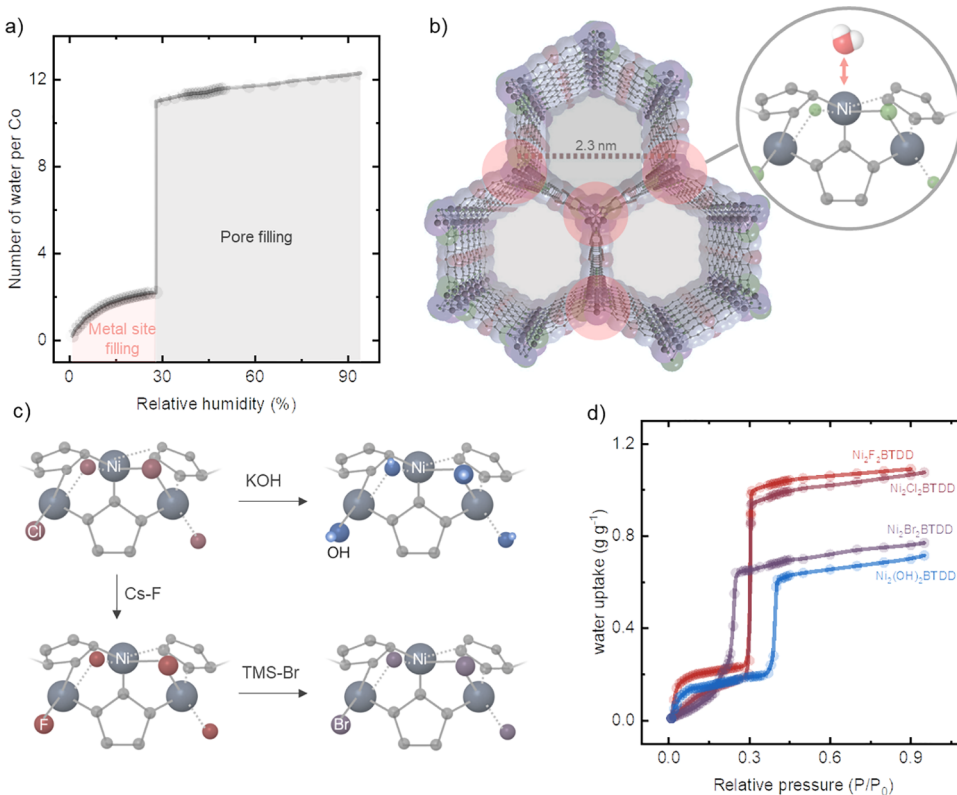


Figure 10. Water adsorption enthalpy in isostructural MOFs. (a) Experimental water adsorption isotherm at 298 K for Co₂Cl₂BTDD. The range corresponds to water occupying metal sites and filling the pores colored by red and gray, respectively.²⁰⁹ (b) Crystal structure of Co₂Cl₂BTDD (H₂BTDD = bis(1H-1,2,3-triazolo[4,5-*b*],[4',5'-*i*])dibenzo[1,4]dioxin). The metal sites and the pore space to accommodate water are colored by red and gray, respectively.²⁰⁹ Panels (a) and (b) are adapted with permission from ref 209. Copyright 2019 open access article distributed under CC BY License 4.0. (c) Scheme of modifying Ni₂X₂BTDD by anion (X) exchange (X = Cl, F, Br, OH) of the metal nodes.²¹⁰ Adapted with permission from ref 210. Copyright 2019 American Chemical Society. (d) Water vapor adsorption (closed symbols) and desorption (open symbols) isotherms of Ni₂Br₂BTDD, Ni₂Cl₂BTDD, Ni₂F_{0.83}Cl_{0.17}BTDD, and Ni₂(OH)₂BTDD measured at 298 K.²¹⁰ The decrease in the relative humidity onset of pore-filling upon anion substitution of OH⁻ can be attributed to the contraction of the pore diameter and weakening of the hydrogen bonding network, which increases the density of unsaturated hydrogen bonds and therefore attracts more water molecules. Reproduced with permission from ref 210. Copyright 2019 American Chemical Society.

porous solids can be used to tune the thermodynamics and properties of water in the confined environment.

3.3.1. Pure Water Adsorption Enthalpy within Cavities. Water adsorption isotherms are used to determine the strength of interaction between water and cavities. Representative measurements of such an isotherm using Co₂Cl₂BTDD (H₂BTDD = bis(1H-1,2,3-triazolo[4,5-*b*],[4',5'-*i*])dibenzo[1,4]dioxin) are shown in Figure 10a,²⁰⁵ which exhibits a step increase in the uptake of water molecules at 28% relative humidity, attributable to the onset of pore filling of water. Before this step, the water molecules only absorb on the strong binding sites (e.g., water interaction with the metal sites by a ligation bond and/or hydrogen bond, Figure 10b, red).²⁰⁵ In the pore filling step, water molecules interact with each other through hydrogen bonds (Figure 10b, gray).²⁰⁵ Water adsorption enthalpy²⁰⁶ can be derived from the water adsorption isotherms at different temperatures according to the Clausius–Clapeyron equation:

$$\Delta h_{isos} = R \left(\frac{d(\ln P)}{d\left(-\frac{1}{T}\right)} \right)_w \quad (10)$$

where Δh_{isos} , R , P , T and w represent the isosteric (i.e., equal valence electrons) enthalpy of adsorption, universal gas

constant, pressure, temperature and water uptake, respectively. Following this formalism, the water adsorption enthalpies have been measured to range from 43 to 85 kJ mol⁻¹ in MOFs and zeolites, as summarized in Table S3 and Figure S6. Most MOFs have been measured to exhibit similar water adsorption enthalpy values during the pore-filling step (40–50 kJ mol⁻¹)^{207,208} approaching the energy of hydrogen bonds (24 kJ mol⁻¹).^{123,139,140} However, some MOFs have also been measured to strongly favor water adsorption. For example, the water adsorption enthalpy of MIL-100(Fe) can reach 85 kJ mol⁻¹ when the water uptake approaches 0 (i.e., before pore-filling), indicating that the metal sites interact strongly with water molecules.²¹¹ Similarly, the hydrophilic Al³⁺ sites in MIL-100(Al) can also exhibit a strong adsorption enthalpy (higher than 80 kJ mol⁻¹) similar to that of Fe³⁺ in MIL-100(Fe).²¹¹ The onset humidity for the pore filling step correlates with the accessibility of water to the hydrophilic (i.e., strong binding) sites within cavities, where the higher onset humidity indicates that the cavity walls can accommodate more adsorbed water.²³

The onset humidity for pore filling can be modified by tuning the metal clusters and organic linkers of the framework. For example, by changing the anions within the metal nodes of Ni₂X₂BTDD (X = Cl⁻, OH⁻, Br⁻, or F⁻) (Figure 10c), pore filling onset humidity can be varied from ~20% to 40% (Figure

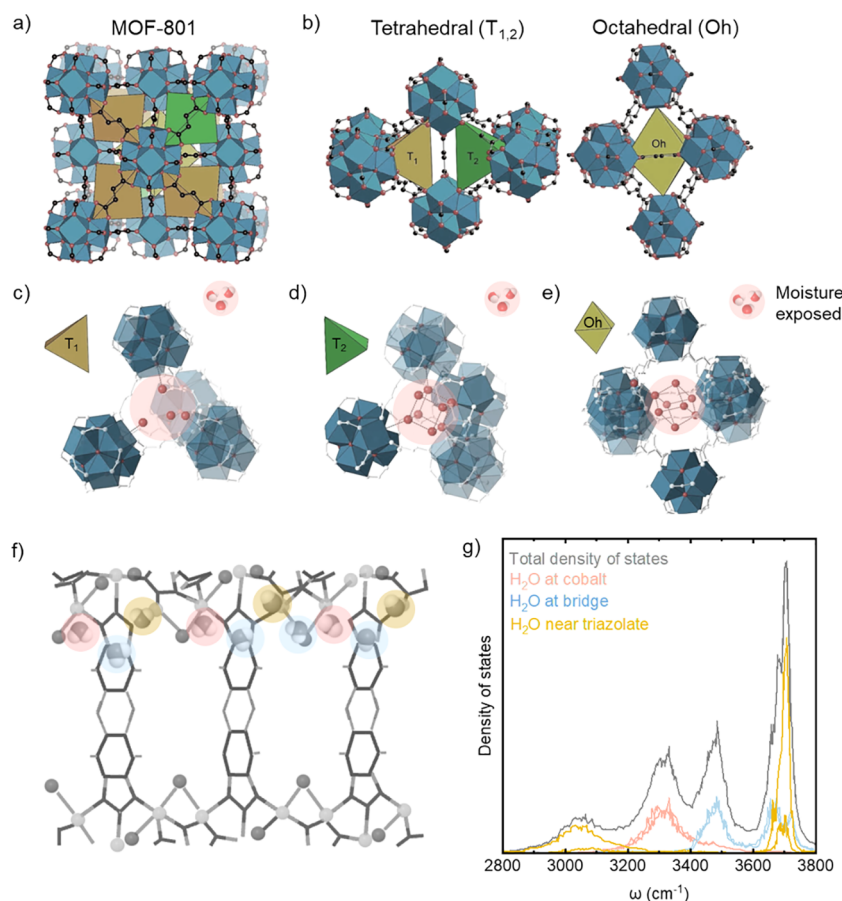


Figure 11. Water structures in Metal Organic Frameworks (MOF). The framework structure (a, b) and water clusters (c–e) formed within MOF-801 as determined by single-crystal XRD. (a) The structure of MOF-801 which contains (b) two tetrahedral cages and large central octahedral cages within MOF-801.²² (c) Stabilized water by $\mu_3\text{-OH}$ sites in the SBUs within a tetrahedral cavity. (d) The cubane structure of water which forms in tetrahedral cavities at low water uptake. (e) The cubane-like structure formed in octahedral cavities only at high water uptake. Due to the unique cavity geometries and interactions with the SBUs, water is able to adopt a rarely seen cubic structure within the MOF. The locations of water clusters are indicated in pink.²² Panels a–e are adapted with permission from ref 22. Copyright 2014 American Chemical Society. (f) The proposed structure of water molecules and (g) density of states of their corresponding theoretical IR spectra obtained from MD simulations in $\text{Co}_2\text{Cl}_2\text{BTDD}$.²⁰⁹ The different highlight colors designate water molecules with different bound identities: pink are water molecules bound to Co^{2+} sites, blue are water molecules bound to triazolate groups, and yellow are bridging water molecules unbound to the framework.²⁰⁹ Panels f and g are adapted with permission from ref 209. Copyright 2019 open access article distributed under CC BY License 4.0.

10d), with the OH^- based materials showing the highest onset of pore filling and Br^- based material showing the lowest.²¹⁰ Surprisingly, more hydrophilic bridging anions within the metal nodes, such as F^- or OH^- compared to Cl^- , had little effect on the water uptake profile of these materials. Rather, the water uptake profile seems to be more dependent on the pore diameter and degree of unsaturated hydrogen bonds within the pore (i.e., rigidity of hydrogen bonding network), which was evidenced by $\text{Ni}_2\text{Br}_2\text{BTDD}$ showing a hydrogen bonding network that is half-liquid-like and half-ice-like at a lower relative humidity ($\sim 15\%$) than those for the other analogues ($\sim 25\%$). On the other hand, incorporating hydrophilic Co^{2+} in MFU-4l (Zn) via cation exchange can decrease the pore-filling onset humidity from 60% to 30% due to increasing the number of sites where water molecules tend to bind and initiate water clustering.²¹² Moreover, using progressively elongated ligands, the pore-filling onset humidity increased from 5% to 40% while the total water uptake increased from 0.4 to 0.9 $\text{g}_{\text{water}}/\text{g}_{\text{MOFs}}$.²¹³

3.3.2. Characterization of H-Bonding Structures of Pure Water in Cavities.

Single-crystal X-ray diffraction, IR spectroscopy and MD simulation have been used to study the

structure of water within cavities. Using single-crystal X-ray diffraction, Yaghi and co-workers have studied the structure of water within the cavities of MOF-801 (Figure 11a),²² a Zr-based MOF that has been well-studied as a water adsorbent,²¹⁴ and found that the water within the MOF adopted different structures and occupancies based on the size and geometry of the cavity (e.g., tetrahedral vs octahedral cavity shape, as shown in Figure 11b).²² For instance, at low relative water uptake, the octahedral cavities remained empty while within tetrahedral cavities water molecules were found to adopt a rarely seen cubane structure (Figure 11c–d), where $\mu_3\text{-OH}$ sites within the structural building units (SBUs) provide the hydrogen bonds necessary to stabilize the structure. On the other hand, at high water uptake, the water molecules in octahedral cavities also exhibited a cubic-like structure (Figure 11e), but initiated instead by the hydrogen bonds between water molecules, whereas some tetrahedral pores showed defected cubane structures, where one atom is missing.²² Temperature-dependent powder X-ray diffraction has been used to monitor the change of water structures with heating, which acts as a proxy for the temperature swing of water

adsorption cycling.²¹⁵ Water molecules at different binding sites (adsorbed on metal sites or H-bonded) have different desorption temperatures, resulting in the change of water cluster structures upon heating.²¹⁵ While the occupancy of hydrogen-bonded water clusters in the channel (O5–O8) gradually decreases from 303 to 393 K, the coordinating water on the Co²⁺ sites only starts to desorb at 378 K (Figure S7),²¹⁵ as also indicated by the adsorption isotherms. Moreover, one recent study acquired IR spectra of Co₂Cl₂BTDD (pore size: 2.3 nm) under different relative humidities (Figure 11f–g).²⁰⁹ At low humidities, water exists as 1D chains of hydrogen-bonded water molecules in three distinct configurations: water bound to open Co²⁺ sites, water bound to triazolate groups, and water unbound to the framework but instead acting as a bridging water molecule, as indicated by the pink, blue and yellow colors (Figure 11f–g), respectively. At high humidities, the configurations change into the characteristic hydrogen-bonded networks at high humidities during pore filling.²⁰⁹ Such a change is further confirmed by MD simulations as the water molecules initially coordinated with Co at a H₂O/Co ratio of 1 form 1D chains bridging multiple cobalt sites when the H₂O/Co ratio is increased to 4. When the H₂O/Co ratio is further increased to 11, a complete hydrogen-bonded network characteristic for water is formed.²⁰⁹ As such, the structure of water within MOFs is dictated largely by the cavity size and geometry, the affinity of metal sites to bind water molecules, and the relative water uptake.

The physical characteristics and chemical properties of water in the pores of zeolites can be tailored by the microporous topology and the chemical nature of hydrophilic sites in pores.²⁰ In the all-silica zeolite, MFI has been commonly adopted to serve as a model system for studying water adsorption. For example, through microcalorimetry of all-silica MFI, where there is an absence of Bronsted or Lewis acid sites, the water absorption strength ranges from ~44–50 kJ mol⁻¹ at any pressure greater than 0.5 Torr, similar to the typical binding energies of water in most MOFs. Only in vacuum does the adsorption energy of water significantly increase, reaching nearly 160 kJ mol⁻¹. Furthermore, MD simulations have shown that water molecules in MFI are arranged in long-range, 1-D extended H-bonding chains, significantly departing from the typical tetrahedral arrangement of water molecules,²⁴ as shown in Figure 12a. The confinement can also shorten the lifetime of H-bonds and increase the frequency of H-bonding fluctuations compared with those of bulk due to the restriction in the reorientation for individual water switching H-bonded neighbors (Figure 12b).

Incorporating defects in the pores of zeolites can increase their hydrophilicity.^{20,21} For example, the Si-Beta framework is a relatively hydrophobic zeolite, where immediate transitions occur from isolated chains to pore-filling water networks at high water chemical potentials.²¹ However, incorporation of Sn within the framework or creation of a hydrated Si site (i.e., silanol nest with four hydroxyl groups) has been shown to stabilize the confined water due to the increased hydrophilicity of the defects relative to the defect-free sites.^{21,39} In addition, different behaviors of water accumulating around defects of Sn and Si have been observed, where Sn defects tend to localize water clusters via H-bonding interaction, which results in decreased water entropy.²¹ On the other hand, Si defects cannot nucleate the water clusters since the OH moieties in silanol nests prefer to be H-bonded with each other, leading to the tendency to stabilize delocalized water molecules instead of

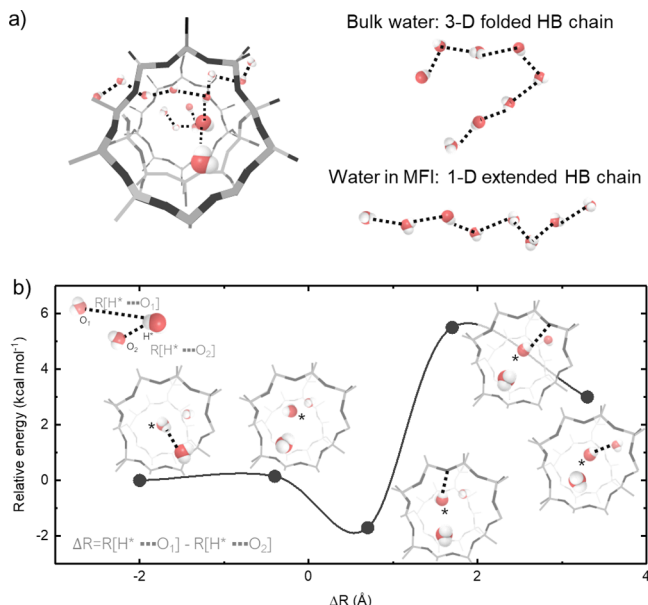


Figure 12. Water structure in zeolites. (a) Snapshots of water confined in the pore of zeolite (MFI).²⁴ In bulk water, a vast amount of structures can be observed, such as the representative 3D folded chain. However, in MFI an extended 1D HB chain can be observed that is not typically found in bulk water. (b) The calculated energy barrier for water rotating in the pore of zeolites, indicating the rotation is inhibited. Due to the reaction barrier of ~8 kcal mol⁻¹, water does not favor switching H-bonded neighbors. In fact, the most favorable configuration is when the water interacts more strongly with the MFI cavity walls than adjacent water molecules. H-bonds are designated by dashed lines.²⁴ Adapted with permission from ref 24. Copyright 2017 American Chemical Society.

high-density clustered water.²¹ Moreover, greater hydrophilic Al³⁺ sites in aluminosilicate zeolites have been shown to increase the water adsorption with increasing Al³⁺ site density, with the trade-off that water clusters tend to be smaller in size.²¹⁶ Furthermore, incorporating ions such as Li⁺, Na⁺, and Mg²⁺ in zeolites can also increase the adsorbed water content, where the formation of water hexamers induced by Na⁺ has been observed by neutron scattering studies.²¹⁷ Therefore, the number and density of hydrophilic defects such as hydroxyl moieties (SiOH), silanol nests (SiOH)₄, and local defect functionalization (e.g., Al³⁺, Na⁺ substitution) can be used effectively to control the framework's hydrophilicity (i.e., water uptake) and structure of water clusters within zeolite pores.^{21,39}

Protonated water in acidic zeolites like aluminosilicates can have different structures from water molecules found in zeolites without acidic sites. The structure of small water clusters (2–9 waters) around the Brønsted acid sites in zeolites has been reported from neutron scattering,²¹⁸ H NMR,¹³⁴ and ab initio MD measurements.^{218–221} The proton can transfer from acidic sites to water clusters,²¹⁸ where at least two water molecules are required to stabilize each hydronium molecule,²²⁰ consistent with previous Al NMR measurements²²² that reveal that each acid site requires three water molecules to assist proton transfer.^{70,222} When the water content increases to eight water molecules per pore, the molecules can organize a strong hydrogen bonding network around the hydronium molecule, which has been suggested to be sensitive to their entropic contribution to the free energy.⁷⁰ Beyond the structure of protonated water clusters, the dynamic picture of

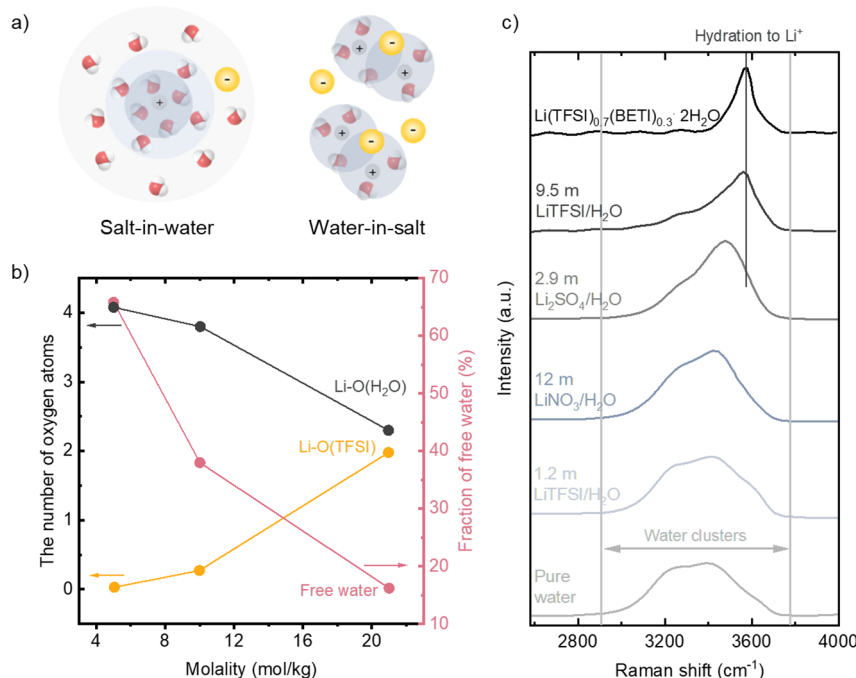


Figure 13. Solvation structure of water-in-salt electrolytes. (a) Schematic of dilute (left) and highly concentrated (right) regimes of water and salt systems, where LiTFSI in water is used as an example. In the dilute regime water solvates Li⁺ cations in the primary solvation sheath, while in the concentrated water-in-salt regime anions can populate the primary solvation sheath of Li⁺.²²⁵ (b) Number of oxygen atoms coordinated to Li⁺ cation (left axis) and fraction of free water (right axis) as a function of ion concentration according to MD simulations for Li⁺TFSI⁻ in water, covering the dilute regime (<5 mol kg⁻¹ or Li⁺:H₂O ratio of 1:12) and concentrated regime (20 mol kg⁻¹ or Li⁺:H₂O of 1:2.8).²²⁵ Panels a and b are reproduced with permission from ref 225. Copyright 2015 AAAS. (c) Raman spectra in the OH-stretching region of pure water, saturated Li₂SO₄ in water (2.9 mol kg⁻¹), saturated LiNO₃ in water (12 mol kg⁻¹), and LiTFSI in water with increasing concentration toward the Li(TFSI)_{0.7}(BETI)_{0.3}·2H₂O hydrate melt.²²⁴ The broad bands bounded by gray lines indicate water clusters in various H-bonding environments. The high wavenumber at 3565 cm⁻¹ indicated by the black line represents the isolated water around Li⁺ cation that is not hydrogen-bonded, most pronounced in the hydrate melt system.²²⁴ Adapted with permission from ref 224. Copyright 2016 Springer Nature.

proton shuttling along a water chain confined in zeolites has been demonstrated by AIMD.²²³

In the context of electrocatalytic applications, the confinement of water molecules in 3D confinement *in the presence of* electrolyte cations and anions will need to be investigated. Techniques such as X-ray diffraction, ultrafast IR spectroscopy and MD simulations to characterize the MOF and zeolite structures of pure water described above can be applied to study the structure and dynamics of solvated ions in the 3D structures.

3.4. Water Molecules Confined by High Concentration Ions and/or Solvents

The electric fields around ions in water solutions lead to the formation of hydration shells whose hydrogen bonding structures and properties are dictated by the structure-making and breaking cations (see Section 2.2). In all cases described until now, the concentrations of ions are generally dilute (<0.1 M range, corresponding to >550 water molecules per ion), where enough water molecules are able to fully screen the electrostatic interactions of ions, and pure bulk water domains can exist in between ion-affected domains. As we increase the salt concentration, to the limit where hydration shells are no longer independent and can overlap, ion pairing can occur and pure water domains will be suppressed as water molecules are strongly confined by the abundant ions.^{224–226} Based on THz-FTIR spectroscopy, the effective number of water molecules in the hydration shell, defined as the number of water molecules which possess subpicosecond H-bond dynamics and results in

a THz adsorption spectrum differing from that of bulk water, has been estimated to be between 2 and 30 water molecules per ion depending on the identity of the salt, corresponding to a concentration of >~2M.²²⁷ We note that this is a situation where significant overlaps of at least the second hydration shell can be expected.²²⁷ The strong water confinement by abundant ions results in significant deviations in the structure, energetics and retarded dynamics compared to pure water and can provide significant opportunities for tuning rates of (electro)catalytic reactions.

In this section, we discuss the properties of water confined by high-concentration salts (called water-in-salt electrolytes, Section 3.4.1) and water confined by aprotic solvents (Section 3.4.2).

3.4.1. Water-in-Salt Electrolytes. “Water-in-salt” electrolytes (Figure 13a) that can engender distinct structural and physiochemical properties to the water are of significant interest particularly in the aqueous battery communities, as they allow for an extended electrochemical stability window of >3 V (compared to that of bulk liquid water at 1.23 V), which has been correlated to the distinct structure of confined water.^{225,226,228} Suo and co-workers have investigated the change in cation–water and cation–anion interactions as a function of LiTFSI concentration using molecular dynamics simulations (Figure 13b).²²⁵ In the dilute regime (<5 mol_{salt} kg⁻¹_{water}, or Li:H₂O ratio of below 1:11.2), each Li⁺ remains well-hydrated with Li⁺-O(H₂O) coordination number >4 (Figure 13b, black) as well as a large fraction of free bulk liquid-like water available (Figure 13b, red). In contrast, above

20 mol kg⁻¹ (Li:H₂O ratio of 1:2.80 or higher) an average of two anions populate the primary solvation sheath of Li⁺ (Figure 13b, yellow) with a significant decrease in the fraction of free water.²²⁹ Interestingly, free water population is still found to exist despite the insufficient average number of water molecules to fully solvate Li⁺ ion. The nanoscale heterogeneity in the water structure with highly concentrated Li⁺ salt electrolyte has been observed experimentally using small-angle neutron scattering,²²⁹ which reveals the existence of two solvation structures: Li⁺(H₂O)₄, where Li⁺ is fully surrounded by water, and the anion-rich solvation, where Li⁺TFSI⁻_x(H₂O)_{4-x} exists with $x > 1$.²²⁹ The formation of an anion-rich solvation environment around the cation has also been characterized in other alkali metal (such as Na⁺²³⁰ and K⁺²³¹) and multivalent cations (Zn²⁺²³² and Al³⁺²³³) water-in-salt electrolytes, but the retention of a water-rich domain around Li⁺ may be unique to Li (or small cations) due to its strong water hydration enthalpy and structure-making entropy (see Section 2.2).

Raman spectroscopy in the OH-bending regime (2900–3700 cm⁻¹) has been employed to elucidate the water bonding environment of water-in-salt electrolytes, as shown in Figure 13c. For bulk liquid water (without any ions), the O–H stretching corresponds to a broad Raman band which can be attributed to the different possible molecular environments which are indicative of the dynamic fluctuations of water.²³⁴ The Raman spectra of saturated Li₂SO₄ (2.9 mol kg⁻¹) and LiNO₃ (12 mol kg⁻¹) solutions also show a similarly broad Raman band,²²⁴ although with a more pronounced intensity at ~3400 cm⁻¹ likely due to the increased population of asymmetric H-bonded water (where water molecules are H-bonded to one other water).¹⁷⁴ Changing the anion to TFSI⁻ leads to the emergence of a high wavenumber peak at 3565–3580 cm⁻¹,²²⁴ which can be attributed to isolated water population¹⁷⁴ (where a water molecule exhibits no hydrogen bonding with other water molecules), which becomes more pronounced in the saturation limit for LiTFSI in water and, in the most extreme case, the Li(TFSI)_{0.7}(BETI)_{0.3}·2H₂O (Figure 13c, black) and other hydrate melts.^{231,235,236} The origin of the extended anodic potential stability of water-in-salt electrolytes has been attributed to the lowered highest occupied molecular orbital (HOMO) level in concentrated electrolytes, in which all water molecules were coordinated with Li⁺. When coordinated with Li⁺ (a Lewis acid), a water molecule donates its electron from the lone pair of the oxygen atom to the Li⁺, which lowers its HOMO level and thus raises its oxidation potential,²³⁶ which was supported by ab initio molecular orbital calculations.²³⁷ These observations demonstrate the ability of confinement by salts at high concentrations to alter the thermodynamic properties and the activity of water.

Beyond the cations discussed above, protons can also have a distinct effect on the water structure around them, which has a hydration energy of -11.5 eV,²³⁸ allowing the binding of waters in the first solvation shell through the covalent bond and the strong hydrogen bond. In high concentration protons, although the bonding between proton and water is much stronger than that of cations, the proton is not fixed by surrounding water molecules and can form stable ion–water clusters due to the extremely high mobility of protons via the water network by the Grotthuss mechanism.²³⁹ The rapid proton transfer occurring spontaneously results in a short life of individual proton-water clusters. Therefore, revealing the specific structure of H-bonds for accommodating protons in

complex water networks is challenging but essential to understand proton transfer. Due to the rapid developments in vibrational spectroscopy, particularly when equipped with an ultrafast pump–probe at femtosecond resolution and mass spectroscopy capabilities, the molecular-level picture of proton transfer via H-bond has become clearer.¹¹ Researchers have found that the proton accommodation in water is mainly present in two forms: (1) the Zundel form (H₂O···H⁺···OH₂) with a localized charge on the proton at the midpoint of the hydrogen bond and (2) the Eigen form (H₃O⁺···2(H₂O)) with more delocalized charge in the cluster (Figure 14a). Recently,

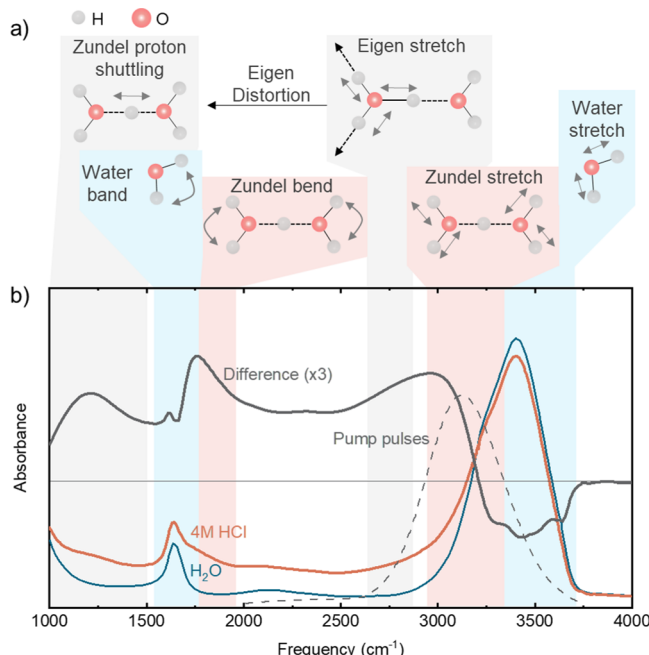


Figure 14. Spectroscopic characterization of water in solutions. (a) Schematics of vibrations of the solvated proton, i.e. the Zundel and Eigen forms. (b) Infrared spectra for water (blue trace) and 4 M HCl (red trace) obtained by Thämer et al.¹¹ The black solid trace indicates the difference spectrum between the two, whereas the horizontal dashed line is the zero line for it. The vibration of the excess proton is shaded in green, the one of bulk water in blue and the one of flanking water molecules in red. The dashed trace represents the spectrum of the pump pulses used in the ultrafast two-dimensional IR spectroscopy experiments which identify the presence of different solvation structures of the excess proton in HCl solutions and follow their evolution on the femtosecond time scale. The center frequency of 3150 cm⁻¹ is tuned to the red side of the O–H stretching band to preferentially excite strongly hydrogen-bonded water species that participate in proton hydration.¹⁹⁹ Reproduced with permission from ref 11. Copyright 2015 AAAS.

Thämer et al. have observed a large population of Zundel-type water clusters in 4 M HCl aqueous solution by ultrafast two-dimensional infrared (2D IR) spectroscopy (Figure 14b).¹¹ The time-dependent shifts of the stretch–bend cross peak of the Zundel cation reveal the kinetic process of proton transfer, which indicates that the persistence time of the long-range proton transfer event via the Zundel configuration is >480 fs.¹¹ In addition, the detailed H-bonding structure for proton transfer has been revealed with Eigen-type heavy water clusters (D₃O⁺···2(D₂O)).²⁴⁰ By changing the proton acceptor in the second solvation shell of the Eigen-type heavy water cluster at low temperature (~20 K) with molecules having increased

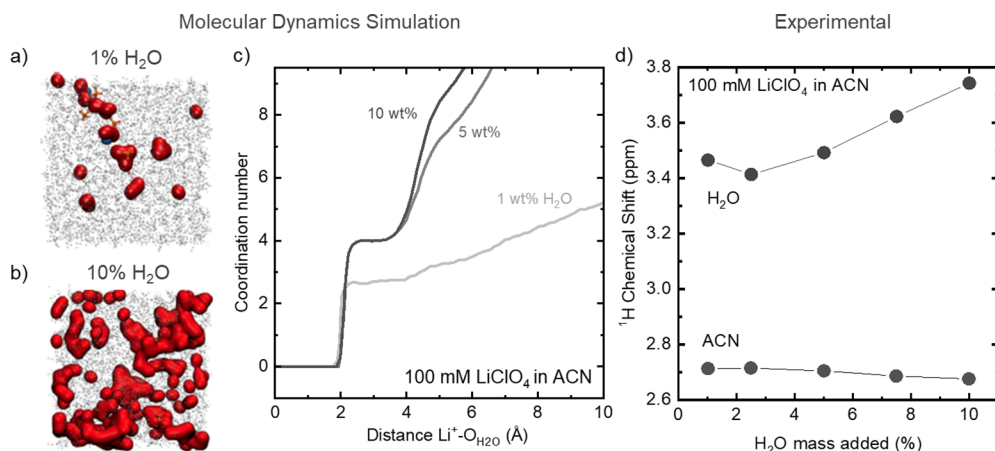


Figure 15. Water structure in water-in-solvent electrolytes. (a) Snapshots of 1% (0.420 M) and (b) 10% water by mass (3.95 M) in the presence of 100 mM LiClO₄ in acetonitrile from MD simulations. Water, Li⁺ and acetonitrile are colored red, blue and gray, respectively. Even at low water concentration, water clusters attached to Li⁺ are forming.²⁵⁷ (c) Li-O(H₂O) coordination number from the MD simulations shown in panels a and b, where lines correspond to 1, 5, and 10 wt % respectively. Even at low water concentration, a pronounced water solvation is observed in the primary solvation shell of Li⁺.²⁵⁷ (d) ¹H NMR characterization of water-in-acetonitrile electrolyte containing 100 mM LiClO₄, where the U-shaped trend of water is consistent with heterogeneous water structure consisting of shielded water (water-cation and water-water) and unshielded water (free water in solvent) populations.²⁵⁷ Adapted with permission from ref 257. Copyright 2020 Springer Nature.

proton affinities (D₂, N₂, CO, and D₂O),²⁴⁰ the structure of the Eigen cation could be distorted and the deuterium was incrementally pulled closer to the solvated water molecule, which is probed by vibrational spectroscopies showing proton transfer at collective reaction coordinates.²⁴⁰ Moreover, to probe the water structure in the second solvation shell of protons, the infrared spectra of protonated water clusters H⁺ (H₂O)_n (*n* > 5) in the gas phase, size-selected via mass spectrometry, have been studied^{241–244} as a model system for understanding the H-bonding network around protons in liquid.^{245–248} Both Eigen and Zundel ion cores have been observed in the protonated water cluster of H⁺ (H₂O)_n (*n* = 5–11),^{241,243} where the three- and five-membered cyclic H-bonding structures have been identified by IR spectra combined with DFT simulation, which is different with the four- and six-membered structures observed in neutral water clusters of (H₂O)₆,^{241,243} revealing the effect on water structure originating from protons.²⁴¹ Employing tandem mass filter-type spectrometers, larger clusters of H⁺ (H₂O)_n (*n* = 4–27) have also been prepared and studied, showing the shift from the two dimensional network to the three dimensional cage when *n* > 21, where each molecule is located at the vertex of the polyhedral cages due to the tetrahedral coordination nature of the water.^{242,244} The formation of 3D cages requires such a large size (*n* > 21) because the core of Eigen and Zundel ions prefers planar coordination.²⁴² While distinct H-bonding structures around protons have been revealed in the gas phase, further development of ultrafast spectroscopy is needed to understand the dynamics of protons on water structures in liquids. In addition to IR spectroscopy, other techniques such as NMR^{249–252} and neutron scattering²⁵³ can be used to study the dynamics of confined water and its effect on proton transport kinetics.

3.4.2. Water-in-Solvent Electrolytes. When water is confined in organic solvents (without any ions), the hydrogen bonding structure can significantly deviate from the tetrahedrally oriented hydrogen bond network in liquid bulk. The nature by which the hydrogen bonding network is altered depends on the polarity of the diluting solvent. Lange and co-workers investigated the difference in hydrogen bonding

structure of water polar and nonpolar solvents.²⁵⁴ Using Oxygen K-edge X-ray absorption spectroscopy, the water spectrum of 1 vol % water in acetonitrile solution (1 water per 34 acetonitrile, suggesting that water is surrounded mostly by the solvent) differs greatly from that of bulk liquid water and resembles that of gas-phase water, where the pre- and main-edges of the mixture's spectrum correlate with the 4a₁ and 2b₂ orbital resonances of a free water molecule.^{254,255} The overall edge positions are still blue-shifted relative to those of gas molecules, as many water molecules can still form 2–3 strong hydrogen bonds in acetonitrile.²⁵⁴ Such spectral change is similar to the effect of the increasing temperature of liquid water, where an increase in the broken hydrogen-bond donor sites and a decrease in long-range tetrahedral order is correlated with higher temperature from 1.5 to 39 °C.^{255,256} In contrast, water confined in nonpolar/hydrophobic solvents such as benzene and chloroform exhibits spectral characteristics resembling those of ice, indicative of strong water aggregation in hydrophobic solvents, or in the case of benzene, a clathrate-like structure containing C₆H₆-(H₂O)_n clusters.²⁵⁴

The formation of water aggregates/domains in organic solvents in the presence of salts has also been studied at a charged interface where an electrochemical reaction occurs and can be triggered not only by increasing water concentration but also by adding ions in the electrolyte. The work by Dubouis and co-workers revealed the role of structure-making cations in creating water nanodomains in acetonitrile containing 1–10 wt % water (0.42–3.95 M) and 100 mM LiClO₄ using molecular dynamic simulations and Nuclear Magnetic Resonance Spectroscopy²⁵⁷ (Figure 15). From classical Molecular Dynamics (MD), water molecules are found to preferentially coordinate to Li⁺ (Figure 15a), as evidenced by the higher Li⁺-H₂O coordination number at the low water content (1% by mass) (Figure 15c), where the energy required to extract a water molecule from the Li⁺ solvation shell (~200 meV) is larger than the energy required to separate two water molecules (~80 meV).²⁵⁷ As a result of the strong Li-H₂O interaction, increasing the water concentration to an intermediate value leads to only more free water in the electrolyte while a further increase leads to the

formation of larger water aggregates. Such an explanation is consistent with the U-shaped trend in the ^1H NMR spectra²⁵⁷ in Figure 15d, which probes the average chemical environment of protons in water and enables the distinction between free water in solvent (unshielded environment) and water–cation or water–water coordination (shielded environment). The formation of these water-rich domains in water-in-solvent electrolyte despite the insufficient number of water on average relative to $\text{Li}^+\text{H}_2\text{O}$ coordination of 4 or 5²²⁴ can be contrasted with hydrophobic cations such as TBA^+ (where such preferential water-rich domain formation is absent)²⁵⁷ and resembles the observation in the water-in-salt case²²⁹ described above, owing to the structure-making property of the Li^+ cation. Moreover, increasing the salt concentration from 100 mM to 1 M at 10% water is found to enlarge the size of water-rich domains rather than the number of domains.²²⁹ Such behavior of larger nanoscale water domain formations in bulk has been found to translate into that at the electrified interface based on MD simulations and correlates with higher water reduction kinetics for water-in-solvent electrolyte,^{257,258} where for instance the hydrogen bond network can promote channels for fast proton transport such as via the Grotthuss mechanism.

In this section, we have seen how 1D, 2D, and 3D structures as well as water confinement by ions can provide a practical approach for tuning water structure in catalytic and electrocatalytic systems, where the variation in local water structure can regulate the thermodynamic and dielectric properties. In Section 4, we attempt to draw the relationship between confined water structure and its influence on parameters governing kinetics of chemical reactions.

4. TUNING REACTION RATES WITH CONFINED WATER

According to transition state theory for reaction kinetics, the rate of an elementary chemical reaction can be expressed in eq 11 following the Eyring equation, where the reactants are assumed to be in quasi-equilibrium with the activated transition state complexes:

$$k = \frac{\kappa k_B T}{h} \exp\left(-\frac{\Delta G^\ddagger}{RT}\right) = \frac{\kappa k_B T}{h} \exp\left(\frac{\Delta S^\ddagger}{R}\right) \exp\left(-\frac{\Delta H^\ddagger}{RT}\right) \quad (11)$$

where k is the rate constant of an elementary reaction, k_B the Boltzmann constant, κ the transmission coefficient, and ΔG^\ddagger the Gibbs energy of activation, which can be expressed in terms of the enthalpy and entropy of activation, $\Delta G^\ddagger = \Delta H^\ddagger - T\Delta S^\ddagger$. The expression can be paralleled with the Arrhenius equation $k = A \exp\left(-\frac{E_a}{RT}\right)$, where E_a is the activation energy and A the prefactor. Comparison with eq 11 shows that the activation energy E_a corresponds to the enthalpy of activation ΔH^\ddagger , while the Arrhenius prefactor A is dictated by the entropy of activation through $\exp\left(\frac{\Delta S^\ddagger}{R}\right)$ as well as the frequency of effective collisions $\frac{\kappa k_B T}{h}$. The latter would be affected by a multitude of factors, such as partial orders with respect to reactant concentrations^{259,260} (e.g., surface sites, adsorbate coverage, species availability such as protons in proton-relevant electrochemical steps, etc.) and individual and collective lattice vibrations²⁶¹ (e.g., nature of the catalyst surface). Proton transfer-relevant electrocatalytic processes can contribute to the pre-exponential factor,²⁶² such as proton

tunnelling in proton transfer-relevant electrocatalytic processes (i.e., by changing the proton availability).²⁶² However, they are not the only factor and their occurrence still remains debated. Other effects which are more generally inscribed in ΔS^\ddagger might dominate in the measured pre-exponential factor.

In the next sections, we will discuss ways in which water confinement can impact reaction rates, with an emphasis on electrochemical reactions. Section 4.1. discusses the role of confined electrolytes and their influence on the enthalpic and entropic components of the activation barrier (ΔG^\ddagger , the extent of which will be evaluated in relation to the rate-determining steps. Section 4.2 discusses the electron transfers in influencing reaction rates in the framework of Marcus theory through altering the reorganization energy. Section 4.3. discusses changes in the pre-exponential factor by tuning proton transfer kinetics.

4.1. Tuning the Enthalpy and Entropy of Activation via Confined Water

The hydrogen bonding network at the electrified interface can influence the thermodynamics of the redox species (such as half-cell reaction entropy) and reaction barrier (i.e., activation entropy) of outer- and inner-sphere reactions (e.g., proton transfer barrier from proton donor like water molecules to proton acceptor like reaction intermediates on the electrode surface), which can be modified by cations, anions, concentrations, electrode surfaces and the potential as well as confinement of water and ions. The relationship between the thermodynamic properties of water molecules and electrolytes in bulk to the activation barrier of the reaction rates can be bridged by invoking the free energy relation, which connects the thermodynamic barrier to the kinetic barrier.²⁶³ In catalytic kinetics, the enthalpy and entropy of the transition state can be regulated by the thermodynamics of water under confinement in the local reaction environment. For instance, the water structure is well modified by the confinement of enzymes, where the entropies of the transition state and the catalytic kinetics are distinct from those that occurred in bulk water (Figure 16).^{19,70} Specifically, water molecules are frozen in the preorganized hydrogen bond network in the peptidyl trans-

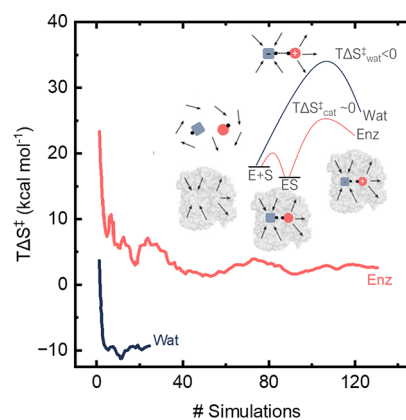


Figure 16. The transition entropy tuned by enzymes. Calculated $T\Delta S^\ddagger$ penalty for the concerted hydrolytic cytidine deamination in enzyme (blue) and water (red),²⁶⁴ where the enzyme-catalyzed reaction has a lower penalty. When solvent reorganization dominates the entropy loss in water, the enzymes can eliminate the penalty by reorganizing the solvent structure around active sites^{19,264} (see inset schematic).¹⁹ Adapted with permission from ref 19. Copyright 2017 American Chemical Society.

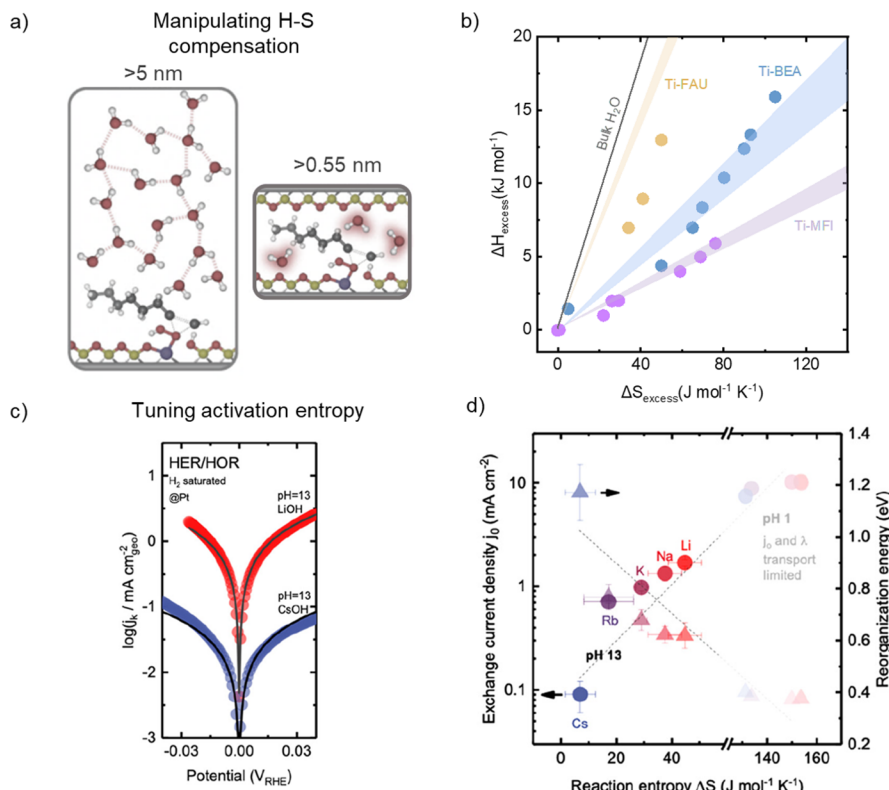


Figure 17. Confined water for tuning reaction barriers. (a) Schematic of C₈H₁₆ epoxidation solvated with various confined water structures in pores of different sizes.³⁸ (b) The enthalpy–entropy compensation relationship of confined water dependent on the size of pores in zeolites, which results in distinct catalytic kinetics.³⁸ Panels a and b are adapted with permission from ref 38. Copyright 2021 Springer Nature. (c) Effect of alkali metal cations on reaction kinetics for HER/HOR on polycrystalline Pt in alkaline electrolyte. (d) Correlation between exchange current densities and reorganization energy (extracted from the MHC theory) on the reaction entropy. Panels c and d are adapted with permission from ref 33. Copyright 2021 American Chemical Society.

ferase center of the ribosome, which can minimize the reorientation of solvent during the peptide bond formation reaction.⁶⁵ Due to this confinement, near-zero activation entropy has been observed via temperature dependent experiments for peptide bond formation in RNA catalyzed by ribosome, even though the activation energy (E_a) of the enzyme-catalyzed reaction is $\sim 18 \text{ kJ mol}^{-1}$ higher than that of the corresponding reaction in bulk water. The acceleration in reaction rates catalyzed by the enzyme is attributed to the more negative value of the activation entropy.⁶⁴

Reaction rates can be influenced by the free energy of the reaction intermediates, which can be tuned by the water confinements engendered by the pores in MOF and zeolites. Bregante et al. have reported that the most hydrophilic Ti-BEAs give epoxidation turnover rates in excess of 100 times larger than those of the defect-free zeolites, while rates of decomposition of H₂O₂ are similar for all silanol nest densities.⁴⁰ These catalytic differences are not due to electronic structure changes of Ti-OOH intermediates but instead result from favorable entropy gains for epoxidation transition states produced by the disruption of hydrogen-bonded water clusters anchored to silanol nests near active sites, which decrease the reaction barrier and facilitate increased reaction rates.³⁴ Moreover, different structures of confined water in FAU, BEA, MFI and CDO zeolites can tune the reaction kinetics.³⁸ They have found that the water molecules can coalesce into confined 1D chains as pore dimension decreases from 1.3 to 0.45 nm, while the water structure within the 1.3 nm pore of FAU zeolites is similar to that of the bulk water (>5 nm)

(Figure 17a). The enthalpy–entropy (H – S) compensation relationships can be regulated when the confined water structure is altered in pores (Figure 17b), which can decrease the enthalpy penalty of alkene epoxidation with increasing entropy during the reaction process (low slope in the H – S compensation relationships, Figure 17b)⁴⁰ and accelerate the reaction rate by >400 times, consequently.

Noncovalent interactions between water molecules and ions in the electrolyte and reaction intermediates at the electrified interface (such as proton donors and proton acceptors in the reactions limited by PCET) can influence the entropy of activation and consequently the reaction rates, particularly where both reactant dissociation and proton transfers are involved in the rate-limiting step of the reaction. Considering HER/HOR on the Pt surface, which can spontaneously dissociate H and involves H⁺/OH[−] transfer in the RDS, the pH and cation-dependent reaction kinetics appear to be strongly manifested in the activation entropy term. The exchange current densities of HER/HOR for Pt in acid (tested in a PEMFC-based hydrogen pump measurement to overcome the transport limitations of the extremely fast kinetics in acid^{265,266}) and alkaline electrolytes differ by ~ 3 orders of magnitude ($\sim 600 \text{ mA cm}^{-2}$ ^{265,266} in PEM vs $\sim 0.5\text{--}0.6 \text{ mA cm}^{-2}$ ²⁶⁷ in 0.1 M KOH @ 80 °C), even though the activation energy is similar ($\sim 0.25 \text{ eV}$ ²⁶⁵ and 0.29 eV,²⁶⁷ respectively). Similarly, Huang et al. have shown that by adopting water structure making cations in electrolytes, the reaction rate of HER on Pt can be increased in the order of (Li⁺ > Na⁺ > K⁺ > Rb⁺ > Cs⁺) (Figure 17c).³³ In that work, the

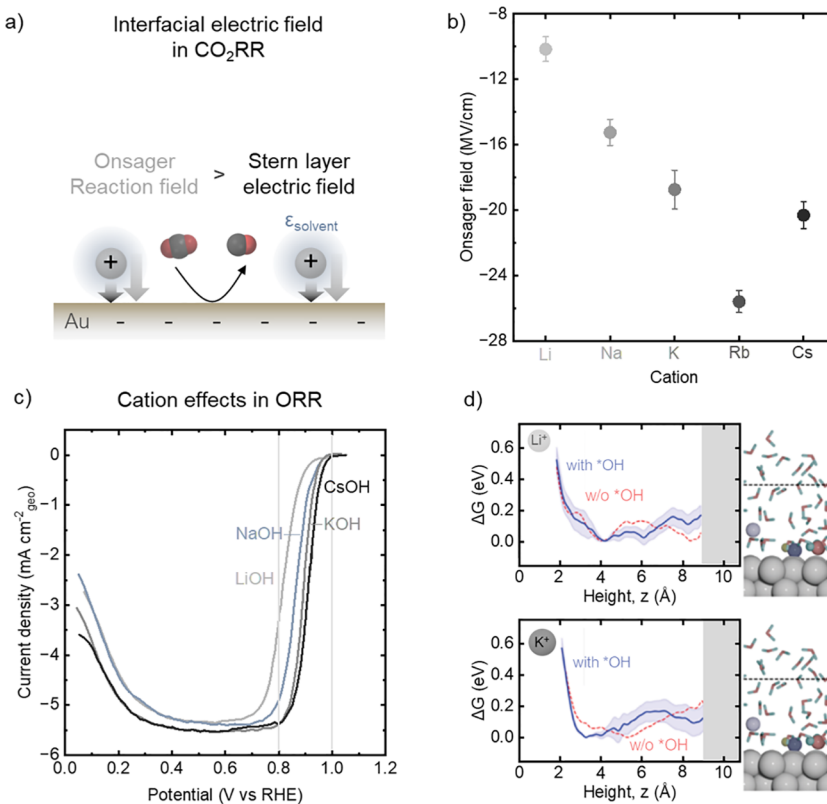


Figure 18. Cation effects on electrocatalysis of CO₂RR and ORR. (a) Schematic of interfacial electric field contributed from Stern field and the solvent-induced Onsager field.²⁷⁸ (b) The strength of the Onsager field was extracted from the CO frequency at the PZC with different ions, and the Onsager field induced by the different water arrangements in the ion's hydration shell dictates the activity and selectivity of CO₂ reduction (CO₂RR).²⁷⁸ Panels a and b are reproduced with permission from ref 278. Copyright 2022 American Chemical Society. (c) Polarization curves for the ORR on Pt(111) in electrolytes that contain various cations, exhibiting the effect of noncovalent interaction on ORR kinetics.²⁸⁷ Data is extracted from ref 287. (d) The adsorption–solvation free energy profile as a function of height above the Pt(111) surface calculated by metadynamics, showing that the confined water in the Li⁺ hydration shell can stabilize the OH intermediate while that of K⁺ tends to destabilize the OH intermediate.²⁸⁸ Reproduced with permission from ref 288. Copyright 2020 Royal Society of Chemistry.

cation-dependence of the HER/HOR reorganization energy on Pt (i.e., a measure of the free energy barrier) is strongly driven by changes in the activation entropy: the reorganization energies of Cs⁺ (~1 eV) and Li⁺ (~0.3 eV) alkaline electrolytes are strongly correlated with an increase in the reaction entropy (and invoking the linear free energy relationship to relate the thermodynamic reaction entropy to the kinetic barrier free energy, Figure 17d). Meanwhile, the *H adsorption energy which is interpreted from the peak potential position of the H/OH exchange in the hydrogen underpotential deposition (HUPD) is unchanged.^{33,268} We surmise that the electrolyte-dependent entropy of activation, which can be tuned via confinement strategies (i.e., via 1D, 2D, and 3D structures or with ions/solvent), can promote reaction rates in which the transfer of ions/protons contributes most significantly in the rate-determining step. One example to demonstrate this idea is the regulation of CO₂RR to methanol selectivity on a molecular catalyst which involves a proton-coupled electron transfer (PCET) in the rate-determining step (i.e., *CHO + H₂O + e⁻ → *CH₂O + OH⁻, RDS identified based on the consistent evidence of kinetic isotope experiments and DFT calculations).²⁶⁹ Smaller cations (Li⁺) possessing a strongly bound hydration shell with an interfacial hydrogen bonding network accelerate PCET kinetics for methanol production.²⁶⁹

The electrolyte-dependent HER/HOR reaction rates on Pt, driven predominantly by changes in the activation entropy, can be contrasted with nondissociative metal surfaces such as Hg having a positive hydrogen adsorption free energy as reported by Conway et al.^{270,271} The activation enthalpy and activation entropy for HER on Hg are shown to depend on the applied potential and the choice of protic electrolytes,²⁷¹ and E_a and log A are related in a compensation relationship.²⁷⁰ In this compensation relationship, the activation enthalpy for HER on Hg can vary significantly in aqueous electrolytes (between ~+1 and +2 eV), and similar observations in the electrolyte-dependent activation enthalpy and activation entropy have been noted on Ag and Au.^{272–274} On these weak-binding metal surfaces having positive hydrogen adsorption free energy, the RDS of HER/HOR may be related to the H₂ dissociation/association (e.g., Tafel step, 2*H_{ad} ↔ H₂₊ 2*) or undissociated reaction steps²⁷⁴ (Heyrovsky step, H₂ ↔ *H_{ad} + H⁺ + e⁻ in acid or H₂ + OH⁻ + * ↔ *H_{ad} + H₂O + e⁻ in base), and the free energy of activation (i.e., ~1 eV for Hg in acid) is dominated by the positive free energy of *H adsorption ($\Delta G_{\text{Had}} = +1.18$ eV for Hg, + 0.69 eV for Ag and +0.47 eV for Au).²⁷⁴ The compensation relationship between activation enthalpy and activation entropy has also been plotted for HER across 14 polycrystalline transition metal surfaces in acidic media,^{259,275} where the span of activation enthalpy values may be dictated by the range of H adsorption energies (i.e., metal–

H covalent interaction) across the transition metal surfaces investigated. Therefore, the electrolyte dependence may be manifested in the enthalpy and entropy of activation for reactions where the reaction rates are limited by both covalent interactions (e.g., reactant adsorption or bond making/breaking step) and noncovalent interactions (e.g., proton transfer rates as influenced by interfacial water/ion structures).^{259,275} The comparison of HER (and HOR on Pt) between Hg and Pt highlights different rate-determining steps, where the electrolyte design presents fruitful opportunities to control reaction kinetics.

Beyond HER/HOR, noncovalent interactions such as cation effects have been observed to influence the activity and selectivity of other electrocatalytic reactions such as CO₂RR, ORR and methanol oxidation reaction (MOR), which have been explained by different schools of thought. One school of thought attributes changes in the reaction kinetics to an enthalpic origin, whereby the interfacial water structures and the interfacial electric fields engendered by the cations can provide stabilization of the reaction intermediates adsorption energy.^{28,44} Chan et al. have systematically studied the electric field effect on CO₂RR (Figure 18a-b),^{28,42,44,276} showing that the induced electric field can stabilize or destabilize the intermediates with different dipole moments and, consequently, steer the barrier for different pathways. Specifically, the adsorption of energy of *CO₂, *OC₂O and *OC₂OH decreases with increasing strength of local electric field, which enhances the CO₂RR selectivity toward HCOOH, C₂H₄ and C₂H₅OH.⁴⁴ Such learning has been further examined in the study by Baker et al., which shows that the electric field effect on CO₂RR originates from the Onsager reaction field^{114,277,278} (from the dipole moment of solvent molecules surrounding the cations) but not from the Stern field^{279–281} (electric field present between finite-sized cations at the closest-distance approach and the electrode surface, Figure 18a), indicating the importance of the cation-dependent interfacial water structure (Figure 18b).²⁷⁸ Moreover, the enthalpic effect can stem from the changes in the number of H-bond interactions with the reaction intermediate, which could be used to steer the selectivity of products such as in CO₂RR. For example, Li et al. have shown that the quaternary alkyl ammonium cations (such as methyl₄N⁺ and ethyl₄N⁺) can enhance the interaction between *CO and interfacial water, which can induce the formation of *CO dimer via water H-bonds and promote the production of ethylene.²⁸² Consistently, Banerjee et al. have found that the presence of CTAB on Cu can replace the hydrated cations, which suppresses the H-bonding interaction between interfacial water and *CO, resulting in lower production of ethylene (C₂H₄).²⁸³ However, these results could also be interpreted based on their entropic effects (see below), where for example the cation-dependent structure of the electric double layer could lead to changes in the activation entropy toward forming the transition state of the relevant rate-limiting step,²⁸⁴ such as in the case of water dissociation on bipolar membranes.^{284,285} Understanding and deconvoluting the enthalpic and entropic contributions of cation effects in electrocatalysis is an active research area which requires further studies.

The other school of thought relates the cation-dependent interfacial water structure to an entropic effect to the reaction barrier. For example, the work of Noh et al. showed that the potential-dependent reaction rates of CO₂RR to CO on Ag in acetonitrile in the presence of 1-ethyl-3-methylimidazolium

(EMIM⁺) cation occur through the bias-dependent activation entropy ($\log A$), while the enthalpy of activation (F_a) is near-zero, based on onset potential and temperature-dependent measurements.²⁸⁶ It is hypothesized that the higher entropy of activation (i.e., lower barrier) is attributed to the formation of an ordered structure of the EMIM⁺ cations with the applied bias, facilitating the electron transfer transition state.²⁸⁶ Similarly, entropy contributions in the intermediates adsorption processes have been considered to explain the cation-dependent reaction rates for ORR (Figure 18c) and methanol oxidation reaction (MOR) on Pt in base,²⁸⁷ as well as OER on RuO₂(110) in base, where reaction rates trend in the order of Cs⁺ > K⁺ > Na⁺ > Li⁺. Analyses of cation-*OH interactions in ORR on Pt via AIMD²⁸⁸ demonstrate that the free energy change of OH⁻ adsorption into *OH with different cations is dominated by the entropic component of adsorption free energy, which can be expected to translate into the activation entropy by invoking the linear free energy relationship. In this work, the internal energy of the Pt/water interface due to *OH interaction the solvation shell of Li⁺ and K⁺ stabilizes by -0.3 eV and -0.4 eV, respectively, while the free energy in the presence of Li⁺ and K⁺ changes only by -0.1 eV and +0.1 eV, respectively (Figure 18d),²⁸⁸ suggesting that the destabilization of intermediates via noncovalent interactions is due to the change in the adsorption entropy. Overall, considering the different possible origins of electrolyte effects on electrocatalytic reaction rates and selectivity, the development of simulation methods and in situ characterization techniques should be pursued to further elucidate the mechanistic details. Nevertheless, these studies highlight the key role of the interfacial water structure and the opportunity to use water confinement strategies to tune reaction rates.^{270,271}

In summary, the modified water network under confinement can help to tune the enthalpy and entropy of reaction intermediates and the enthalpy and entropy of activation, which provides opportunities to improve the activity and selectivity of (electro-)catalysis via water structure engineering. However, considering the energy of static states (reactants, intermediates and products) is insufficient for evaluating the energy cost for driving the reactions.²⁸⁹ Aside from the barrier changes originated from the free energy changes in the transition state, solvent dynamics is another essential factor to tune the reaction kinetics for the chemical reactions in liquids,^{289–292} which will be discussed in detail in the next section.

4.2. Tuning the Reorganization Process for Electrochemical Reaction Rates

4.2.1. Relating the Reorganization Process to Reaction Kinetics via the Marcus Theory.

Electrochemical reactions in aqueous solution generally involve electron transfer (ET) and proton transfer (PT). The charge separation during the reaction process induces the reorganization of solvent molecules around the redox center. Therefore, the kinetics of electrochemical reactions are sensitive to the local water structures. The quantitative correlation between the reorganization process and ET kinetics has been established by Marcus,^{230,231} where the driving force of an ET reaction can be altered by the applied potential of the electrode, but the reorganization energy, a measure of the free-energy penalty associated with the reactant/product and environmental rearrangements that accompany ET, is a key parameter dictating rate constants. Marcus theory has been applied to

Faradaic reaction kinetics, including interfacial ET on the metal surfaces,³⁷ lithium electrodeposition/stripping,²⁹³ lithium-ion intercalation at solid–solid interfaces^{294,295} and proton coupled electron transfer (PCET) reactions (e.g., H₂ evolution/oxidation (HER/HOR) on nickel-based molecular electrocatalyst²⁹⁶ and the reduction of water-superoxide ion complex on glassy carbon electrode²⁹⁷). The rate constant for ET between molecules is depicted in eq 12, which shows that the reaction kinetics is driven by electrochemical potential to overcome the energy penalty of solvent reorganization. Solvent dynamics across the charge transfer process in the framework of the Marcus theory depicts the variation of solvent structure around the charge donor and acceptor during the reaction. Specifically, the collective solvent coordinate can be defined by the difference in potential energy between the redox center's reduced and oxidized states at a fixed nuclear configuration.²⁹⁸ In a reaction involving proton transfer, such as HER, the reaction coordinate *R* can be the combination of the solvent coordinate and the proton coordinate, which has been discussed by Schmickler,²⁹⁹ and also in the PCET theory of Sharon Hammes-Schiffer.²⁶² Moreover, the electronic structure of the electrode should be considered for the rate constant of ET processes between molecules and electrodes, as indicated in eq 13 obtained from Marcus–Hush–Chidsey (MHC) theory:

$$k = k_0 \exp\left(\frac{(\Delta G \pm \lambda)^2}{4\lambda k_B T}\right) \quad (12)$$

$$k = A \int_{-\infty}^{+\infty} \exp\left(-\frac{(x + \lambda \pm \eta)^2}{4\lambda k_B T}\right) \frac{dx}{1 + \exp(x/k_B T)} \quad (13)$$

where λ is the reorganization energy, k_B is the Boltzmann constant, T is temperature, η is the overpotential, A is the pre-exponential factor, accounting for the electronic coupling strength and the electronic density of states (DOS) of the electrode, and x accounts for the Fermi statistics of the electron energy distribution around the electrode potential. The first term in the integrand is the classical Marcus rate for the transfer of an electron of energy x relative to the Fermi level, and the second factor is the Fermi–Dirac distribution assuming a uniform DOS. In these equations, reorganization energy (λ) is the key quantity for evaluating the solvent reorganization effect on kinetics, which is defined as the dissipated Gibbs energy when a system that has undergone a vertical electron transfer obeying the Franck–Condon principle relaxes to the equilibrium state and adopts its new charge distribution.³⁰⁰ Generally, the total reorganization is the sum of an inner contribution and an outer contribution. The inner reorganization energy counts the energy change resulting from the variation of the coordination environment around the redox center. The outer reorganization energy originates from the solvent reorganization, which could be approximately described by the Born energy of solvation:²³⁷

$$\lambda_{out} \approx \frac{e^2}{8\pi\epsilon_0 k_B T} \left(\frac{1}{a_0} - \frac{1}{2d} \right) \left(\frac{1}{\epsilon_{op}} - \frac{1}{\epsilon_s} \right) \quad (14)$$

where ϵ_0 is the permittivity of free space, a_0 the effective radius of the reactant of the electrode, d the distance from the center of the reactant to the surface of the electrode, ϵ_{op} the optical dielectric constant and ϵ_s the static dielectric constant. For bulk

water, the static and optical dielectric constants are 72 and 1.8, respectively.

The kinetics of electron transfer described in the MHC formalism is dictated by the reorganization process of the redox species upon the electron and/or proton transfer event. In the next section, experimental and computational works which characterize the modes and time-scales of water reorganization in bulk or under confinement will be discussed.

4.2.2. Characterization of Reorganization Dynamics of Water. The dynamics of water reorganization is central to the kinetics of chemical reactions in liquids, which correlates to reactant diffusion,^{301,302} energy exchange,^{303–305} and even the reaction coordinates of transition states.^{306–310} For general reactions in solvent (Figure 19), the reactants A and BC

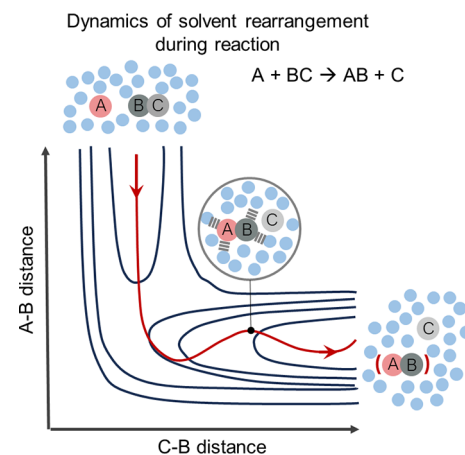
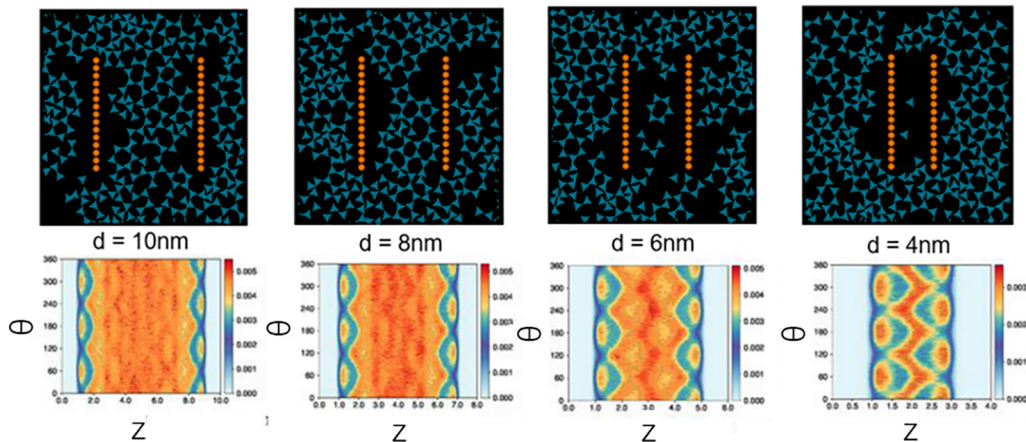


Figure 19. Reaction dynamics in liquid solution. Schematic representation of the potential energy surface of the chemical reaction influenced by solvent interaction. Getting to the transition state necessitates the solvents around the reactants to undergo rearrangement. Once transition state is achieved, the reaction will drive forward via thermal fluctuations.²⁸⁹

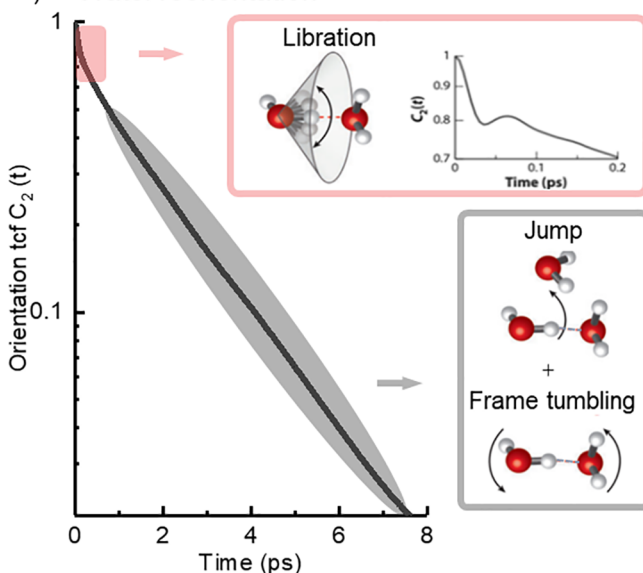
should diffuse to create a solvent cage that can accommodate the intermediate {A-BC},²⁸⁹ where the energy exchange between solvent and redox species (A, BC and A-BC) would happen. Some solvent molecules can acquire excess energy from fluctuations and transfer their energy to the reactants via collision, which drives the reaction forward.^{305,311,312} During these processes, H-bonding networks of water should change the geometry to accommodate the reactant complex and also respond to the variation of local dipole moments by reorientating, diffusing and exchanging H-bonds of individual water molecules. Therefore, the dynamics of reorganization get involved in several elementary steps of chemical reactions, closely linking this process to the reaction kinetics in water.

It is challenging to capture the collective motion of water networks during the reorganization process, hindering the establishment of a quantitative correlation between reorganization dynamics and reaction kinetics at this stage. To address this challenge, extensive works have been devoted in this field to first identify the essential molecular motions during the reorganization process by adopting simulation and experimental methods. For instance, a simplified model named the Mercedes-Benz (MB) model has been adopted widely to illustrate the water network variation in simulations,^{313–315} where the water molecule is simplified as a 2D disk, with three radial arms presenting three hydrogen bonds (Figure 20a).

a) Collective behavior of water reorganization



b) Water reorientation



c) Tunneling in orientation

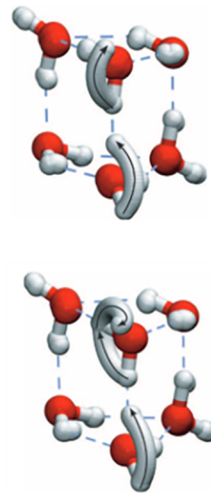


Figure 20. The reorganization process of water. (a) The representative snapshots and the corresponding orientation map of water confined within two hydrophobic rods at different inter-rod separations d . θ is the angle between the arms of the MB particles and the z -axis. The left rod is set as $z = 0$, the probability distribution of θ is plotted along z , and color indicates the probability.³²¹ Adapted with permission from ref 321 with the permission of AIP Publishing. (b) Second-rank orientation time-correlation function ($C_2(t)$) for a water OH bond extracted by MD simulations, suggesting libration initiates the reorientation of water, the large-amplitude angular jumps, and the frame reorientations are two essential reorientation mechanisms.^{322,341} Adapted with permission from ref 322. Copyright 2011 Annual Reviews. (c) The antigeared and geared pathways of water reorientation via quantum tunneling in the water hexamer prism.³⁶⁸ Adapted with permission from ref 368. Copyright 2016 AAAS.

The energy variation due to fluctuations of the H-bonding network is simulated by Lennard-Jones (LJ) attraction and repulsion and the orientation dependent H-bonding interaction.^{316–320} The MB model provides flexibility in yielding insights and elucidating concepts with a macroscopic water network, without requiring substantial computer resources. It can also act as a foundational framework for the development and analysis of more accurate theoretical methods. Recent work has used the MB model to illustrate the water network reorganization under the confinement of two hydrophobic rods,²¹¹ which serve as a model system to analyze the hydrophobic effect for driving water reorganization when two hydrophobic centers join in one solvation cage in reactions. The network structures with water (represented by MB particles, a disk with 3 arms) with decreased distance between two rods are depicted in Figure 20a. The distribution of the water orientation is also plotted in the lower panel of Figure 20a, where θ is defined as the angle between the arms of the

MB particles and the z -axis, i.e., the axis normal to the rods. The simulation highlights that the orientation of water plays an essential role in triggering the reorganization process. At the early stage of the reorganization process, the variation of the oriented heterogeneity of the water network appears near the rod and drives the two rods to assemble into one individual solvent cavity. As two rods are brought closer, the inference among the oppositely oriented heterogeneity increases, decreasing the heterogeneity and lowering the free energy of the system. In addition, the local ice-like hexagonal structure can be observed in the initial state of the water reorganization, which can trigger the assembly process by forming more H-bonds, hence lowering the free energy of the water network.³²¹ Although the simulations using simplified models, such as the MB model, can extract the network information from complicated large systems, much chemical information is neglected in this kind of analysis, which could be further studied with experiments and MD simulations.

Focusing on the molecular picture of the H-bonding network rearrangement, reorientation of water is one of the crucial motions for H-bonding exchange.^{322,323} An accurate depiction of the reorientation dynamics of a water molecule is encapsulated by the time-correlation function (TCF) of its molecular orientation (Figure 20b). This function quantitatively assesses the rate at which the initial orientation of a water molecule, represented by a specific body-fixed vector such as the OH bond or the molecular dipole moment, diminishes over time. The TCF can be measured by IR pump–probe spectroscopy^{2,324–330} or nuclear magnetic resonance (NMR) spectroscopy^{331–335} or extracted from MD simulations.^{323,336–341} Figure 20b illustrates a representative TCF for bulk water at ambient temperature extracted from MD simulations.³⁴¹ When analyzed on a logarithmic scale, this function reveals that water reorientation occurs through distinct stages with varying rates and mechanisms. Initially, there is a rapid (sub-picosecond) partial reorientation, which is succeeded by a more gradual (picoseconds) complete reorientation. The initial inertial rotation is named as libration, which is quickly constrained by the H-bonds formed with nearby molecules. These H-bonds exert restorative torques, effectively maintaining the molecule around a mean orientation. Experimental results including neutron scattering experiments^{342,343} and mid-IR femtosecond pump–probe spectroscopy³⁴⁴ agree with the point that the librational motion initiates the H-bonding network rearrangement in bulk water (Figure 20b), indicating that the spectroscopic feature of the libration frequency can be a descriptor for water network rearrangement. The variation of the libration IR signal has been analyzed in confined water. Venables et al. have revealed that the size of the confinement can influence the libration peak position of water confined in a reverse micelle, which can be shifted from 660 to 510 cm⁻¹ when the size of the micelle decreased.³⁴⁵ The confinement effect on water libration can also be observed in zeolites, where the signal of the libration peak decreased and shifted slightly, because of the reduced coordination of H-bonds in hydrophobic pores, and consequently influenced the properties of local catalytic environments in zeolites.³⁹ Beyond libration, MD simulations have captured the later stages of the reorientation dynamics of water and revealed that the process is comprised of two different motions, i.e., the large-amplitude angular jumps and frame reorientations of the intact hydrogen bond axis (Figure 20b).^{323,346} Laage and Hynes have determined that the reorientation of bulk water is composed of mainly the large-amplitude angular jumps, of which the relaxation time is faster than frame reorientation.^{322,323,346}

Dielectric spectroscopy has also been adopted to study water reorganization processes, which can extract the TCF from the frequency dependent dielectric function.³⁴⁷ The dielectric spectrum of bulk water in the low-frequency region corresponds to Debye relaxation processes and exhibits two time constants of 8.2 and 1.02 ps.³⁴⁸ On the other hand, the spectra in the high-frequency region are contributed from many vibration modes, including the intramolecular vibration of O–H···O (\sim 200 cm⁻¹) and the libration mode (\sim 680 cm⁻¹). The molecular probe has been adopted to capture the reorganization dynamic, which is nonpolar or nearly nonpolar in the ground state but is highly polar in the excited state.³⁴⁷ Therefore, the water structure remains randomly oriented in the ground state and reorganized by the polarized center in the excited state. When the excited state relaxed to the ground

state, the time dependent energy emission originated from the water reorganization process can be captured by the fluorescence Stokes shift.^{347,349} The results show that water can respond quickly to the dipole variation.^{104,350} The initial part occurs within a few tens femtoseconds and contributes more than 60% to the total reorganization process, followed by a relative slow relaxation in the picosecond time scale.³⁵⁰ Further theoretical works suggested that the initial part of water reorganization described by a Gaussian component is contributed by the 200 cm⁻¹ intermolecular vibrational mode, and the libration mode (\sim 680 cm⁻¹) also important in a short time.^{351–353} These results suggest the close correlation between the vibration features of water and reorganization dynamics.

Whether the confinement of water by ions leads to faster or slower water dynamics is still debated. On one hand, when water is confined in concentrated salt solutions, the reorientation dynamics become slower than those of pure water,^{354–356} where the frame reorientation dominates,²²¹ and the presence of hydrated ion clusters slows down the collective component of water rotation.³⁵⁷ On the other hand, the recent work using 2D Raman-terahertz spectroscopy revealed the inhomogeneity of aqueous salt solutions,³⁵⁸ where Cs⁺ can slightly accelerate the water dynamics around the cation.³⁵⁸ In contrast, the significantly slower relaxation dynamic of water in concentrated alkali halide solutions was observed in the 1D Raman technique.³⁵⁹ The distinct dynamics around Cs⁺ has been explained in another simulation work,³⁶⁰ showing that cations can influence H-bond exchange in two ways. First, a local excluded volume created by cations can hinder the new H-bond partner to approach and consequently retard the dynamics. Second, cations can perturb the local H-bonding network to reduce the energy penalty for elongating the H-bond, which should benefit the dynamics of the exchange between H-bonds.³⁶⁰ For Cs⁺, the latter effect surpasses the former one, so the water dynamics accelerates.³⁶⁰ In addition, the energy cost for reorientation of bulk water has been explored, where the structure-dynamic relationship has been established to predict the barrier for H-bond exchange based on the radial distribution function in liquid water.³⁶¹ Based on computation, the results show the Gibbs free energy of the transition state in water reorientation is mainly determined by the activation enthalpy (2.58 ± 0.06 kcal mol⁻¹ or 10.8 ± 0.25 kJ mol⁻¹), while the experimentally determined activation barrier (E_a) is found to be in close agreement at \sim 3–4 kcal mol⁻¹ or 12.6–16.7 kJ mol⁻¹).³⁶¹ Consistently, E_a of reorientation in bulk water measured by dielectric spectroscopy is around 15 kJ mol⁻¹,³⁶² which can increase to 40–52 kJ mol⁻¹ under confinement of silica nanopores or organic mixtures.^{363–365} The kinetics of water reorientation plays the essential role in tuning the barrier in proton transfer^{366,367} and proton transport,^{239,246} where it can be the rate determining step to influence the reactions. By using ultrafast spectroscopy techniques, quantitatively correlating the water structures and the energy cost of water reorientation is a promising future direction to relate the microscopic molecular picture of dynamics to the macroscopic reaction kinetics.

Moreover, the reorientation process of water has been described by the quantum nature of H-bonds.^{369,370} Paesani et al. have compared the relaxation time of reorientation simulated by classical MD and quantum MD, where quantum MD exhibits better agreement with the corresponding experimental results while classical MD has significantly slower

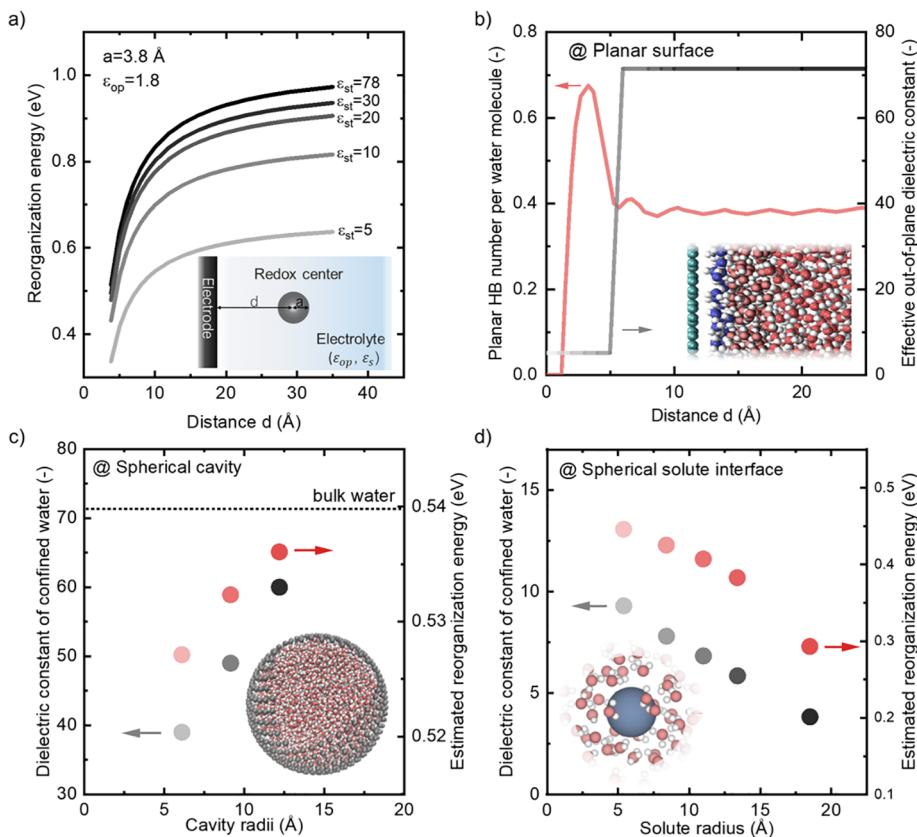


Figure 21. Altering reorganization energy of ET by tuning interfacial dielectric properties. (a) Reorganization energy of ET estimated by $\lambda \approx \frac{e^2}{8\pi\epsilon_0 k_B T} \left(\frac{1}{a_0} - \frac{1}{2d} \right) \left(\frac{1}{\epsilon_{op}} - \frac{1}{\epsilon_s} \right)$ for static dielectric constant ϵ_s ranging 5–78, assuming optical dielectric constant ϵ_s at 1.8 and ionic radii of redox center a at 3.8 Å (e.g., ferri/ferrocyanide). The figure is created by the authors. The inset schematic depicts the parameters of the reorganization energy of ET at a metallic electrode surface. (b) Distribution of planar hydrogen bonds per molecule for water and effective out-of-plane dielectric constant at the graphene surface at different regions for a 25 Å channel in the MD simulation.³⁸⁸ The inset schematic shows confined water on the graphene channel.³⁸⁸ The inset is adapted with permission from ref 388. Copyright 2019 American Chemical Society. (c) Dielectric constant of water confined by different radii of spherical cavity¹⁰⁹ and ET reorganization energy for $d = a = 3.8$ Å and $\epsilon_{op} = 1.8$ estimated by eq 14. The inset schematic shows water confinement in a spherical cavity.³⁸⁹ The inset is adapted with permission from ref 389. Copyright 2016 AIP Publishing. (d) Dielectric constant of water confined by different radii of the spherical solvation surface³⁹⁰ and ET reorganization energy for $d = a = 3.8$ Å and $\epsilon_{op} = 1.8$ estimated by eq 14. Adapted with permission from ref 390. Copyright 2016 AIP Publishing. The inset schematic shows water confinement in spherical solvation.³⁹¹

reorientation dynamics.³⁶⁹ Wilkins et al. have adopted ring polymer molecular dynamics to quantify the nuclear quantum effect on reorientation of water at 298 K. Their results suggest that by taking into account nuclear quantum effects, the water dynamic relaxation time is only ~13% faster than classical MD simulations, while the reorientation mechanism and the jump amplitude distribution of water remain unchanged between quantum vs classical MD. The acceleration is mainly due to decreased structuring of the OO radial distribution function when the nuclear quantum effect is considered.³⁷⁰ While the effect is rather minor for bulk water, the tunneling contribution can become significant when water is fixed in a network at low temperatures or under confinement. Richardson et al. have observed the tunneling pathways that involve the concerted breaking of two hydrogen bonds in hexamer clusters (Figure 20c),³⁶⁸ indicating that the water network can rearrange by proton tunneling without the motion of oxygen atoms. This quantum process without the barrier required for the classical mechanism of water rearrangement may provide a novel reaction pathway in the confined water environment because of the distinct water dynamics. For example, water dimers

confined on a metal surface (Pd (111)) exhibit a higher diffusion rate than monomers.³⁷¹ In this situation, the quantum mechanism of H-bond rearrangement through tunnelling has been proposed to be one possible reason for the accelerated dynamics.^{372,373} However, experimentally quantifying the contribution of tunneling to water rearrangement remains challenging at this stage. Future works are required to examine this hypothesis, which has been mainly based on theoretical simulation.

In summary, confinement can influence the rearrangement behavior of the H-bonding network of water, which can tune the kinetics and dynamics of chemical reactions in liquids. However, the strict quantitative correlation between the water dynamics and the energy penalty of reorganization^{374–377} is not established yet. Detailed measurements and development in ultrafast spectroscopies and simulation methods are required to address the challenge of probing reaction dynamics in liquids.²⁸⁹ On the other hand, the reorganization process for reactions involving charge transfer has been extensively studied,^{374–377} of which the energy penalty can be extracted

with the dielectric continuum treatment developed by Born, and the rate constant deduced based on Marcus theory.

4.2.3. Reorganization Energy Trends for Electrochemical Reactions. The reorganization energy of ET on the electrode surface has been measured by experimental studies and analyzed by the Born model,^{378–385} where a self-assembly monolayer was adopted to control the distance between the electrode and redox center. The results showed that the reorganization energy reduces markedly with decreasing distance (Figure 21a). By adopting the Born model, the reduced reorganization energy is attributed to the decreased charge transfer distance and the lower static dielectric constant of the solvent under confinement at the interface. However, the dielectric continuum treatment neglects the effects of explicit hydrogen bonding of the solvent to the redox center, as well as the detailed structures of the water under confinement. Moreover, it also neglects the dynamic effects of the system and the electronic structure of the electrode. Molecular dynamics (MD) studies with explicit solvent and ions, combined with an atomic-level treatment of the electrode, would provide further insights. Using MD simulation, the reorganization energy can be extracted by calculating the Marcus free-energy profiles for ET between a metallic electrode and a redox species in the solution phase between the initial state M^+ and the final state M^{2+} ($M^{2+/+}$) such as $Ru^{3+/2+}$ ³⁸⁵ and $Ag^{2+/+}$.^{386,387} By examining the electrostatic potential fluctuations experienced by ionic species in the vicinity of an electrode surface, Limaye et al. have revealed that the effect of image charges supported by the electrodes plays a dominant role in determining the vertical energy gap and hence the reorganization energy, as one approaches the electrode surface.³⁸⁷ Furthermore, water molecules can be strongly attracted to and ordered at the electrode surface and affect the probability of ions reaching the surfaces,²⁵¹ where the ordering can be different from the water structure indicated from continuum models of electrode interfaces. Hammes-Schiffer and co-workers have developed a computational model to include the effects of the double layer and ionic environment of the diffuse layer when calculating the solvent reorganization energy for Electron Transfer (ET) and Proton-Coupled Electron Transfer (PCET) between the redox species and the electrode. In the method, the accurate electronic charge distribution of the species within a molecular-shaped cavity (in lieu of ionic representation as a point charge) has been used along with a dielectric continuum treatment of the solvent, ions, and electrode.³⁷⁸ Consequently, a reorganization energy model including the effects of the double layer and ionic environment of the diffuse layer has been developed.³⁷⁸ Compared with the classical Born model, the model in MD simulations can consider comprehensive effects on the local dipole moment (dielectric constant) of water originated from confinement of the electrode, charge distribution in the double layer and interaction with ions, which can predict the reorganization energy more precisely.

While obtaining reorganization energy from MD simulation is a relatively complicated and expensive calculation, the dielectric constant of water (a more accessible parameter) has been shown to be the key descriptor connecting local water properties and reorganization energy for an electrode, which can be reduced under confinement and most-likely correlated with the changes in the hydrogen bonding network.^{32,388–390} This phenomenon was attributed to the reduced rotational diffusion coefficient for water molecules close to the solid

surface.³⁸⁸ The suppressed rotation, in turn, affects the orientational polarization of water, leading to a low value for the dielectric constant at the interface.³⁸⁸ The water in the interfacial regions tends to be much more energetically stable than that in bulk even though the interfaces form a lesser number of hydrogen bonds compared with the bulk (Figure 21b). Consequently, the effective out-of-plane dielectric constant of water decreases to 5.1 in the vicinity of the surface from 72 for the bulk water (Figure 21b). The experimental evidence of the vanishing perpendicular dielectric constant of water is from a scanning dielectric microscopy study based on electrostatic force detection with AFM,³² where interfacial water confined between two atomically flat hydrophobic hexagonal boron nitride (hBN) walls has an out-of-plane ϵ only ~ 2 , close to the optical dielectric constant of water (1.8) with electronic polarization only.³² The near-surface layer with $\epsilon = 2.1$ and thickness $h \approx 7.5 \pm 1.5$ Å is two to three molecular diameters, in agreement with simulation studies,³⁹² whereas the remainder of the channel contains the ordinary bulk water.³² While the near-surface layer value $\epsilon = 2.1$ is obtained experimentally, several studies based on classical MD simulations have predicted different values for the out-of-plane dielectric constants (e.g., $\epsilon > \sim 10$ based on the simulation of graphene confined in two graphene walls), highlighting understanding the origin of the out-of-plane dielectric constant being an active area of research. Similarly, the shape of the dielectric constant profile between the near-surface region and the bulk can be system-dependent. For example, the hBN confinement described above shows a smooth and gradual increase in the out-of-plane dielectric constant as the water channel size increases and only approaches the bulk water value at channel size > 100 nm. In contrast, the MD simulation by Bonthius et al.³⁹³ for water-on-diamond surfaces shows an oscillatory profile of the dielectric constant which only spans over a much shorter range (<15 Å) width between the near-surface and bulk water regions. The MD simulation study of Majumdar et al.,³⁹⁴ which simulated water layers in between two graphene sheets, shows a smooth transition over a distance of ~ 10 Å ahead of the graphene interface. As an active area of research, the discrepancies in the observed value and profile can be potentially due to the specific surfaces used in simulating water confinement,³⁹⁵ channel size of confinement (e.g., single interface vs symmetric two electrode systems) and levels of theory in the MD simulations.³⁵

Similar to planar surfaces, the dielectric properties of water confined in a nanodimensional spherical cavity⁶⁹ and spherical solvation of ions³⁹⁰ are shown by MD simulation to be significantly smaller than those of bulk water from MD. A nearly 50% decrease of the dielectric constant is observed when water is confined in a cavity of about 6 Å in radii¹⁰⁹ (Figure 21c). In that work, the fictitious cavity wall was created by using a Lennard-Jones potential to keep water molecules inside the cavity. As a result, the wall is nonpolarizable ($\epsilon_{cavity\ wall}$ equals unity) and has zero charge. Therefore, the reduction of the dielectric constant observed in the study originates not from electrostatic interactions but purely from geometric confinement, where the spatial and orientational order of water in the cavity reduces the ability of water molecules to respond to an external electric field. In a more realistic situation, real surfaces are polarizable, and so in addition to the geometric confinement effect, the electrostatic interaction can further lock water molecules in place and

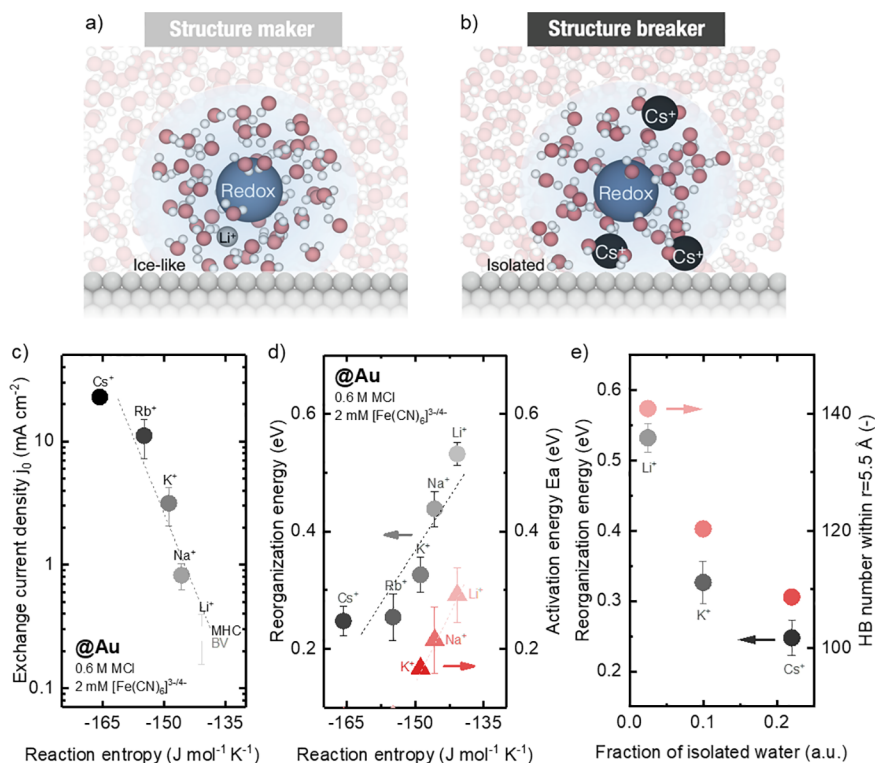


Figure 22. Altering reorganization energy of ET by tuning interfacial water structure. (a) Structure-breaking cations (Cs^+) could promote weakly H-bonded water molecules at the metal surface and make the redox solvation shell disordered with loosely bonded water molecules. (b) Structure-making cations (Li^+) could promote a strongly hydrogen-bonded (ice-like) interfacial water layer and make the redox solvation shell ordered with tightly bonded water molecules. (c) Cation-dependent exchange current density j_0 as a function of reaction entropy, which is extracted via the MHC formalism of 2 mM equimolar $[\text{Fe}(\text{CN})_6]^{3-}/[\text{Fe}(\text{CN})_6]^{4-}$ in an Ar-saturated aqueous solution of 0.6 M chloride salts of Li, Na, K, Rb and Cs on the Au RDE electrode.³⁷ (d) Reorganization energy extracted via the MHC formalism as a function of entropy.³⁷ (e) Cation dependent dielectric constants extracted from entropy and reorganization energy via the Born model.³⁷ Panels c–e are adapted with permission from ref 37. Copyright 2021 American Chemical Society.

suppresses the interfacial water's dielectric response. Moreover, water interfacing spherical ions (Figure 21d) exhibit significantly lower effective dielectric constant than its bulk, which depends on the solvation size, where the effective dielectric constant changes from 9 to 4 when the solvation sphere radius is increased from ~ 5 to 18 \AA .³⁹⁰

With regulated dielectric constants of water under confinement, the kinetics (exchange current density and reorganization energy) of electrochemical reaction involving ET can be tuned. For example, the kinetics of $[\text{Fe}(\text{CN})_6]^{3-}/^{4-}$ redox (an outer-sphere ET reaction) has been measured (Figure 22), where the confined water properties are tuned by cations to form the disordering/ordering of the water network around the redox centers at the electrode surface (Figure 22a–b).^{33,37} When the cationic radius decreases, the reorganization energy increases (Figure 22d) and the exchange current density decreases (Figure 22c).³³ The dielectric constant at the interface can be extracted from the entropy and reorganization energy via the Born model, exhibiting a higher dielectric constant with Li^+ compared with Cs^+ (Figure 22e). On the other hand, for cation-dependent kinetics of PCET reactions such as HER and HOR, where the activity decreases when cation radii increases ($\text{Li}^+ > \text{Na}^+ > \text{K}^+ > \text{Rb}^+ > \text{Cs}^+$), the trend can be attributed to increased reorganization energy because of proton transfer (see Section 4.1). Meanwhile, the increasing reaction entropy is evidently accompanied by decreasing reorganization energy and increasing exchange current density, which is a measure of the disordering of solvation environ-

ments at electrified interfaces, and can be used to extract the interfacial dielectric constant, suggesting that cation-dependent reaction entropy is associated with cation-dependent interfacial water structure. Rossmeisl et al.³⁹⁶ have suggested that the entropic barrier of proton transfer across the Helmholtz layer might be a possible explanation for pH-dependent HER/HOR kinetics for catalysts such as Pt. Given the influence of interfacial water structure and the solvation structure of the negatively charged redox molecules on the reaction kinetics, such an approach provides an exciting opportunity to alter the reaction rates of individual reactions (such as CO_2RR and NRR, during which HER inevitable occurs due to the negative applied potential) and hence tune the selectivity in electrochemical reactions.

In addition, cations can also have a significant influence on the activity of CO_2RR . The first ET step of CO_2RR has been determined as the rate determined step for CO_2RR on Au.³⁹⁷ Koper et al. observe that CO_2RR can only occur with cations on a Au surface.³⁹⁷ Recently, Qin et al. has adopted constrained DFT-MD and slow-growth DFT-MD quantitatively extracted the barrier for outer-sphere ET and inner-sphere ET of CO_2 on Au with and without the inclusion of alkali metal cations (Figure 23a–b).³⁹⁸ The results show that CO_2 prefers inner-sphere ET with cations on the surface and consequently forms CO_2^- adsorbed on Au. K^+ can reduce the barrier of inner-sphere ET by 0.3 eV compared with that of Li^+ (Figure 23d, f). On the other hand, the Au/water interface without cations prefers outer-sphere ET, where the reorganiza-

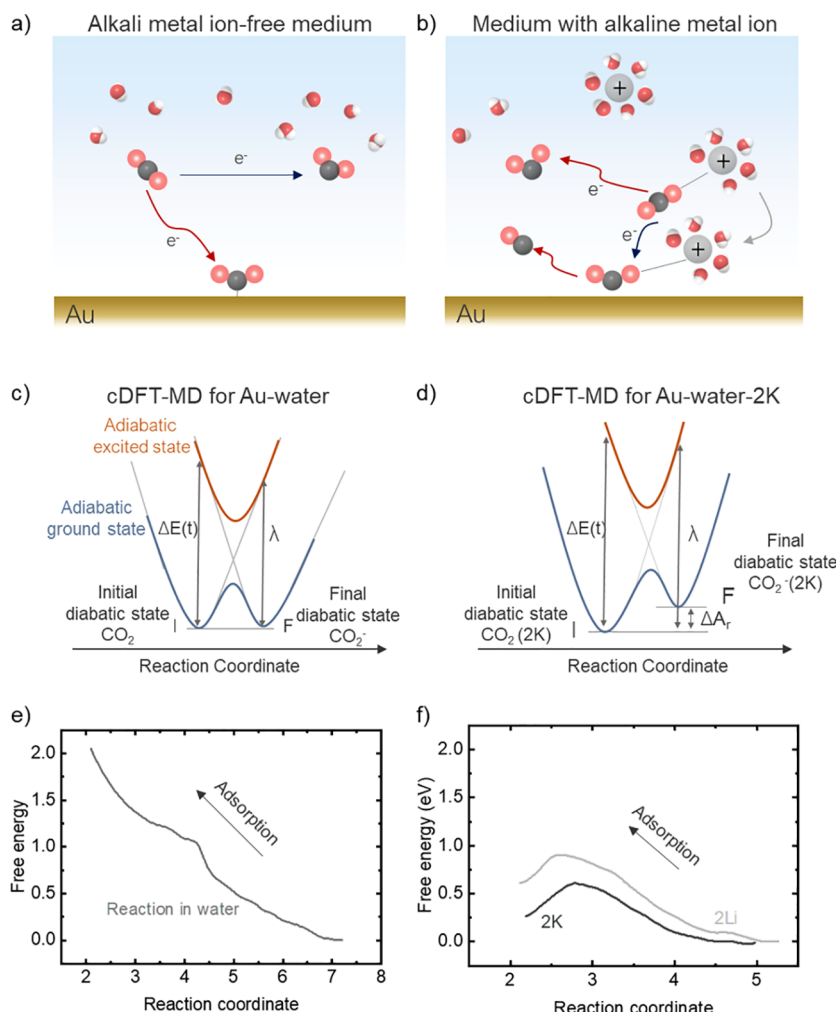


Figure 23. Reorganization energy for CO₂RR with and without cations. (a, b) Schematics of CO₂RR in cation-free medium (a) and medium with K⁺ cations (b).³⁹⁸ (c, d) Schematic views of the Marcus theory of diabatic states of outer-sphere ET shown at the Au-water (c) and Au-water-K⁺ (d) interfaces.³⁹⁸ (e, f) Free energy profiles of inner-sphere-ET at the Au-water (e) and Au-water-K⁺ (f) interfaces, with the free energy curve at the Au-water-Li⁺ interfaces inserted for comparison.³⁹⁸ Adapted from ref 398. Copyright 2023 open access article distributed under CC BY-NC-ND License 4.0.

tion energy is as high as 4.82 eV and results in the barrier of 1.21 eV for CO₂RR, showing that the ET step without cation (1.21 eV) is much higher than that with K⁺ (0.61 eV) and Li⁺ (0.91 eV) (Figure 23c, e). Koper et al. also constructed the theoretical model describing the effect of cation coupled electron transfer in CO₂RR, which highlights the short-range interaction between ions and intermediates.³⁹⁹ Therefore, the reorganization energy is one of the key factors ruling the electrochemical kinetics in aqueous solution, which can be tuned by regulating the water structure under confinement, local dielectric constant, reaction entropy and the ions-intermediates interaction dominated by the solvation structure.

4.3. Tuning Proton Kinetics via H-Bonds

PT and ET processes exhibit evident quantum behavior, where the tunneling probability is sensitive with the transferring distance, especially for protons, of which the mass is significantly higher than that of electrons. The transferring distance of PT always correlates with H-bonding structure, of which the equilibrium bond length and dynamics can dictate the tunneling probabilities. The kinetic equations of homogeneous PCET have been developed by several groups,^{262,400–402} with the framework of Marcus theory to deal with the solvent

effect and highlight the quantum effect of proton transfer by the Franck–Condon overlap. One of the kinetic equations developed by the Sharon Hammes-Schiffer group²⁶² is depicted in eq 15:

$$k = \sum_{\mu,\nu} P_\mu \frac{(V^{\text{el}} S_{\mu,\nu})^2}{\hbar} \sqrt{\frac{\pi}{\lambda k_B T}} \exp\left[-\frac{(\Delta G_{\mu,\nu}^0 + \lambda \pm \epsilon\eta)^2}{4\lambda k_B T}\right] \quad (15)$$

where T is the temperature for reactions and $\Delta G_{\mu,\nu}^0$ is the energy difference between oxidized states and reduced states. V^{el} is the electronic coupling. P_μ is the Boltzmann probability of protons in different vibrational states, and $S_{\mu,\nu}$ represents the vibronic coupling of protons in different states. $S_{\mu,\nu}$ is the key factor to evaluate the proton tunneling probability for the specific vibrational state, while the hydrogen bonding dynamic can also influence the distribution probability of protons in different states. Based on these theoretical models, the H-bonding effect on ORR kinetics by adopting ionic liquid as proton donor has been highlighted; with the favorable pK_a value of the proton donor to increase the bond strength of interfacial H-bonds, the PCET kinetics of ORR can be

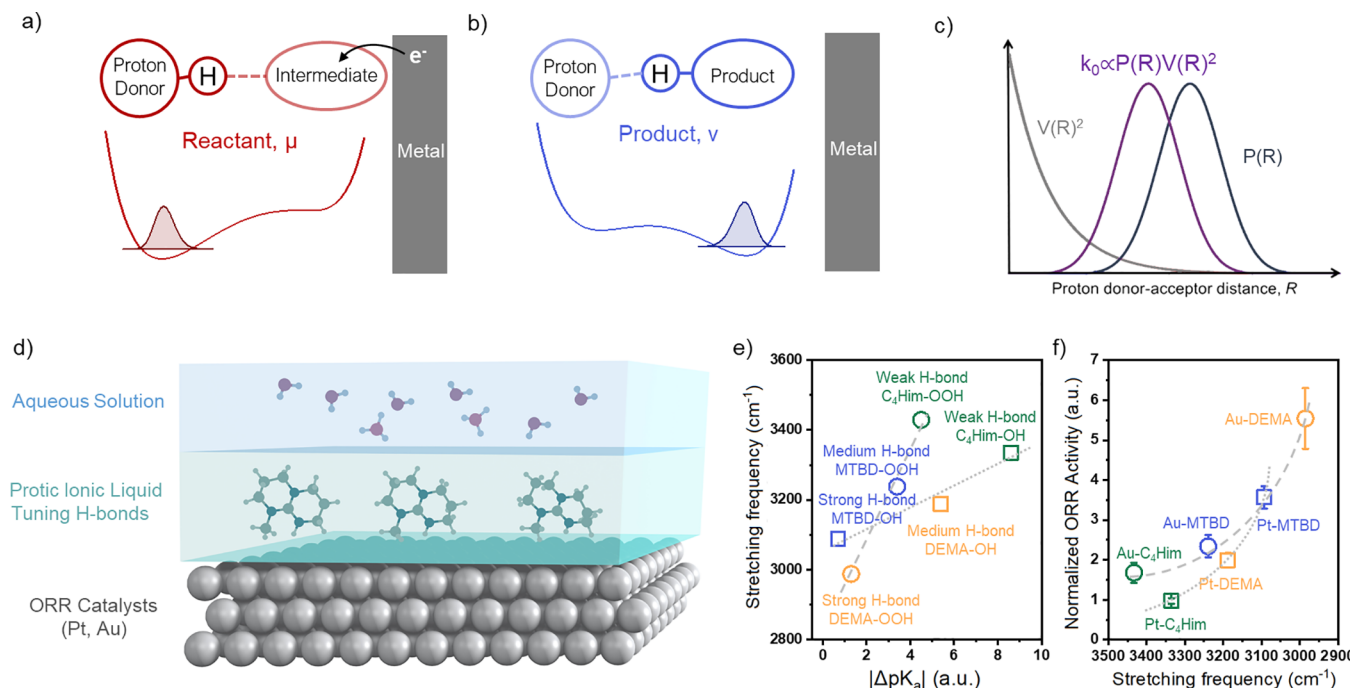


Figure 24. Hydrogen bonding structure dictates the kinetics of proton transfer (PT) and proton coupled electron transfer (PCET) via the water network. (a, b) Schemes of the PCET reaction at the H-bonded interface at the state of reactant (a) and product (b).⁴⁵ (c) Schematic depiction of the square of vibronic coupling $V(R)$ in gray, the probability distribution function $P(R)$ in dark gray, and the product of these two factors in purple, as functions of the proton donor-acceptor distance R . The overall rate constant (k_0) is the integral of the purple curve over R .⁴⁰⁴ (d) Schematic depiction of an ionic-liquid-modified metal surface, where protic cations of ionic liquids can serve as proton relays for delivering a proton from an aqueous electrolyte to a surface and tuning the pK_a of the proton donor for ORR.⁴⁵ (e) The correlation between the stretching frequency of a H-bonding species ($N-\text{H}\cdots\text{O}$) and ΔpK_a ($\Delta pK_a = pK_a^{\text{donor}} - pK_a^{\text{acceptor}}$).⁴⁵ (f) The relationship between the stretching frequency of the H-bonding species ($N-\text{H}\cdots\text{O}$) and the normalized ORR activity catalyzed by ionic-liquid-modified Au/C and Pt/C, which are normalized by the ORR activity of pristine Au/C and Pt/C, respectively.⁴⁵ The curves only serve as a guide to the eyes. Adapted with permission by the authors from ref 45. Copyright 2021 Springer Nature.

accelerated,⁴⁵ suggesting the important role of the H-bonding structure for ruling electrochemical kinetics (Figure 24). Besides, the expression of the PCET rate constant considering the quantum effect of protons has been developed for analyzing the Volmer step in adiabatic and nonadiabatic limits recently,⁴⁰³ where the contribution of the adiabatic rate constant is insignificant for metals. The rate constant is dominated by the nonadiabatic rate constant that exhibits a similar mathematical form compared to MHC theory.⁴⁰³ The protonic vibronic coupling is also emphasized in this expression developed for the heterogeneous electrochemical PCET processes. Therefore, the general effect of H-bonds on PCET kinetics can be described in Figure 24c. Generally, the vibronic coupling increases dramatically when transferring distance decreases, and the total rate can be quantified by considering both the vibronic coupling and distribution probability of the transferring distance that dominates by H-bonding dynamics. Interestingly, the peak of the reaction rate (indicated by the purple curve k_0 in Figure 24c) is not located at the equilibrium state of an H-bond ($P(R)$ in Figure 24c), indicating that the fluctuation of the bonds around the mean distance can contribute more significantly to the total rate constant and can result in higher kinetics. Therefore, we highlight the opportunity of altering the rigidity of H-bonds via confinement strategies to tune the probability of the transferring distance $P(R)$ in order to influence reaction rates k_0 .

While the work by Wang et al. on the H-bonding effect on ORR kinetics points to the effect of proton tunnelling on

reaction kinetics, whether proton-tunnelling occurs especially in HER is still debated. Schmickler et al. have discussed the temperature dependence of the Tafel slope in the context of proton tunneling, suggesting that if both tunneling and classical transitions can occur in parallel, their relative contributions vary with temperature, with tunneling becoming more significant at low temperatures.^{299,405,406} They also argue that proton tunneling would produce two different Tafel slopes for HER between light (H_2O) and heavy (D_2O) water on a mercury electrode, but the Tafel slopes for hydrogen and deuterium run parallel, suggesting a lack of evidence for proton tunneling.²⁹⁹ On the other hand, Krishnalik et al. have claimed evidence for proton tunneling for HER on Hg ,⁴⁰⁷ which is further corroborated by simulation works of Nazmutdinov et al.⁴⁰⁸ We note that the contribution of proton tunnelling remains debated. The pre-exponential factor generally contains the activation entropy (see Section 4), and thus the idea of proton tunnelling is not necessarily needed to explain changes in the pre-exponential factor unless presented with more evidence.

The kinetic effect of the rigidity of the water network confined on the electrode surface has been discussed extensively. Ledezma-Yanez et al.⁴⁰⁹ have performed laser-induced temperature-jump measurements to illustrate that the reorientation kinetics of water and the rigidity of the H-bonding network can be tuned by the surface charge. When the applied potential becomes more negative than the PZC, the local electric field can confine water more strictly, which results in the increased rigidity of the water network and decreased

HER and HOR activity of Pt in alkaline solution. This opinion was further elaborated by the theoretical work of Huang et al.,^{410,411} where the influence of water rigidity on the surface was considered in the model Hamiltonian, showing that the increasing rigidity of the water network can raise the barrier for the Volmer step. These works suggest that when water reorientation is free, protons can more easily approach the surface and increase the reactivity, so that the lower rigidity of confined water can result in higher HER/HOR activity.

The equilibrium structure of the H-bonding structure can be studied by *in situ* spectroscopy, which suggests that tuning the proportion of H-down water with dangling O–H bonds on the surface can increase the electrochemical activity. For instance, Shen and co-workers have studied HER on Pt and PtNi surfaces with *in situ* Raman Spectroscopy.⁴¹² More dangling O–H bonds were observed on the PtNi surface, which has been attributed to the physical origin of enhanced HER activity, indicating that the H-down water is associated with a lower barrier for dissociating proton to the Pt surface. A recent study also agrees with this opinion; Wang et al. have observed the Na⁺ present in the electric double layer can decrease the distance between hydrogen to the surface and enhance the HER activity.⁴¹³ Consistently, recent studies combining *in situ* IR and AIMD simulations have revealed that the interfacial water has high probability to approach ORR active sites⁴¹⁴ or CO₂RR intermediates⁴¹⁵ can increase the reaction kinetics as well.

The connectivity of the water network was found to influence the HER kinetics and proton diffusion. Chen et al. have adopted AIMD and IR spectroscopy to study the water network confined on Pt and analyzed the correlation between HER activity with H-bonding structure.⁴¹⁶ The results revealed that comparing the interfacial structure for HER in acid and alkaline, the accumulated cations on the surface in alkaline environment can place a gap of H-bonds between interfacial water and bulk water,⁴¹⁶ which make it difficult for protons to diffuse to the surface and for OH⁻ to diffuse out, resulting in an evident energy penalty for the reactions.⁴¹⁷ When Ru is introduced to the Pt surface, the connectivity of the water network increases due to OH adsorption on Ru sites, consequently enhancing the HER activity in alkaline solution. In addition, the network structures can also influence the proton diffusion kinetics in the diffusion layer of electrocatalysis wherein the reaction rate is suppressed by more than 10 times upon addition of 1.3 M K⁺ cations into acidic electrolytes.⁴¹⁸ Such drastic inhibition of the proton diffusion kinetics cannot be explained by the classical electromigration (driven by excess cations accumulating on the negatively charged electrode surface at operating potentials). Instead, the addition of cations disrupts the hydrogen-bonding network of bulk water and localizes protons in its hydration shell, preventing it from hopping across the bulk.⁴¹⁸ Moreover, the diffusion rate can also be tuned within carbon nanotubes, where the 1D water chain formed in carbon nanotubes always shows more than 1 order of magnitude enhancement in proton transfer kinetics.⁴¹⁹ Previous simulations suggest that the proton transfer within carbon nanotubes occurs via the Zundel–Zundel mechanism with H₇O₃⁺ intermediates,⁴²⁰ while a slower Eigen–Zundel–Eigen mechanism has been suggested in bulk water⁴²¹ (Figure 25a–b). The faster kinetics of the Zundel–Zundel mechanism than the Eigen–Zundel–Eigen mechanism is attributed to the excess energy cost required for the reorientation of water in the first solvation shell in the Eigen–Zundel–Eigen process, while

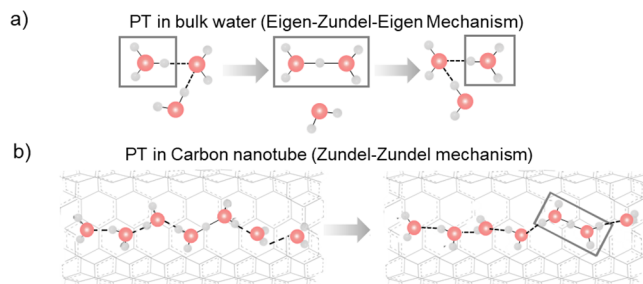


Figure 25. (a, b) The different PT mechanisms in bulk water (a, Eigen–Zundel–Eigen)⁴²¹ and in a nanoconfined water chain in a carbon nanotube (b, Zundel–Zundel).⁴²⁰ Adapted with permission from ref 420. Copyright 2008 American Chemical Society.

protons can directly hop along the water chain without reorganization in the Zundel–Zundel process. Therefore, while confinement can retard the rotational dynamics of water, proton transport can still be enhanced due to the faster mechanisms of proton transport in confined water (e.g., Zundel–Zundel mechanism or proton tunnelling) versus bulk water (e.g., Eigen–Zundel–Eigen).

Perfluorinated sulfonic acid (PFSA) polymer electrolytes, e.g. Nafion, are another ideal platform to explore the behavior with confined water. The key parameter for proton transport is the formation of a hydrogen-bonded water network, which grows with increasing water content.^{422–424} When a proton is separated from the sulfonate group, it is first transferred to water molecules (forming hydronium ions) and then it needs to diffuse through confined water. The addition of water molecules in the hydration shell allows for the formation of more complex protonic species, i.e. Zundel or Eigen ions.^{239,423} MD simulations provide insights at the nanoscale into the evolution of the hydrogen bond network and proton transport mechanism of water under confinement inside PFSA ionomers.^{425–427} At low water content, with an incomplete network of hydrogen bonds, proton conduction occurs at the interface between water and ionomer via a vehicular mechanism, which is the result of the competition between the electrostatic interactions between sulfonate groups and protons and their solvation energy. For low water content, proton mobility is generally low due to the incomplete dissociation and the disconnected hydrophilic domains. With increasing water content, water occupies the space beyond the first hydration shell where it is more mobile, i.e. less affected by the electrostatic interaction with sulfonate groups and with a higher rotational mobility. At this stage, water starts pulling hydronium ions away from sulfonate groups, making their separation more favorable. Due to their increased mobility, protons can hop from one water molecule to another one by the Grotthus mechanism,²³⁹ which is described as a coordinated transfer (sequence of breaking and forming steps) via the hydrogen bond network, forming Zundel or Eigen ions.^{421,428,429} Although many works begin to consider the role of water structure on electrocatalysis and proton diffusion kinetics, the water network and its dynamics possess a high level of complexity to be resolved comprehensively. Future work is needed to explore the role of the specific H-bonding structure in water networks on the PT, ET and PCET reaction rate.

Beyond the H-bonds composed of water, some molecular electrocatalysts have been designed to modify the proton transfer kinetics by changing the properties of proton donors

for the PT or PCET reaction. For example, a series of hangman iron porphyrins with hanging groups of differing proton-donating abilities have been synthesized to evaluate their electrocatalytic hydrogen-evolving ability at various H^+ concentrations.^{430–432} Hangman iron porphyrins with low pK_a functional groups tend to be more active at higher H^+ concentrations (Figure S8). In addition to tuning the kinetics of proton transfer, the geometry of the water network can also influence the tunneling probability of the electron. For example, in the pocket of *Pseudomonas aeruginosa* azurin,⁴³³ confined water is able to induce the formation and disturbance of local hydrogen bond networks and consequently tune the electron transfer kinetics.⁴³³ In the reactant basin (Figure 26a),

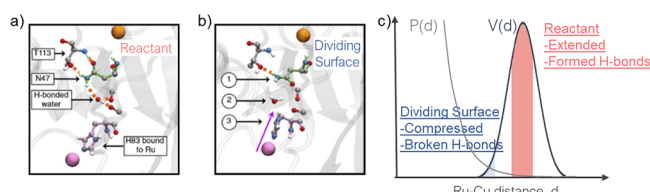


Figure 26. H-bonding structure of confined water alters the ET kinetics. (a) In the pocket of *Pseudomonas aeruginosa* azurin, the reactant basin exhibits a hydrogen-bond network between N47, the neighboring T113, a water molecule present in the pocket between N47 and H83, and nearby backbone oxygens. (b) The dividing surface is characterized by changes that include (1) breaking of the hydrogen bonds around N47, (2) displacement of the water molecule from the pocket, and (3) compression of H83 into the pocket. Hydrogen bonds are indicated by orange-dashed lines; the Cu center is in orange, residue 47 is highlighted in green, and the Ru center and H83 are highlighted in pink. (c) Schematic illustration of the atomistic features governing ET in azurin. The black curve corresponds to the probability distribution, $P(d)$, of Ru–Cu distances, d , while the green-dashed curve corresponds to the distance-dependent electronic coupling, $V(d)$. Reactant basin and dividing surface configurations are indicated in red and blue, respectively.⁴³³ Adapted from ref 433. Copyright 2018 open access article distributed under CC BY-NC-ND License 4.0.

the hydrogen bond network is formed, causing the structure of the protein extended and the electron transfer distance between two metal centers long. When the water is rotated and displaced from the network, the local hydrogen bond network is broken and the structure of the proteins is compressed (Figure 26b). As a result, the distance between two metal centers becomes shorter and the electronic coupling becomes higher to facilitate the ET reaction (Figure 26c).⁴³³ A similar mechanism for tuning reaction selectivity can be found in the electro-reduction of aldehydes on Au (111), which is a PCET process. When aldehydes approach the first solvation of Au (111), the vibronic coupling between Au (111) and aldehydes, which can be extracted by integrating the overlap between the wave function of the electron in the Fermi level of Au and in the lowest unoccupied molecular orbital (LUMO) of aldehydes, is high enough to trigger the reduction reaction.⁴³⁴ Mixing alcohol in water has been found to disturb the structure of the electric interface, rotate molecules to be unfavorable for the wave function overlap and consequently decrease the reduction activity (Figure S9).⁴³⁵

5. CONCLUSIONS

The distinct H-bonding structure of water in confined environments significantly influences the catalytic activity and

selectivity, but it is still challenging to reveal the physical origin of the effect of water structure variation. Here we have reviewed the H-bonding effects of confined water on the thermodynamics and kinetics of the energy conversion and catalytic process. The geometry restriction in confined environments can lower the average number of H-bonds of water clusters and result in the enthalpy penalty of water within pores. The hydrophilic interaction between water and cavities or special H-bonding structure formed under confinement (which can be achieved via 1D, 2D, or 3D structures and confinement by ions/solvents) can further decrease the enthalpy, providing great tunability for the adsorption enthalpy and configuration of the transition state for heterogeneous (electro)catalysis. Moreover, the H-bonding structure of confined water can also affect the reaction entropy, because of the decrease in translational and rotational degree of freedom of water molecules in the local solvation environment of the reaction. The restriction of configuration during transition, as suggested by entropy variation under confinement, can have an impact on the reorganization energy, especially for charge transfer reactions (ET, PT, PCET). According to the Born model, reorganization energy is dictated by the dielectric constant, which will decrease dramatically in confined environment since the suppressed rotation in turn affects the orientational polarization of water. Therefore, the modified solvation environment in cavities can assist in relieving the free energy penalty resulting from water rearrangement during the charge transfer process. Moreover, the kinetics of the proton involved reaction is discussed via PCET theory, where the H-bonding structure can influence the proton kinetics, which may be modeled via the change in the probability of proton tunneling. The strengthened H-bond can facilitate the proton transfer since the shorter distance is required for the proton to travel. The vibronic coupling of electrons is also sensitive to the transfer distance between donor and acceptor, which is potentially dictated by the structural fluctuation of the water H-bonding network in the protein pocket and electrode surface.

The understanding of the dynamics of the confined water structure in the catalytic process is essential for pursuing the fundamental study of the water structure effect on kinetics. However, it is mainly explored by simulation works, while experimental observation of water dynamics in local reaction environments remains a significant challenge. Techniques such as dielectric spectroscopy, NMR, and ultrafast vibrational spectroscopy have traditionally been used to study the dynamics of bulk water. It is imperative to extend these insights to the catalytic and electrocatalytic interfaces. Sum Frequency Generation (SFG) is a surface-sensitive, ultrafast spectroscopic technique that could play a key role in exploring confined water structures at these interfaces.^{436–439} Additionally, the recently developed Attenuated Total Reflectance Two-Dimensional Infrared Spectroscopy (ATR-2D-IR) offers a powerful method for investigating water and proton dynamics.^{11,439,440} NMR has also been applied to study how interfacial water interacts with proteins.^{441,442} Adapting these methodologies to catalytic systems could yield crucial insights into the role of water in reaction environments. Although experimental studies on the dynamics of confined water in catalysis are currently limited, developing surface-sensitive, ultrafast characterization techniques could significantly advance our understanding of (electro)catalysis.

ASSOCIATED CONTENT**Supporting Information**

The Supporting Information is available free of charge at <https://pubs.acs.org/doi/10.1021/acs.chemrev.4c00274>.

Figures S1–S9 and Tables S1–S3: Schematic of the origin of surface charge; Schematic of transition state free energy, reaction free energy and reorganization energy; Dielectric constant of bulk and confined water as a function of temperature and pressure; Examples of spectroscopic measurements of water–solid interfaces; Comparison of water adsorption enthalpy across metal oxides, MOFs and zeolites; More examples of water confinement for tuning electrocatalytic kinetics; Tabulated DFT calculated adsorption energies and diffusion barriers of monomers and dimers on various surfaces; Tabulated values of ion–molecule distance and coordination number of first hydration shells of ions; Tabulated values of water adsorption enthalpy on 3D structures ([PDF](#))

AUTHOR INFORMATION**Corresponding Authors**

Jiayu Peng — *Electrochemical Energy Laboratory, Massachusetts Institute of Technology, Cambridge, Massachusetts 02139, United States; Department of Materials Science and Engineering, Massachusetts Institute of Technology, Cambridge, Massachusetts 02139, United States;*  [0000-0003-3696-770X](https://orcid.org/0000-0003-3696-770X); Email: jypeng@mit.edu

Reshma R. Rao — *Department of Materials, Imperial College London, London SW7 2AZ, U.K.; Grantham Institute – Climate Change and the Environment, London SW7 2AZ, United Kingdom;*  [0000-0002-6655-3105](https://orcid.org/0000-0002-6655-3105); Email: reshma.rao@imperial.ac.uk

Yang Shao-Horn — *Electrochemical Energy Laboratory, Massachusetts Institute of Technology, Cambridge, Massachusetts 02139, United States; Research Laboratory of Electronics, Department of Materials Science and Engineering, and Department of Mechanical Engineering, Massachusetts Institute of Technology, Cambridge, Massachusetts 02139, United States;*  [0000-0001-8714-2121](https://orcid.org/0000-0001-8714-2121); Email: shaohorn@mit.edu

Authors

Tao Wang — *Electrochemical Energy Laboratory, Massachusetts Institute of Technology, Cambridge, Massachusetts 02139, United States; Research Laboratory of Electronics, Massachusetts Institute of Technology, Cambridge, Massachusetts 02139, United States; Collaborative Innovation Center of Chemistry for Energy Materials, State Key Laboratory for Physical Chemistry of Solid Surfaces, College of Chemistry and Chemical Engineering, Xiamen University, Xiamen 361005, China;*  [0000-0002-3013-1947](https://orcid.org/0000-0002-3013-1947)

Haldrian Iriawan — *Electrochemical Energy Laboratory, Massachusetts Institute of Technology, Cambridge, Massachusetts 02139, United States; Department of Materials Science and Engineering, Massachusetts Institute of Technology, Cambridge, Massachusetts 02139, United States;*  [0000-0002-2997-1180](https://orcid.org/0000-0002-2997-1180)

Botao Huang — *Electrochemical Energy Laboratory, Massachusetts Institute of Technology, Cambridge, Massachusetts 02139, United States; Research Laboratory of Electronics, Massachusetts Institute of Technology, Cambridge, Massachusetts 02139, United States;*  [0000-0001-5634-5620](https://orcid.org/0000-0001-5634-5620)

Daniel Zheng — *Electrochemical Energy Laboratory, Massachusetts Institute of Technology, Cambridge, Massachusetts 02139, United States; Department of Materials Science and Engineering, Massachusetts Institute of Technology, Cambridge, Massachusetts 02139, United States;*  [0000-0002-9471-6856](https://orcid.org/0000-0002-9471-6856)

David Menga — *Electrochemical Energy Laboratory, Massachusetts Institute of Technology, Cambridge, Massachusetts 02139, United States; Research Laboratory of Electronics, Massachusetts Institute of Technology, Cambridge, Massachusetts 02139, United States*

Abhishek Aggarwal — *Electrochemical Energy Laboratory, Massachusetts Institute of Technology, Cambridge, Massachusetts 02139, United States; Research Laboratory of Electronics and Department of Materials Science and Engineering, Massachusetts Institute of Technology, Cambridge, Massachusetts 02139, United States;*  [0000-0002-3342-6484](https://orcid.org/0000-0002-3342-6484)

Shuai Yuan — *Electrochemical Energy Laboratory, Massachusetts Institute of Technology, Cambridge, Massachusetts 02139, United States; Research Laboratory of Electronics, Massachusetts Institute of Technology, Cambridge, Massachusetts 02139, United States*

John Eom — *Electrochemical Energy Laboratory, Massachusetts Institute of Technology, Cambridge, Massachusetts 02139, United States; Research Laboratory of Electronics, Massachusetts Institute of Technology, Cambridge, Massachusetts 02139, United States*

Yirui Zhang — *Electrochemical Energy Laboratory, Massachusetts Institute of Technology, Cambridge, Massachusetts 02139, United States; Department of Mechanical Engineering, Massachusetts Institute of Technology, Cambridge, Massachusetts 02139, United States*

Kaylee McCormack — *Department of Chemical Engineering, Massachusetts Institute of Technology, Cambridge, Massachusetts 02139, United States*

Yuriy Román-Leshkov — *Department of Chemical Engineering, Massachusetts Institute of Technology, Cambridge, Massachusetts 02139, United States;*  [0000-0002-0025-4233](https://orcid.org/0000-0002-0025-4233)

Jeffrey Grossman — *Department of Materials Science and Engineering, Massachusetts Institute of Technology, Cambridge, Massachusetts 02139, United States;*  [0000-0003-1281-2359](https://orcid.org/0000-0003-1281-2359)

Complete contact information is available at:
<https://pubs.acs.org/10.1021/acs.chemrev.4c00274>

Author Contributions

[†]T.W. and H.I. contributed equally to this work. CRediT: **Tao Wang** conceptualization, data curation, formal analysis, investigation, methodology, validation, writing - original draft, writing - review & editing; **Haldrian Iriawan** conceptualization, data curation, formal analysis, investigation, methodology, project administration, resources, software, validation, visualization, writing - original draft, writing - review & editing; **Jiayu Peng** data curation, formal analysis,

investigation, writing - original draft; **Reshma R. Rao** conceptualization, data curation, formal analysis, investigation, methodology, supervision, validation, writing - original draft, writing - review & editing; **Botao Huang** data curation, formal analysis, investigation, methodology, validation, visualization, writing - original draft; **Daniel J. Zheng** data curation, investigation, project administration, writing - original draft, writing - review & editing; **Davide Menga** data curation, formal analysis, investigation, project administration, writing - original draft, writing - review & editing; **Abhishek Aggarwal** visualization, writing - review & editing; **Shuai Yuan** data curation, formal analysis, investigation, writing - original draft; **John Eom** data curation, formal analysis, investigation, methodology, writing - original draft; **Yirui Zhang** data curation, formal analysis, investigation, methodology, writing - original draft; **Kaylee McCormack** data curation, formal analysis, funding acquisition, investigation, methodology, writing - original draft; **Yuriy Román-Leshkov** conceptualization, investigation, resources, writing - review & editing; **Jeffrey C. Grossman** conceptualization, investigation, resources, writing - review & editing; **Yang Shao-Horn** conceptualization, funding acquisition, investigation, methodology, project administration, resources, supervision, validation, writing - original draft, writing - review & editing.

Notes

The authors declare no competing financial interest.

Biographies

Tao Wang received his Ph.D. degree at Xiamen University in 2019. During 2018 to 2019, he conducted research at Massachusetts Institute of Technology under the supervisor of Prof. Yang Shao-Horn. Afterwards, he worked as a postdoctoral researcher in the group of Prof. Shi-Gang Sun at Xiamen University. Presently, he is a professor in Xiamen University. His research mainly focuses on electrolyte effects of electrocatalysis, which is investigated through *in situ* spectroscopy and molecular dynamics simulations.

Haldrian Iriawan is a Ph.D. candidate in the Department of Materials Science and Engineering at the Massachusetts Institute of Technology (MIT), advised by Prof. Yang Shao-Horn. His research focuses on tailored approaches for the electrocatalytic activation of small molecules in aqueous and nonaqueous systems for the decarbonization of fuels and chemicals. Prior to MIT, he earned his undergraduate degree in Materials Science and Engineering from Imperial College London in 2021, where he worked on modelling nitrogen electrocatalysis on transition metal oxides.

Jiayu Peng is an incoming Assistant Professor (starting in January 2025) in the Department of Materials Design and Innovation at the University at Buffalo. He obtained his Ph.D. in Materials Science and Engineering from the Massachusetts Institute of Technology (MIT) in 2022, after which he was a Postdoctoral Associate in the same department at MIT. His research group aims to combine data science and machine learning with materials physics and surface chemistry to elucidate new physical principles and accelerate materials discovery for transformative opportunities in decarbonization and sustainability.

Reshma R Rao is a Royal Academy of Engineering Research Fellow in the Department of Materials and Grantham Institute–Climate Change and the Environment, Imperial College London. She obtained her Ph.D. under the supervision of Prof. Yang Shao-Horn at the Massachusetts Institute of Technology in 2019. Her research focusses on understanding electrochemical reactivity at solid–liquid interfaces

using operando spectroscopic techniques to design active, stable, selective and low-cost catalysts for energy conversion technologies.

Botao Huang is a research scientist at the Electrochemical Energy Lab (EEL) and the Research Laboratory of Electronics (RLE) at the Massachusetts Institute of Technology (MIT). He earned his Ph.D. in Chemical and Process Engineering from the University of Lorraine in 2012, where he investigated degradation mechanisms in proton-exchange membrane (PEM) fuel cells. His research focuses on the interplay between electrolytes and (proton-coupled) electron transfer kinetics, particularly the relationship between electrochemical reaction rates, selectivity, and liquid/solid interfacial structures.

Daniel Zheng is a PhD candidate in the Department of Materials Science and Engineering at the Massachusetts Institute of Technology (MIT), coadvised by Prof. Yang Shao-Horn and Prof. Yuriy Román-Leshkov. His research aims to advance the understanding and design of supramolecular chemistries as electrocatalysts for energy conversion technologies. He also works on developing high throughput synthesis and screening techniques to discover new descriptors of transition metal oxides and high entropy alloy electrocatalysts. Prior to joining MIT, he earned his BS in Materials Science and Engineering from Cornell University in 2019, where he researched postsynthetic methods for synthesizing metastable nanoparticles for electrocatalysis applications.

Davide Menga is currently a postdoctoral researcher in the Electrochemical Energy Lab at the Massachusetts Institute of Technology, working with Professor Yang Shao-Horn. He earned his Ph.D. from the Technical University of Munich, where he worked in the group of Professor Hubert Gasteiger on the development of catalysts for the oxygen reduction reaction. His research spans both fundamental studies, where he focuses on understanding reaction mechanisms and tuning interfaces to enhance reaction rates, as well as applied work on the device level, aimed at improving the performance and scalability of electrochemical systems.

Abhishek Aggarwal is a postdoctoral associate working with Prof. Subramanian Sankaranarayanan at the Argonne National Laboratory and the University of Illinois Chicago since April 2024. He received his Ph.D. in Physics in 2022 from the Indian Institute of Science under the supervision of Prof. Prabal K Maiti. During his Ph.D., he used various state-of-the-art computational tools, such as MD, DFT, and ML techniques, to understand the charge transport properties of biomolecular systems. Immediately after receiving his Ph.D., he worked at MIT for the next two years as a postdoctoral associate from March 2022–2024 and was coadvised by Prof. Yang Shao-Horn and Prof. Jeffrey Grossman. While at MIT, his research focused on modeling the electrolyte-electrode interfaces, liquid electrolytes, and polymer electrolytes. He is currently working on water–oil interfaces and ice formation on glass substrates in the Sankaranarayanan group.

Shuai Yuan received his B.S. in Chemistry from Shandong University in 2013 and his Ph.D. in Chemistry from Texas A&M University in 2018. His thesis focuses on the synthesis and functionalization of stable metal–organic frameworks. He then moved to MIT for postdoctoral research, where he explored the application of MOFs for electrocatalysis. In 2021, he joined Nanjing University as a Professor of Chemistry. His research focused on the design of synergistic catalysts using multicomponent metal–organic frameworks.

John Eom earned his Ph.D. from Cornell University in 2020, where he worked on *in situ* spectroscopy of electrochemically interesting materials for fuel cell and battery applications and was advised by Prof. Jin Suntivich. He then joined the Massachusetts Institute of Technology as a Postdoctoral Associate, advised by Prof. Yang Shao-

Horn. He is now a Senior Member of the Technical Staff at QuantumScape.

Yirui Zhang is a Schmidt Science Fellow at Stanford University. She received her Ph.D. in Mechanical Engineering from the Massachusetts Institute of Technology in 2022 and her B.S. in Mechanical Engineering from Tsinghua University, China, in 2017. Her research focuses on understanding and advancing material interfaces for energy storage and biosensing applications. Specifically, she develops *in situ* spectroscopy and electrochemical methods to gain molecular-scale insights that inform design principles for electrochemical and photochemical conversion.

Kaylee McCormack is a Ph.D. candidate in Yuriy Roman's lab studying heterogeneous transition metal catalysis toward applications in sustainable energy. She completed a master's thesis in chemical engineering on industrial methanol to formaldehyde catalyst deactivation at DTU as part of a Fulbright Grant in 2018 and earned her Master's in chemical engineering practice under Yuriy Román in 2023. Her research interests include leveraging catalytic design principles toward liquid organic hydrogen carriers and fuel cells. She will defend her thesis in 2025.

Yuriy Román-Leshkov is the Robert T. Haslam (1911) Professor in Chemical Engineering at MIT, with a joint appointment in the Department of Chemistry at MIT. He earned his B.S.E. in Chemical Engineering from the University of Pennsylvania in 2002. After working in industry for a year, he received his Ph.D. in Chemical and Biological Engineering from the University of Wisconsin—Madison in 2008, working under the supervision of Professor James A. Dumesic. He then moved to the California Institute of Technology to do postdoctoral research in the group of Professor Mark E. Davis. At MIT, his research lies at the interface of heterogeneous catalysis and materials design to tackle relevant problems associated with sustainable energy, biofuels, and renewable chemicals. His group applies a wide range of synthetic, spectroscopic, and reaction engineering tools to study the chemical transformation of molecules on catalytic surfaces. Among his honors are the Paul H. Emmett Award in Fundamental Catalysis, the ACS Early Career in Catalysis Award, an NSF Career Award, and the Rutherford Aris Award. He was named a Blavatnik Finalist in 2022.

Jeffrey Grossman earned a BA in physics at Johns Hopkins University in 1991 and did graduate work at the University of Illinois Urbana-Champaign, earning a Ph.D. in theoretical physics in 1996. He was a postdoctoral researcher at the University of California at Berkeley and then a Lawrence Fellow at the Lawrence Livermore National Laboratory. In 2009 he joined MIT, where he developed a research program known for its contributions to energy conversion, energy storage, membranes, and clean-water technologies. He has published more than 200 scientific papers, holds 17 current or pending patents, and recently cofounded two Massachusetts companies to commercialize novel membrane materials for efficient industrial separations.

Yang Shao-Horn is the JR East Professor of Engineering and a faculty member in the Department of Mechanical Engineering, Department of Materials Science and Engineering and the Research Laboratory of Electronics at MIT. Her research is centered on physical/material chemistry to tune kinetics and dynamics in enabling energy storage and making chemicals and fuels. Yang is a scientist and entrepreneur in electrochemical science and engineering with 400+ publications. She has advised 100+ students and postdocs at MIT, who are now pursuing successful careers in industry including Tesla, Amazon and Apple, startups, and academia (~40) across the US, Europe and Asia. Yang is a member of the National Academy of Engineering and a fellow of the American Association for the Advancement of Science,

the Electrochemical Society, the National Academy of Inventors and the International Society of Electrochemistry.

ACKNOWLEDGMENTS

Research support at MIT by the DOE-BES through the Energy Frontier Research Center DE-SC0023415 (Center for Electrochemical Dynamics And Reaction on Surfaces) is acknowledged. This work was supported by the Advanced Research Projects Agency Energy (ARPA-E), US Department of Energy under award number DE-AR0001220, and the Toyota Research Institute through the Accelerated Materials Design and Discovery programme. H.I. and Y.S.-H. acknowledge support from the MIT Climate Grand Challenge - Center for Electrification and Decarbonization of Industry (MIT-CEDI) Thrust 4 - Ammonia. We acknowledge the gift to the MIT Electrochemical Energy Laboratory from Tosoh and the Mathworks Seed Fund from MIT Department of Mechanical Engineering.

REFERENCES

- (1) Amann-Winkel, K.; Bellissent-Funel, M.-C.; Bove, L. E.; Loerting, T.; Nilsson, A.; Paciaroni, A.; Schlesinger, D.; Skinner, L. X-Ray and Neutron Scattering of Water. *Chem. Rev.* **2016**, *116* (13), 7570–7589.
- (2) Bakker, H. J.; Skinner, J. L. Vibrational Spectroscopy as a Probe of Structure and Dynamics in Liquid Water. *Chem. Rev.* **2010**, *110* (3), 1498–1517.
- (3) Skinner, L. B.; Huang, C.; Schlesinger, D.; Pettersson, L. G. M.; Nilsson, A.; Benmore, C. J. Benchmark Oxygen-Oxygen Pair-Distribution Function of Ambient Water from x-Ray Diffraction Measurements with a Wide Q -Range. *J. Chem. Phys.* **2013**, *138* (7), DOI: [10.1063/1.4790861](https://doi.org/10.1063/1.4790861).
- (4) Pople, J. A. Molecular Association in Liquids II. A Theory of the Structure of Water. *Proc. R. Soc. Lond A Math Phys. Sci.* **1951**, *205* (1081), 163–178.
- (5) Soper, A. K.; Ricci, M. A. Structures of High-Density and Low-Density Water. *Phys. Rev. Lett.* **2000**, *84* (13), 2881–2884.
- (6) Kim, K. H.; Amann-Winkel, K.; Giovambattista, N.; Späh, A.; Perakis, F.; Pathak, H.; Parada, M. L.; Yang, C.; Mariedahl, D.; Eklund, T.; Lane, Thomas. J.; You, S.; Jeong, S.; Weston, M.; Lee, J. H.; Eom, I.; Kim, M.; Park, J.; Chun, S. H.; Poole, P. H.; Nilsson, A. Experimental Observation of the Liquid-Liquid Transition in Bulk Supercooled Water under Pressure. *Science* **2020**, *370* (6519), 978–982.
- (7) Li, F.; Cui, Q.; He, Z.; Cui, T.; Zhang, J.; Zhou, Q.; Zou, G.; Sasaki, S. High Pressure-Temperature Brillouin Study of Liquid Water: Evidence of the Structural Transition from Low-Density Water to High-Density Water. *J. Chem. Phys.* **2005**, *123* (17), 174511.
- (8) Bertram, C.; Fang, W.; Pedevilla, P.; Michaelides, A.; Morgenstern, K. Anomalously Low Barrier for Water Dimer Diffusion on Cu(111). *Nano Lett.* **2019**, *19* (5), 3049–3056.
- (9) Nilekar, A. U.; Greeley, J.; Mavrikakis, M. A Simple Rule of Thumb for Diffusion on Transition-Metal Surfaces. *Angew. Chem., Int. Ed.* **2006**, *45* (42), 7046–7049.
- (10) Zhang, C.; Galli, G. Dipolar Correlations in Liquid Water. *J. Chem. Phys.* **2014**, *141* (8), 084504.
- (11) Thämer, M.; De Marco, L.; Ramasesha, K.; Mandal, A.; Tokmakoff, A. Ultrafast 2D IR Spectroscopy of the Excess Proton in Liquid Water. *Science* **2015**, *350* (6256), 78–82.
- (12) Yang, J.; Dettori, R.; Nunes, J. P. F.; List, N. H.; Biasin, E.; Centurion, M.; Chen, Z.; Cordones, A. A.; Deponte, D. P.; Heinz, T. F.; Kozina, M. E.; Ledbetter, K.; Lin, M.-F.; Lindenberg, A. M.; Mo, M.; Nilsson, A.; Shen, X.; Wolf, T. J. A.; Donadio, D.; Gaffney, K. J.; Martinez, T. J.; Wang, X. Direct Observation of Ultrafast Hydrogen Bond Strengthening in Liquid Water. *Nature* **2021**, *596* (7873), 531–535.

- (13) Corridoni, T.; Mancinelli, R.; Ricci, M. A.; Bruni, F. Viscosity of Aqueous Solutions and Local Microscopic Structure. *J. Phys. Chem. B* **2011**, *115* (48), 14008–14013.
- (14) Horne, R. A.; Johnson, D. S. The Viscosity of Water under Pressure. *J. Phys. Chem.* **1966**, *70* (7), 2182–2190.
- (15) Zhu, Y.; Granick, S. Viscosity of Interfacial Water. *Phys. Rev. Lett.* **2001**, *87* (9), 096104.
- (16) Brini, E.; Fennell, C. J.; Fernandez-Serra, M.; Hribar-Lee, B.; Lukšić, M.; Dill, K. A. How Water's Properties Are Encoded in Its Molecular Structure and Energies. *Chem. Rev.* **2017**, *117* (19), 12385–12414.
- (17) Eisenberg, D.; Kauzmann, W. *The Structure and Properties of Water*; Oxford University Press, 2005; Vol. 9780198570264. DOI: [10.1093/acprof:oso/9780198570264.001.0001](https://doi.org/10.1093/acprof:oso/9780198570264.001.0001).
- (18) Snyder, P. W.; Lockett, M. R.; Moustakas, D. T.; Whitesides, G. M. Is It the Shape of the Cavity, or the Shape of the Water in the Cavity? *Eur. Phys. J. Spec Top.* **2014**, *223* (5), 853–891.
- (19) Åqvist, J.; Kazemi, M.; Isaksen, G. V.; Brandsdal, B. O. Entropy and Enzyme Catalysis. *Acc. Chem. Res.* **2017**, *50* (2), 199–207.
- (20) Resasco, D. E.; Crossley, S. P.; Wang, B.; White, J. L. Interaction of Water with Zeolites: A Review. *Catalysis Reviews* **2021**, *63* (2), 302–362.
- (21) Bukowski, B. C.; Bates, J. S.; Gounder, R.; Greeley, J. Defect-Mediated Ordering of Condensed Water Structures in Microporous Zeolites. *Angew. Chem., Int. Ed.* **2019**, *58* (46), 16422–16426.
- (22) Furukawa, H.; Gándara, F.; Zhang, Y.-B.; Jiang, J.; Queen, W. L.; Hudson, M. R.; Yaghi, O. M. Water Adsorption in Porous Metal-Organic Frameworks and Related Materials. *J. Am. Chem. Soc.* **2014**, *136* (11), 4369–4381.
- (23) Xu, W.; Yaghi, O. M. Metal-Organic Frameworks for Water Harvesting from Air, Anywhere, Anytime. *ACS Cent Sci.* **2020**, *6* (8), 1348–1354.
- (24) Zhou, T.; Bai, P.; Siepmann, J. I.; Clark, A. E. Deconstructing the Confinement Effect upon the Organization and Dynamics of Water in Hydrophobic Nanoporous Materials: Lessons Learned from Zeolites. *J. Phys. Chem. C* **2017**, *121* (40), 22015–22024.
- (25) Shen, Y. R.; Ostroverkhov, V. Sum-Frequency Vibrational Spectroscopy on Water Interfaces: Polar Orientation of Water Molecules at Interfaces. *Chem. Rev.* **2006**, *106* (4), 1140–1154.
- (26) Nihonyanagi, S.; Yamaguchi, S.; Tahara, T. Direct Evidence for Orientational Flip-Flop of Water Molecules at Charged Interfaces: A Heterodyne-Detected Vibrational Sum Frequency Generation Study. *J. Chem. Phys.* **2009**, *130* (20), 204704.
- (27) Gonella, G.; Backus, E. H. G.; Nagata, Y.; Bonthuis, D. J.; Loche, P.; Schlaich, A.; Netz, R. R.; Kühlne, A.; McCrum, I. T.; Koper, M. T. M.; Wolf, M.; Winter, B.; Meijer, G.; Campen, R. K.; Bonn, M. Water at Charged Interfaces. *Nat. Rev. Chem.* **2021**, *5* (7), 466–485.
- (28) Xu, A.; Govindarajan, N.; Kastlunger, G.; Vijay, S.; Chan, K. Theories for Electrolyte Effects in CO₂ Electroreduction. *Acc. Chem. Res.* **2022**, *55* (4), 495–503.
- (29) Toney, M. F.; Howard, J. N.; Richer, J.; Borges, G. L.; Gordon, J. G.; Melroy, O. R.; Wiesler, D. G.; Yee, D.; Sorensen, L. B. Voltage-Dependent Ordering of Water Molecules at an Electrode-Electrolyte Interface. *Nature* **1994**, *368* (6470), 444–446.
- (30) Wang, J.; Ocko, B. M.; Davenport, A. J.; Isaacs, H. S. *In Situ* x-Ray-Diffraction and -Reflectivity Studies of the Au(111)/Electrolyte Interface: Reconstruction and Anion Adsorption. *Phys. Rev. B* **1992**, *46* (16), 10321–10338.
- (31) Danielewicz-Ferchmin, I. Phase Diagram of Hydration Shells in Ionic Solutions. *J. Phys. Chem.* **1995**, *99* (15), 5658–5665.
- (32) Fumagalli, L.; Esfandiar, A.; Fabregas, R.; Hu, S.; Ares, P.; Janardanan, A.; Yang, Q.; Radha, B.; Taniguchi, T.; Watanabe, K.; Gomila, G.; Novoselov, K. S.; Geim, A. K. Anomalously Low Dielectric Constant of Confined Water. *Science* **2018**, *360* (6395), 1339–1342.
- (33) Huang, B.; Rao, R. R.; You, S.; Hpone Myint, K.; Song, Y.; Wang, Y.; Ding, W.; Giordano, L.; Zhang, Y.; Wang, T.; Muy, S.; Katayama, Y.; Grossman, J. C.; Willard, A. P.; Xu, K.; Jiang, Y.; Shao-Horn, Y. Cation- and PH-Dependent Hydrogen Evolution and Oxidation Reaction Kinetics. *JACS Au* **2021**, *1* (10), 1674–1687.
- (34) Sugahara, A.; Ando, Y.; Kajiyama, S.; Yazawa, K.; Gotoh, K.; Otani, M.; Okubo, M.; Yamada, A. Negative Dielectric Constant of Water Confined in Nanosheets. *Nat. Commun.* **2019**, *10* (1), 850.
- (35) Pascal, T. A.; Goddard, W. A.; Jung, Y. Entropy and the Driving Force for the Filling of Carbon Nanotubes with Water. *Proc. Natl. Acad. Sci. U. S. A.* **2011**, *108* (29), 11794–11798.
- (36) Bangle, R. E.; Schneider, J.; Conroy, D. T.; Aramburu-Trošelj, B. M.; Meyer, G. J. Kinetic Evidence That the Solvent Barrier for Electron Transfer Is Absent in the Electric Double Layer. *J. Am. Chem. Soc.* **2020**, *142* (35), 14940–14946.
- (37) Huang, B.; Myint, K. H.; Wang, Y.; Zhang, Y.; Rao, R. R.; Sun, J.; Muy, S.; Katayama, Y.; Corchado Garcia, J.; Fragedakis, D.; Grossman, J. C.; Bazant, M. Z.; Xu, K.; Willard, A. P.; Shao-Horn, Y. Cation-Dependent Interfacial Structures and Kinetics for Outer-Sphere Electron-Transfer Reactions. *J. Phys. Chem. C* **2021**, *125* (8), 4397–4411.
- (38) Bregante, D. T.; Chan, M. C.; Tan, J. Z.; Ayla, E. Z.; Nicholas, C. P.; Shukla, D.; Flaherty, D. W. The Shape of Water in Zeolites and Its Impact on Epoxidation Catalysis. *Nat. Catal.* **2021**, *4* (9), 797–808.
- (39) Bregante, D. T.; Flaherty, D. W. Impact of Specific Interactions Among Reactive Surface Intermediates and Confined Water on Epoxidation Catalysis and Adsorption in Lewis Acid Zeolites. *ACS Catal.* **2019**, *9* (12), 10951–10962.
- (40) Bregante, D. T.; Johnson, A. M.; Patel, A. Y.; Ayla, E. Z.; Cordon, M. J.; Bukowski, B. C.; Greeley, J.; Gounder, R.; Flaherty, D. W. Cooperative Effects between Hydrophilic Pores and Solvents: Catalytic Consequences of Hydrogen Bonding on Alkene Epoxidation in Zeolites. *J. Am. Chem. Soc.* **2019**, *141* (18), 7302–7319.
- (41) Potts, D. S.; Bregante, D. T.; Adams, J. S.; Torres, C.; Flaherty, D. W. Influence of Solvent Structure and Hydrogen Bonding on Catalysis at Solid-Liquid Interfaces. *Chem. Soc. Rev.* **2021**, *50* (22), 12308–12337.
- (42) Chen, L. D.; Urushihara, M.; Chan, K.; Nørskov, J. K. Electric Field Effects in Electrochemical CO₂ Reduction. *ACS Catal.* **2016**, *6* (10), 7133–7139.
- (43) Ludwig, T.; Gauthier, J. A.; Brown, K. S.; Ringe, S.; Nørskov, J. K.; Chan, K. Solvent-Adsorbate Interactions and Adsorbate-Specific Solvent Structure in Carbon Dioxide Reduction on a Stepped Cu Surface. *J. Phys. Chem. C* **2019**, *123* (10), 5999–6009.
- (44) Resasco, J.; Chen, L. D.; Clark, E.; Tsai, C.; Hahn, C.; Jaramillo, T. F.; Chan, K.; Bell, A. T. Promoter Effects of Alkali Metal Cations on the Electrochemical Reduction of Carbon Dioxide. *J. Am. Chem. Soc.* **2017**, *139* (32), 11277–11287.
- (45) Wang, T.; Zhang, Y.; Huang, B.; Cai, B.; Rao, R. R.; Giordano, L.; Sun, S.-G.; Shao-Horn, Y. Enhancing Oxygen Reduction Electrocatalysis by Tuning Interfacial Hydrogen Bonds. *Nat. Catal.* **2021**, *4* (9), 753–762.
- (46) Marcus, R. A. On the Theory of Oxidation-Reduction Reactions Involving Electron Transfer. I. *J. Chem. Phys.* **1956**, *24* (5), 966–978.
- (47) Marcus, R. A. Electron Transfer Reactions in Chemistry. Theory and Experiment. *Rev. Mod. Phys.* **1993**, *65* (3), 599–610.
- (48) Hillyer, M. B.; Gibb, B. C. Molecular Shape and the Hydrophobic Effect. *Annu. Rev. Phys. Chem.* **2016**, *67*, 307–329.
- (49) Moskowitz, I.; Snyder, M. A.; Mittal, J. Water Transport through Functionalized Nanotubes with Tunable Hydrophobicity. *J. Chem. Phys.* **2014**, *141* (18), 18C532.
- (50) Chong, S.-H.; Ham, S. Dynamics of Hydration Water Plays a Key Role in Determining the Binding Thermodynamics of Protein Complexes. *Sci. Rep.* **2017**, *7* (1), 8744.
- (51) Árnadóttir, L.; Stuve, E. M.; Jónsson, H. Adsorption of Water Monomer and Clusters on Platinum(111) Terrace and Related Steps and Kinks II. Surface Diffusion. *Surf. Sci.* **2012**, *606* (3–4), 233.
- (52) Fang, W.; Chen, J.; Pedevilla, P.; Li, X.-Z.; Richardson, J. O.; Michaelides, A. Origins of Fast Diffusion of Water Dimers on Surfaces. *Nat. Commun.* **2020**, *11* (1), 1689.

- (53) Raju, M.; van Duin, A.; Ihme, M. Phase Transitions of Ordered Ice in Graphene Nanocapillaries and Carbon Nanotubes. *Sci. Rep.* **2018**, *8* (1), 3851.
- (54) McGrath, M. J.; Siepmann, J. I.; Kuo, I.-F. W.; Mundy, C. J. Spatial Correlation of Dipole Fluctuations in Liquid Water. *Mol. Phys.* **2007**, *105* (10), 1411–1417.
- (55) Keutsch, F. N.; Saykally, R. J. Water Clusters: Untangling the Mysteries of the Liquid, One Molecule at a Time. *Proc. Natl. Acad. Sci. U. S. A.* **2001**, *98* (19), 10533–10540.
- (56) Ludwig, R. The Effect of Hydrogen Bonding on the Thermodynamic and Spectroscopic Properties of Molecular Clusters and Liquids. *Phys. Chem. Chem. Phys.* **2002**, *4* (22), 5481–5487.
- (57) Jorgensen, W. L.; Chandrasekhar, J.; Madura, J. D.; Impey, R. W.; Klein, M. L. Comparison of Simple Potential Functions for Simulating Liquid Water. *J. Chem. Phys.* **1983**, *79* (2), 926–935.
- (58) Ball, P. Water Is an Active Matrix of Life for Cell and Molecular Biology. *Proc. Natl. Acad. Sci. U. S. A.* **2017**, *114* (51), 13327–13335.
- (59) Sterpone, F.; Stirnemann, G.; Hynes, J. T.; Laage, D. Water Hydrogen-Bond Dynamics around Amino Acids: The Key Role of Hydrophilic Hydrogen-Bond Acceptor Groups. *J. Phys. Chem. B* **2010**, *114* (5), 2083–2089.
- (60) Wolfenden, R.; Snider, M. J. The Depth of Chemical Time and the Power of Enzymes as Catalysts. *Acc. Chem. Res.* **2001**, *34* (12), 938–945.
- (61) Bruice, T. C.; Lightstone, F. C. Ground State and Transition State Contributions to the Rates of Intramolecular and Enzymatic Reactions. *Acc. Chem. Res.* **1999**, *32* (2), 127–136.
- (62) Shurki, A.; Štrajbl, M.; Villà, J.; Warshel, A. How Much Do Enzymes Really Gain by Restraining Their Reacting Fragments? *J. Am. Chem. Soc.* **2002**, *124* (15), 4097–4107.
- (63) Villà, J.; Štrajbl, M.; Glennon, T. M.; Sham, Y. Y.; Chu, Z. T.; Warshel, A. How Important Are Entropic Contributions to Enzyme Catalysis? *Proc. Natl. Acad. Sci. U. S. A.* **2000**, *97* (22), 11899–11904.
- (64) Sievers, A.; Beringer, M.; Rodnina, M. V.; Wolfenden, R. The Ribosome as an Entropy Trap. *Proc. Natl. Acad. Sci. U. S. A.* **2004**, *101* (21), 7897–7901.
- (65) Trobro, S.; Åqvist, J. Mechanism of Peptide Bond Synthesis on the Ribosome. *Proc. Natl. Acad. Sci. U. S. A.* **2005**, *102* (35), 12395–12400.
- (66) Rudorf, S.; Thommen, M.; Rodnina, M. V.; Lipowsky, R. Deducing the Kinetics of Protein Synthesis In Vivo from the Transition Rates Measured In Vitro. *PLoS Comput. Biol.* **2014**, *10* (10), No. e1003909.
- (67) Bagchi, B. The Entropy of Water. In *Water in Biological and Chemical Processes*; Cambridge University Press: Cambridge, 2013; pp 287–304. DOI: [10.1017/CBO9781139583947.024](https://doi.org/10.1017/CBO9781139583947.024).
- (68) Geissler, P. L.; Dellago, C.; Chandler, D.; Hutter, J.; Parrinello, M. Autoionization in Liquid Water. *Science* **2001**, *291* (5511), 2121–2124.
- (69) Schmidt, K. H.; Ander, S. M. Formation and Recombination of the Hydronium Ion (H_3O^+) and Hydroxide in Irradiated Water. *J. Phys. Chem.* **1969**, *73* (9), 2846–2852.
- (70) Collinge, G.; Yuk, S. F.; Nguyen, M.-T.; Lee, M.-S.; Glezakou, V.-A.; Rousseau, R. Effect of Collective Dynamics and Anharmonicity on Entropy in Heterogenous Catalysis: Building the Case for Advanced Molecular Simulations. *ACS Catal.* **2020**, *10* (16), 9236–9260.
- (71) Li, Y.; Li, L.; Yu, J. Applications of Zeolites in Sustainable Chemistry. *Chem.* **2017**, *3* (6), 928–949.
- (72) Lenton, S.; Rhys, N. H.; Towey, J. J.; Soper, A. K.; Dougan, L. Highly Compressed Water Structure Observed in a Perchlorate Aqueous Solution. *Nat. Commun.* **2017**, *8*, 919.
- (73) Marcus, Y. Effect of Ions on the Structure of Water: Structure Making and Breaking. *Chem. Rev.* **2009**, *109* (3), 1346–1370.
- (74) Frank, H. S.; Evans, M. W. Free Volume and Entropy in Condensed Systems III. Entropy in Binary Liquid Mixtures; Partial Molal Entropy in Dilute Solutions; Structure and Thermodynamics in Aqueous Electrolytes. *J. Chem. Phys.* **1945**, *13* (11), 507–532.
- (75) Corey, V. B. Adiabatic Compressibilities of Some Aqueous Ionic Solutions and Their Variation with Indicated Liquid Structure of the Water. *Phys. Rev.* **1943**, *64* (11–12), 350–357.
- (76) Collins, K. D.; Washabaugh, M. W. The Hofmeister Effect and the Behaviour of Water at Interfaces. *Q. Rev. Biophys.* **1985**, *18* (4), 323–422.
- (77) Stewart, G. W. The Variation in the Structure of Water in Ionic Solutions. II. *J. Chem. Phys.* **1943**, *11* (2), 72–74.
- (78) Kujumzelis, T. G. Über Die Änderung Der Struktur Des Wassers Durch Ionen. *Zeitschrift für Physik* **1938**, *110* (11–12), 742.
- (79) Vinogradov, E. V.; Smirnov, P. R.; Trostin, V. N. Structure of Hydrated Complexes Formed by Metal Ions of Groups I–III of the Periodic Table in Aqueous Electrolyte Solutions under Ambient Conditions. *Russian Chemical Bulletin* **2003**, *52*, 1253–1271.
- (80) Novikov, A. G.; Rodnikova, M. N.; Savostin, V. V.; Sobolev, O. V. The Study of Hydration Effects in Aqueous Solutions of LiCl and CsCl by Inelastic Neutron Scattering. *J. Mol. Liq.* **1999**, *82* (1–2), 83–104.
- (81) Mancinelli, R.; Botti, A.; Bruni, F.; Ricci, M. A.; Soper, A. K. Perturbation of Water Structure Due to Monovalent Ions in Solution. *Phys. Chem. Chem. Phys.* **2007**, *9* (23), 2959.
- (82) Bouazizi, S.; Nasr, S. Local Order in Aqueous Lithium Chloride Solutions as Studied by X-Ray Scattering and Molecular Dynamics Simulations. *J. Mol. Struct.* **2007**, *837* (1–3), 206–213.
- (83) Bouazizi, S.; Nasr, S.; Jaïdane, N.; Bellissent-Funel, M.-C. Local Order in Aqueous NaCl Solutions and Pure Water: X-Ray Scattering and Molecular Dynamics Simulations Study. *J. Phys. Chem. B* **2006**, *110* (46), 23515–23523.
- (84) Harsányi, I.; Jóvári, P.; Mészáros, G.; Pusztai, L.; Bopp, P. A. Neutron and X-Ray Diffraction Studies of Aqueous Rubidium Bromide Solutions. *J. Mol. Liq.* **2007**, *131*–132 (SPEC. ISS.), 60–64.
- (85) Mancinelli, R.; Botti, A.; Bruni, F.; Ricci, M. A.; Soper, A. K. Hydration of Sodium, Potassium, and Chloride Ions in Solution and the Concept of Structure Maker/Breaker. *J. Phys. Chem. B* **2007**, *111* (48), 13570–13577.
- (86) Soper, A. K.; Weckström, K. Ion Solvation and Water Structure in Potassium Halide Aqueous Solutions. *Biophys Chem.* **2006**, *124* (3), 180–191.
- (87) Chen, Y.; Okur, H. I.; Gomopoulos, N.; Macias-Romero, C.; Cremer, P. S.; Petersen, P. B.; Tocci, G.; Wilkins, D. M.; Liang, C.; Ceriotti, M.; Roke, S. Electrolytes Induce Long-Range Orientational Order and Free Energy Changes in the H-Bond Network of Bulk Water. *Sci. Adv.* **2016**, *2* (4), DOI: [10.1126/sciadv.1501891](https://doi.org/10.1126/sciadv.1501891).
- (88) Krestov, G. A. The Thermodynamic Characteristics of Structural Changes in Water Connected with the Hydration of Polyatomic and Complex Ions. *Journal of Structural Chemistry* **1963**, *3* (4), 391–398.
- (89) Abraham, M. H.; Liszi, J. Calculations on Ionic Solvation. Part 2.—Entropies of Solvation of Gaseous Univalent Ions Using a One-Layer Continuum Model. *Journal of the Chemical Society, Faraday Transactions 1: Physical Chemistry in Condensed Phases* **1978**, *74* (0), 2858.
- (90) Abraham, M. H.; Liszi, J.; Papp, E. Calculations on Ionic Solvation. Part 6.—Structure-Making and Structure-Breaking Effects of Alkali Halide Ions from Electrostatic Entropies of Solvation. Correlation with Viscosity B-Coefficients, Nuclear Magnetic Resonance B'-Coefficients and Partial Molal Volumes. *Journal of the Chemical Society, Faraday Transactions 1: Physical Chemistry in Condensed Phases* **1982**, *78* (1), 197.
- (91) Marcus, Y.; Loewenschuss, A. Chapter 4. Standard Entropies of Hydration of Ions. *Annual Reports Section "C" (Physical Chemistry)* **1984**, *81*, 81.
- (92) Marcus, Y. Viscosity B-Coefficients, Structural Entropies and Heat Capacities, and the Effects of Ions on the Structure of Water. *J. Solution Chem.* **1994**, *23* (7), 831–848.
- (93) Marcus, Y. The Hydration Entropies of Ions and Their Effects on the Structure of Water. *Journal of the Chemical Society, Faraday Transactions 1: Physical Chemistry in Condensed Phases* **1986**, *82* (1), 233.

- (94) Hummer, G.; Rasaiah, J. C.; Noworyta, J. P. Water Conduction through the Hydrophobic Channel of a Carbon Nanotube. *Nature* **2001**, *414* (6860), 188–190.
- (95) Koga, K.; Gao, G. T.; Tanaka, H.; Zeng, X. C. Formation of Ordered Ice Nanotubes inside Carbon Nanotubes. *Nature* **2001**, *412* (6849), 802–805.
- (96) Takaiwa, D.; Hatano, I.; Koga, K.; Tanaka, H. Phase Diagram of Water in Carbon Nanotubes. *Proc. Natl. Acad. Sci. U. S. A.* **2008**, *105* (1), 39–43.
- (97) Cambré, S.; Schoeters, B.; Luyckx, S.; Goovaerts, E.; Wenseleers, W. Experimental Observation of Single-File Water Filling of Thin Single-Wall Carbon Nanotubes Down to Chiral Index (5,3). *Phys. Rev. Lett.* **2010**, *104* (20), 207401.
- (98) Chandler, D. Interfaces and the Driving Force of Hydrophobic Assembly. *Nature* **2005**, *437* (7059), 640–647.
- (99) Lin, S.-T.; Maiti, P. K.; Goddard, W. A. Two-Phase Thermodynamic Model for Efficient and Accurate Absolute Entropy of Water from Molecular Dynamics Simulations. *J. Phys. Chem. B* **2010**, *114* (24), 8191–8198.
- (100) Chakraborty, S.; Kumar, H.; Dasgupta, C.; Maiti, P. K. Confined Water: Structure, Dynamics, and Thermodynamics. *Acc. Chem. Res.* **2017**, *50* (9), 2139–2146.
- (101) Kolesnikov, A. I.; Zanotti, J.-M.; Loong, C.-K.; Thiagarajan, P.; Moravsky, A. P.; Loutfy, R. O.; Burnham, C. J. Anomalously Soft Dynamics of Water in a Nanotube: A Revelation of Nanoscale Confinement. *Phys. Rev. Lett.* **2004**, *93* (3), 035503.
- (102) Sprik, M. Hydrogen Bonding and the Static Dielectric Constant in Liquid Water. *J. Chem. Phys.* **1991**, *95* (9), 6762–6769.
- (103) Simulation of Electrostatic Systems in Periodic Boundary Conditions. III. Further Theory and Applications. *Proceedings of the Royal Society of London. A. Mathematical and Physical Sciences* **1983**, *388* (1794), 177.
- (104) Allen, M. P.; Wilson, M. R. Computer Simulation of Liquid Crystals. *J. Comput. Aided Mol. Des.* **1989**, *3* (4), 335–353.
- (105) Popov, I.; Ishai, P. B.; Khamzin, A.; Feldman, Y. The Mechanism of the Dielectric Relaxation in Water. *Phys. Chem. Chem. Phys.* **2016**, *18* (20), 13941–13953.
- (106) Artemov, V. G. A Unified Mechanism for Ice and Water Electrical Conductivity from Direct Current to Terahertz. *Phys. Chem. Chem. Phys.* **2019**, *21* (15), 8067–8072.
- (107) Kerr, G. D.; Hamm, R. N.; Williams, M. W.; Birkhoff, R. D.; Painter, L. R. Optical and Dielectric Properties of Water in the Vacuum Ultraviolet. *Phys. Rev. A (Coll Park)* **1972**, *5* (6), 2523–2527.
- (108) Yeh, I. C.; Berkowitz, M. L. Dielectric Constant of Water at High Electric Fields: Molecular Dynamics Study. *J. Chem. Phys.* **1999**, *110* (16), 7935–7942.
- (109) Senapati, S.; Chandra, A. Dielectric Constant of Water Confined in a Nanocavity. *J. Phys. Chem. B* **2001**, *105* (22), 5106–5109.
- (110) Renou, R.; Szymczyk, A.; Maurin, G.; Malfreyt, P.; Ghoufi, A. Superpermittivity of Nanoconfined Water. *J. Chem. Phys.* **2015**, *142* (18), 184706.
- (111) Booth, F. The Dielectric Constant of Water and the Saturation Effect. *J. Chem. Phys.* **1951**, *19* (4), 391–394.
- (112) Kirkwood, J. G. The Dielectric Polarization of Polar Liquids. *J. Chem. Phys.* **1939**, *7* (10), 911–919.
- (113) Cole, R. H. Theory of Dielectric Constant and Dielectric Loss. *J. Am. Chem. Soc.* **1958**, *80* (18), 5010–5010.
- (114) Onsager, L. Electric Moments of Molecules in Liquids. *J. Am. Chem. Soc.* **1936**, *58* (8), 1486–1493.
- (115) Debye, P. Polar Molecules. *Journal of the Society of Chemical Industry* **1929**, *48* (43), 1036–1037.
- (116) Henderson, M. The Interaction of Water with Solid Surfaces: Fundamental Aspects Revisited. *Surf. Sci. Rep.* **2002**, *46* (1–8), 1–308.
- (117) Morgenstern, K. Scanning Tunnelling Microscopy Investigation of Water in Submonolayer Coverage on Ag(111). *Surf. Sci.* **2002**, *504*, 293–300.
- (118) Tatarkhanov, M.; Ogletree, D. F.; Rose, F.; Mitsui, T.; Fomin, E.; Maier, S.; Rose, M.; Cerdá, J. I.; Salmeron, M. Metal- and Hydrogen-Bonding Competition during Water Adsorption on Pd(111) and Ru(0001). *J. Am. Chem. Soc.* **2009**, *131* (51), 18425–18434.
- (119) Morgenstern, K.; Rieder, K.-H. Formation of the Cyclic Ice Hexamer via Excitation of Vibrational Molecular Modes by the Scanning Tunneling Microscope. *J. Chem. Phys.* **2002**, *116* (13), 5746–5752.
- (120) Gawronski, H.; Morgenstern, K.; Rieder, K.-H. Electronic Excitation of Ice Monomers on Au(111) by Scanning Tunneling Microscopy. *European Physical Journal D* **2005**, *35* (2), 349–353.
- (121) Morgenstern, K.; Rieder, K.-H. Dissociation of Water Molecules with the Scanning Tunnelling Microscope. *Chem. Phys. Lett.* **2002**, *358* (3–4), 250–256.
- (122) Morgenstern, K.; Gawronski, H.; Mehlhorn, M.; Rieder, K.-H. Local Investigation of Electron-Induced Processes in Water-Metal Systems. *J. Mod. Opt.* **2004**, *51* (16–18), 2813–2819.
- (123) Hodgson, A.; Haq, S. Water Adsorption and the Wetting of Metal Surfaces. *Surf. Sci. Rep.* **2009**, *64* (9), 381–451.
- (124) Monroe, J.; Barry, M.; DeStefano, A.; Aydogan Gokturk, P.; Jiao, S.; Robinson-Brown, D.; Webber, T.; Crumlin, E. J.; Han, S.; Shell, M. S. Water Structure and Properties at Hydrophilic and Hydrophobic Surfaces. *Annu. Rev. Chem. Biomol. Eng.* **2020**, *11*, 523–557.
- (125) Davies, J. F.; Miles, R. E. H.; Haddrell, A. E.; Reid, J. P. Influence of Organic Films on the Evaporation and Condensation of Water in Aerosol. *Proc. Natl. Acad. Sci. U. S. A.* **2013**, *110* (22), 8807–8812.
- (126) Björneholm, O.; Hansen, M. H.; Hodgson, A.; Liu, L.-M.; Limmer, D. T.; Michaelides, A.; Pedevilla, P.; Rossmeisl, J.; Shen, H.; Tocci, G.; Tyrode, E.; Walz, M.-M.; Werner, J.; Bluhm, H. Water at Interfaces. *Chem. Rev.* **2016**, *116* (13), 7698–7726.
- (127) Árnadóttir, L.; Stuve, E. M.; Jónsson, H. Adsorption of Water Monomer and Clusters on Platinum(111) Terrace and Related Steps and Kinks. *Surf. Sci.* **2010**, *604* (21–22), 1978–1986.
- (128) Ranea, V. A.; Michaelides, A.; Ramírez, R.; de Andres, P. L.; Vergés, J. A.; King, D. A. Water Dimer Diffusion on Pd{111} Assisted by an H-Bond Donor-Acceptor Tunneling Exchange. *Phys. Rev. Lett.* **2004**, *92* (13), 136104.
- (129) Hammer, B.; Wendt, S.; Besenbacher, F. Water Adsorption on TiO₂. *Top Catal.* **2010**, *53* (5–6), 423–430.
- (130) Calvin, J. J.; Rosen, P. F.; Ross, N. L.; Navrotsky, A.; Woodfield, B. F. Review of Surface Water Interactions with Metal Oxide Nanoparticles. *J. Mater. Res.* **2019**, *34* (3), 416–427.
- (131) Eriksen, S.; Naylor, P. D.; Egddell, R. G. The Adsorption of Water on SrTiO₃ and TiO₂: A Reappraisal. *Spectrochim Acta A* **1987**, *43* (12), 1535–1538.
- (132) Potter, F. H.; Egddell, R. G. The Adsorption of Water on Na_xWO₃(100) Surfaces: A Study by Photoemission. *Surf. Sci.* **1993**, *297* (3), 286–292.
- (133) Warren, S.; Flavell, W. R.; Thomas, A. G.; Hollingworth, J.; Dunwoody, P. M.; Downes, S.; Chen, C. Adsorption of H₂O on Single Crystal CuO. *Surf. Sci.* **1999**, *436* (1–3), 1–8.
- (134) Thiel, P. A.; Madey, T. E. The Interaction of Water with Solid Surfaces: Fundamental Aspects. *Surf. Sci. Rep.* **1987**, *7* (6–8), 211–385.
- (135) Heras, J. M.; Papp, H.; Spiess, W. Face Specificity of the H₂O Adsorption and Decomposition on Co Surfaces - a LEED, UPS, Sp and TPD Study. *Surf. Sci.* **1982**, *117* (1–3), 590.
- (136) Grellner, F.; Klingenberg, B.; Borgmann, D.; Wedler, G. Interaction of H₂O with Co(1120): A Photoelectron Spectroscopic Study. *Surf. Sci.* **1994**, *312* (1–2), 143–150.
- (137) Thiel, P. A.; Hoffmann, F. M.; Weinberg, W. H. Monolayer and Multilayer Adsorption of Water on Ru(001). *J. Chem. Phys.* **1981**, *75* (11), 5556–5572.
- (138) Thiel, P. A.; Hoffmann, F. M.; Weinberg, W. H. Coadsorption of Oxygen and Water on Ru (001): Vibrational and Structural Properties. *Phys. Rev. Lett.* **1982**, *49* (7), 501–504.

- (139) Meng, S.; Wang, E. G.; Gao, S. Water Adsorption on Metal Surfaces: A General Picture from Density Functional Theory Studies. *Phys. Rev. B* **2004**, *69* (19), 195404.
- (140) Podgornik, R. Water and Life: The Unique Properties of H₂O. *J. Biol. Phys.* **2011**, *37* (2), 163–165.
- (141) Li, B.; Li, X.; Gao, W.; Jiang, Q. An Effective Scheme to Determine Surface Energy and Its Relation with Adsorption Energy. *Acta Mater.* **2021**, *212*, 116895.
- (142) Yeandel, S. R.; Freeman, C. L.; Harding, J. H. A General Method for Calculating Solid/Liquid Interfacial Free Energies from Atomistic Simulations: Application to CaSO₄·xH₂O. *J. Chem. Phys.* **2022**, *157* (8), 084117.
- (143) Gim, S.; Cho, K. J.; Lim, H.-K.; Kim, H. Structure, Dynamics, and Wettability of Water at Metal Interfaces. *Sci. Rep.* **2019**, *9* (1), 14805.
- (144) Murono, T.; Hongo, K.; Nakano, K.; Maezono, R. Ab-Initio-Based Interface Modeling and Statistical Analysis for Estimate of the Water Contact Angle on a Metallic Cu(111) Surface. *Surfaces and Interfaces* **2022**, *34*, 102342.
- (145) Wang, R.; Sakai, N.; Fujishima, A.; Watanabe, T.; Hashimoto, K. Studies of Surface Wettability Conversion on TiO₂ Single-Crystal Surfaces. *J. Phys. Chem. B* **1999**, *103* (12), 2188–2194.
- (146) White, M. L. The Wetting of Gold Surfaces by Water¹. *J. Phys. Chem.* **1964**, *68* (10), 3083–3085.
- (147) Whyman, G.; Bormashenko, E.; Stein, T. The Rigorous Derivation of Young, Cassie-Baxter and Wenzel Equations and the Analysis of the Contact Angle Hysteresis Phenomenon. *Chem. Phys. Lett.* **2008**, *450* (4–6), 355–359.
- (148) Marmur, A. Wetting on Hydrophobic Rough Surfaces: To Be Heterogeneous or Not To Be? *Langmuir* **2003**, *19* (20), 8343–8348.
- (149) Josyula, T.; Kumar Malla, L.; Thomas, T. M.; Kalichetty, S. S.; Sinha Mahapatra, P.; Pattamatta, A. Fundamentals and Applications of Surface Wetting. *Langmuir* **2024**, *40* (16), 8293–8326.
- (150) Sinha Mahapatra, P.; Ganguly, R.; Ghosh, A.; Chatterjee, S.; Lowrey, S.; Sommers, A. D.; Megaridis, C. M. Patterning Wettability for Open-Surface Fluidic Manipulation: Fundamentals and Applications. *Chem. Rev.* **2022**, *122* (22), 16752–16801.
- (151) Shimizu, T. K.; Maier, S.; Verdaguera, A.; Velasco-Velez, J.-J.; Salmeron, M. Water at Surfaces and Interfaces: From Molecules to Ice and Bulk Liquid. *Prog. Surf. Sci.* **2018**, *93* (4), 87–107.
- (152) Chaplin, M. Water's Hydrogen Bond Strength. *ArXiv* **2007**, DOI: [10.48550/arXiv.0706.1355](https://doi.org/10.48550/arXiv.0706.1355).
- (153) Michaelides, A.; Morgenstern, K. Ice Nanoclusters at Hydrophobic Metal Surfaces. *Nat. Mater.* **2007**, *6* (8), 597–601.
- (154) Groß, A.; Sakong, S. Ab Initio Simulations of Water/Metal Interfaces. *Chem. Rev.* **2022**, *122* (12), 10746–10776.
- (155) Groß, A.; Gossenberger, F.; Lin, X.; Naderian, M.; Sakong, S.; Roman, T. Water Structures at Metal Electrodes Studied by Ab Initio Molecular Dynamics Simulations. *J. Electrochem. Soc.* **2014**, *161* (8), E3015–E3020.
- (156) Carrasco, J.; Michaelides, A.; Forster, M.; Haq, S.; Raval, R.; Hodgson, A. A One-Dimensional Ice Structure Built from Pentagons. *Nat. Mater.* **2009**, *8* (5), 427–431.
- (157) Baghbanpourasl, A.; Hingerl, K.; Wippermann, S.; Schmidt, W. G. Copper(110) Surface in Thermodynamic Equilibrium with Water Vapor Studied from First Principles. *Surf. Sci.* **2013**, *612*, 82–89.
- (158) Carrasco, J.; Hodgson, A.; Michaelides, A. A Molecular Perspective of Water at Metal Interfaces. *Nat. Mater.* **2012**, *11* (8), 667–674.
- (159) Guo, J.; Meng, X.; Chen, J.; Peng, J.; Sheng, J.; Li, X.-Z.; Xu, L.; Shi, J.-R.; Wang, E.; Jiang, Y. Real-Space Imaging of Interfacial Water with Submolecular Resolution. *Nat. Mater.* **2014**, *13* (2), 184–189.
- (160) Peng, J.; Guo, J.; Hapala, P.; Cao, D.; Ma, R.; Cheng, B.; Xu, L.; Ondráček, M.; Jelinek, P.; Wang, E.; Jiang, Y. Weakly Perturbative Imaging of Interfacial Water with Submolecular Resolution by Atomic Force Microscopy. *Nat. Commun.* **2018**, *9*, 122.
- (161) Meng, X.; Guo, J.; Peng, J.; Chen, J.; Wang, Z.; Shi, J.-R.; Li, X.-Z.; Wang, E.-G.; Jiang, Y. Direct Visualization of Concerted Proton Tunnelling in a Water Nanocluster. *Nat. Phys.* **2015**, *11* (3), 235–239.
- (162) Lee, J.; Sorescu, D. C.; Deng, X.; Jordan, K. D. Water Chain Formation on TiO₂(110). *J. Phys. Chem. Lett.* **2013**, *4* (1), 53–57.
- (163) Meng, S.; Wang, E. G.; Gao, S. Water Adsorption on Metal Surfaces: A General Picture from Density Functional Theory Studies. *Phys. Rev. B* **2004**, *69* (19), 195404.
- (164) Mu, R.; Zhao, Z.; Dohnálek, Z.; Gong, J. Structural Motifs of Water on Metal Oxide Surfaces. *Chem. Soc. Rev.* **2017**, *46* (7), 1785–1806.
- (165) Diebold, U. Perspective: A Controversial Benchmark System for Water-Oxide Interfaces: H₂O/TiO₂(110). *J. Chem. Phys.* **2017**, *147* (4), 040901.
- (166) Brookes, I. M.; Muryn, C. A.; Thornton, G. Imaging Water Dissociation on TiO₂(110). *Phys. Rev. Lett.* **2001**, *87* (26), 266103.
- (167) Kimmel, G. A.; Baer, M.; Petrik, N. G.; VandeVondele, J.; Rousseau, R.; Mundy, C. J. Polarization- and Azimuth-Resolved Infrared Spectroscopy of Water on TiO₂(110): Anisotropy and the Hydrogen-Bonding Network. *J. Phys. Chem. Lett.* **2012**, *3* (6), 778–784.
- (168) He, Y.; Tiloccia, A.; Dulub, O.; Selloni, A.; Diebold, U. Local Ordering and Electronic Signatures of Submonolayer Water on Anatase TiO₂(101). *Nat. Mater.* **2009**, *8* (7), 585–589.
- (169) Henderson, M. A. Structural Sensitivity in the Dissociation of Water on TiO₂ Single-Crystal Surfaces. *Langmuir* **1996**, *12* (21), 5093–5098.
- (170) Rao, R. R.; Kolb, M. J.; Hwang, J.; Pedersen, A. F.; Mehta, A.; You, H.; Stoerzinger, K. A.; Feng, Z.; Zhou, H.; Bluhm, H.; Giordano, L.; Stephens, I. E. L.; Shao-Horn, Y. Surface Orientation Dependent Water Dissociation on Rutile Ruthenium Dioxide. *J. Phys. Chem. C* **2018**, *122* (31), 17802–17811.
- (171) Garlyyev, B.; Xue, S.; Watzele, S.; Scieszka, D.; Bandarenka, A. S. Influence of the Nature of the Alkali Metal Cations on the Electrical Double-Layer Capacitance of Model Pt(111) and Au(111) Electrodes. *J. Phys. Chem. Lett.* **2018**, *9* (8), 1927–1930.
- (172) Tian, Y.; Huang, B.; Song, Y.; Zhang, Y.; Guan, D.; Hong, J.; Cao, D.; Wang, E.; Xu, L.; Shao-Horn, Y.; Jiang, Y. Effect of Ion-Specific Water Structures at Metal Surfaces on Hydrogen Production. *Nat. Commun.* **2024**, *15*, 7834.
- (173) Björneholm, O.; Hansen, M. H.; Hodgson, A.; Liu, L. M.; Limmer, D. T.; Michaelides, A.; Pedevilla, P.; Rossmisl, J.; Shen, H.; Tocci, G.; Tyrode, E.; Walz, M. M.; Werner, J.; Bluhm, H. Water at Interfaces. *Chem. Rev.* **2016**, *116* (13), 7698–7726.
- (174) Ataka, K.; Yotsuyanagi, T.; Osawa, M. Potential-Dependent Reorientation of Water Molecules at an Electrode/Electrolyte Interface Studied by Surface-Enhanced Infrared Absorption Spectroscopy. *J. Phys. Chem.* **1996**, *100* (25), 10664–10672.
- (175) Osawa, M.; Tsushima, M.; Mogami, H.; Samjeské, G.; Yamakata, A. Structure of Water at the Electrified Platinum-Water Interface: A Study by Surface-Enhanced Infrared Absorption Spectroscopy. *J. Phys. Chem. C* **2008**, *112* (11), 4248–4256.
- (176) Velasco-Velez, J.-J.; Wu, C. H.; Pascal, T. A.; Wan, L. F.; Guo, J.; Prendergast, D.; Salmeron, M. The Structure of Interfacial Water on Gold Electrodes Studied by X-Ray Absorption Spectroscopy. *Science* **2014**, *346* (6211), 831–834.
- (177) Li, C.-Y.; Le, J.-B.; Wang, Y.-H.; Chen, S.; Yang, Z.-L.; Li, J.-F.; Cheng, J.; Tian, Z.-Q. In Situ Probing Electrified Interfacial Water Structures at Atomically Flat Surfaces. *Nat. Mater.* **2019**, *18* (7), 697–701.
- (178) Ostroverkhov, V.; Waychunas, G. A.; Shen, Y. R. New Information on Water Interfacial Structure Revealed by Phase-Sensitive Surface Spectroscopy. *Phys. Rev. Lett.* **2005**, *94* (4), 046102.
- (179) Macias-Romero, C.; Nahalka, I.; Okur, H. I.; Roke, S. Optical Imaging of Surface Chemistry and Dynamics in Confinement. *Science* **2017**, *357* (6353), 784–788.
- (180) Brown, G. E.; Henrich, V. E.; Casey, W. H.; Clark, D. L.; Eggleston, C.; Felmy, A.; Goodman, D. W.; Grätzel, M.; Maciel, G.;

- McCarthy, M. I.; Nealon, K. H.; Sverjensky, D. A.; Toney, M. F.; Zachara, J. M. Metal Oxide Surfaces and Their Interactions with Aqueous Solutions and Microbial Organisms. *Chem. Rev.* **1999**, *99* (1), 77–174.
- (181) Verdaguer, A.; Sacha, G. M.; Bluhm, H.; Salmeron, M. Molecular Structure of Water at Interfaces: Wetting at the Nanometer Scale. *Chem. Rev.* **2006**, *106* (4), 1478–1510.
- (182) Fenter, P.; Sturchio, N. C. Mineral-Water Interfacial Structures Revealed by Synchrotron X-Ray Scattering. *Prog. Surf. Sci.* **2004**, *77* (5–8), 171–258.
- (183) Heald, C. L.; Kroll, J. H. The Fuel of Atmospheric Chemistry: Toward a Complete Description of Reactive Organic Carbon. *Sci. Adv.* **2020**, *6* (6), No. eaay8967.
- (184) Liu, X.; Xiao, J.; Peng, H.; Hong, X.; Chan, K.; Nørskov, J. K. Understanding Trends in Electrochemical Carbon Dioxide Reduction Rates. *Nat. Commun.* **2017**, *8*, 15438.
- (185) Ogasawara, H.; Yoshinobu, J.; Kawai, M. Direct Observation of the Molecular Interaction between Chemisorbed CO and Water Overlayer on Pt(111). *Surf. Sci.* **1997**, *386* (1–3), 73–77.
- (186) Wagner, F. T.; Moylan, T. E. Generation of Surface Hydronium from Water and Hydrogen Coadsorbed on Pt(111). *Surf. Sci.* **1988**, *206* (1–2), 187–202.
- (187) Wagner, F. T.; Moylan, T. E.; Schmiege, S. J. Hydrophilic versus Hydrophobic Coadsorption: Carbon Monoxide and Water on Rh(111) versus Pt(111). *Surf. Sci.* **1988**, *195* (3), 403–428.
- (188) Ellis, T. H.; Kruus, E. J.; Wang, H. Substrate Induced Interactions between Water and Carbon Monoxide on Ni(100) and Cu(100). *J. Electron Spectrosc. Relat. Phenom.* **1993**, *64*–*65*, 421–426.
- (189) Ellis, T. H.; Kruus, E. J.; Wang, H. The Interaction between Water and Carbon Monoxide Coadsorbed onto Ni(100). *Surf. Sci.* **1992**, *273* (1–2), 73–87.
- (190) Ehlers, D. H.; Esser, A. P.; Spitzer, A.; Lüth, H. Coadsorption of CO with Methanol, Water and Xenon on Pt(111): Band Suppression in Vibrational Spectroscopy. *Surf. Sci.* **1987**, *191* (3), 466–478.
- (191) Nakamura, M.; Ito, M. Coadsorption of Water Monomers with CO on Ru(001) and Charge Transfer during Hydration Processes. *Chem. Phys. Lett.* **2001**, *335* (3–4), 170–175.
- (192) Rupprechter, G.; Dellwig, T.; Unterhalt, H.; Freund, H. J. High-Pressure Carbon Monoxide Adsorption on Pt(III) Revisited: A Sum Frequency Generation Study. *J. Phys. Chem. B* **2001**, *105* (18), 3797–3802.
- (193) Bedürftig, K.; Völken, S.; Wang, Y.; Wintterlin, J.; Jacobi, K.; Ertl, G. Vibrational and Structural Properties of OH Adsorbed on Pt(111). *J. Chem. Phys.* **1999**, *111* (24), 11147–11154.
- (194) Roudgar, A.; Groß, A. Water Bilayer on the Pd/Au(111) Overlayer System: Coadsorption and Electric Field Effects. *Chem. Phys. Lett.* **2005**, *409* (4–6), 157–162.
- (195) Schnur, S.; Groß, A. Properties of Metal-Water Interfaces Studied from First Principles. *New J. Phys.* **2009**, *11* (12), 125003.
- (196) Rossmeisl, J.; Skúlason, E.; Björkertun, M. E.; Tripkovic, V.; Nørskov, J. K. Modeling the Electrified Solid-Liquid Interface. *Chem. Phys. Lett.* **2008**, *466* (1–3), 68–71.
- (197) Shi, C.; O’Grady, C. P.; Peterson, A. A.; Hansen, H. A.; Nørskov, J. K. Modeling CO₂ Reduction on Pt(111). *Phys. Chem. Chem. Phys.* **2013**, *15* (19), 7114–7122.
- (198) Zhang, Z.-M.; Wang, T.; Cai, Y.-C.; Li, X.-Y.; Ye, J.-Y.; Zhou, Y.; Tian, N.; Zhou, Z.-Y.; Sun, S.-G. Probing Electrolyte Effects on Cation-Enhanced CO₂ Reduction on Copper in Acidic Media. *Nat. Catal.* **2024**, *7* (7), 807–817.
- (199) Xu, P.; Wang, R.; Zhang, H.; Carnevale, V.; Borguet, E.; Suntivich, J. Cation Modifies Interfacial Water Structures on Platinum during Alkaline Hydrogen Electrocatalysis. *J. Am. Chem. Soc.* **2024**, *146* (4), 2426–2434.
- (200) Xu, P.; von Rueden, A. D.; Schimmenti, R.; Mavrikakis, M.; Suntivich, J. Optical Method for Quantifying the Potential of Zero Charge at the Platinum-Water Electrochemical Interface. *Nat. Mater.* **2023**, *22* (4), 503–510.
- (201) Rao, R. R.; Huang, B.; Katayama, Y.; Hwang, J.; Kawaguchi, T.; Lunger, J. R.; Peng, J.; Zhang, Y.; Morinaga, A.; Zhou, H.; You, H.; Shao-Horn, Y. PH- and Cation-Dependent Water Oxidation on Rutile RuO₂ (110). *J. Phys. Chem. C* **2021**, *125* (15), 8195–8207.
- (202) Guo, J.; Jiang, Y. Submolecular Insights into Interfacial Water by Hydrogen-Sensitive Scanning Probe Microscopy. *Acc. Chem. Res.* **2022**, *55* (12), 1680–1692.
- (203) Grifoni, E.; Piccini, G.; Lercher, J. A.; Glezakou, V.-A.; Rousseau, R.; Parrinello, M. Confinement Effects and Acid Strength in Zeolites. *Nat. Commun.* **2021**, *12*, 2630.
- (204) Tan, K.; Nijem, N.; Gao, Y.; Zuluaga, S.; Li, J.; Thonhauser, T.; Chabal, Y. J. Water Interactions in Metal Organic Frameworks. *CrystEngComm* **2015**, *17* (2), 247–260.
- (205) Rieth, A. J.; Yang, S.; Wang, E. N.; Dincă, M. Record Atmospheric Fresh Water Capture and Heat Transfer with a Material Operating at the Water Uptake Reversibility Limit. *ACS Cent Sci.* **2017**, *3* (6), 668–672.
- (206) Kim, H.; Cho, H. J.; Narayanan, S.; Yang, S.; Furukawa, H.; Schiffres, S.; Li, X.; Zhang, Y.-B.; Jiang, J.; Yaghi, O. M.; Wang, E. N. Characterization of Adsorption Enthalpy of Novel Water-Stable Zeolites and Metal-Organic Frameworks. *Sci. Rep.* **2016**, *6*, 19097.
- (207) Khutia, A.; Rammelberg, H. U.; Schmidt, T.; Henninger, S.; Janiak, C. Water Sorption Cycle Measurements on Functionalized MIL-101Cr for Heat Transformation Application. *Chem. Mater.* **2013**, *25* (5), 790–798.
- (208) Henninger, S. K.; Schmidt, F. P.; Henning, H.-M. Water Adsorption Characteristics of Novel Materials for Heat Transformation Applications. *Appl. Therm Eng.* **2010**, *30* (13), 1692–1702.
- (209) Rieth, A. J.; Hunter, K. M.; Dincă, M.; Paesani, F. Hydrogen Bonding Structure of Confined Water Templatated by a Metal-Organic Framework with Open Metal Sites. *Nat. Commun.* **2019**, *10*, 4771.
- (210) Rieth, A. J.; Wright, A. M.; Skorupskii, G.; Mancuso, J. L.; Hendon, C. H.; Dincă, M. Record-Setting Sorbents for Reversible Water Uptake by Systematic Anion Exchanges in Metal-Organic Frameworks. *J. Am. Chem. Soc.* **2019**, *141* (35), 13858–13866.
- (211) Jeremias, F.; Khutia, A.; Henninger, S. K.; Janiak, C. MIL-100(Al, Fe) as Water Adsorbents for Heat Transformation Purposes—a Promising Application. *J. Mater. Chem.* **2012**, *22* (20), 10148–10151.
- (212) Wright, A. M.; Rieth, A. J.; Yang, S.; Wang, E. N.; Dincă, M. Precise Control of Pore Hydrophilicity Enabled by Post-Synthetic Cation Exchange in Metal-Organic Frameworks. *Chem. Sci.* **2018**, *9* (15), 3856–3859.
- (213) Zheng, J.; Vemuri, R. S.; Estevez, L.; Koech, P. K.; Varga, T.; Camaroni, D. M.; Blake, T. A.; McGrail, B. P.; Motkuri, R. K. Pore-Engineered Metal-Organic Frameworks with Excellent Adsorption of Water and Fluorocarbon Refrigerant for Cooling Applications. *J. Am. Chem. Soc.* **2017**, *139* (31), 10601–10604.
- (214) Kim, H.; Yang, S.; Rao, S. R.; Narayanan, S.; Kapustin, E. A.; Furukawa, H.; Umans, A. S.; Yaghi, O. M.; Wang, E. N. Water Harvesting from Air with Metal-Organic Frameworks Powered by Natural Sunlight. *Science* **2017**, *356* (6336), 430–434.
- (215) Dietzel, P. D. C.; Johnsen, R. E.; Blom, R.; Fjellvåg, H. Structural Changes and Coordinatively Unsaturated Metal Atoms on Dehydration of Honeycomb Analogous Microporous Metal-Organic Frameworks. *Chem.—Eur. J.* **2008**, *14* (8), 2389–2397.
- (216) Chen, K.; Kelsey, J.; White, J. L.; Zhang, L.; Resasco, D. Water Interactions in Zeolite Catalysts and Their Hydrophobically Modified Analogs. *ACS Catal.* **2015**, *5* (12), 7480–7487.
- (217) Hunger, J.; Beta, I. A.; Böhligh, H.; Ling, C.; Jobic, H.; Hunger, B. Adsorption Structures of Water in NaX Studied by DRIFT Spectroscopy and Neutron Powder Diffraction. *J. Phys. Chem. B* **2006**, *110* (1), 342–353.
- (218) Jiménez-Ruiz, M.; Gahle, D. S.; Lemishko, T.; Valencia, S.; Sastre, G.; Rey, F. Evidence of Hydronium Formation in Water-Chabazite Zeolite Using Inelastic Neutron Scattering Experiments and Ab Initio Molecular Dynamics Simulations. *J. Phys. Chem. C* **2020**, *124* (9), 5436–5443.

- (219) Wang, M.; Jaegers, N. R.; Lee, M. S.; Wan, C.; Hu, J. Z.; Shi, H.; Mei, D.; Burton, S. D.; Camaioni, D. M.; Gutiérrez, O. Y.; Glezakou, V. A.; Rousseau, R.; Wang, Y.; Lercher, J. A. Genesis and Stability of Hydronium Ions in Zeolite Channels. *J. Am. Chem. Soc.* **2019**, *141* (8), 3444–3455.
- (220) Termath, V.; Haase, F.; Sauer, J.; Hutter, J.; Parrinello, M. Understanding the Nature of Water Bound to Solid Acid Surfaces. Ab Initio Simulation on HSAPO-34. *J. Am. Chem. Soc.* **1998**, *120* (33), 8512–8516.
- (221) Vener, M. V.; Rozanska, X.; Sauer, J. Protonation of Water Clusters in the Cavities of Acidic Zeolites: $(\text{H}_2\text{O})_n\text{-H-Chabazite}$, $n = 1\text{--}4$. *Phys. Chem. Chem. Phys.* **2009**, *11* (11), 1702.
- (222) Kletnieks, P. W.; Ehresmann, J. O.; Nicholas, J. B.; Haw, J. F. Adsorbate Clustering and Proton Transfer in Zeolites: NMR Spectroscopy and Theory. *ChemPhysChem* **2006**, *7* (1), 114–116.
- (223) Li, G.; Wang, B.; Resasco, D. E. Water-Mediated Heterogeneously Catalyzed Reactions. *ACS Catal.* **2020**, *10* (2), 1294–1309.
- (224) Yamada, Y.; Usui, K.; Sodeyama, K.; Ko, S.; Tateyama, Y.; Yamada, A. Hydrate-Melt Electrolytes for High-Energy-Density Aqueous Batteries. *Nat. Energy* **2016**, *1* (10), 16129.
- (225) Suo, L.; Borodin, O.; Gao, T.; Olguin, M.; Ho, J.; Fan, X.; Luo, C.; Wang, C.; Xu, K. Water-in-Salt” Electrolyte Enables High-Voltage Aqueous Lithium-Ion Chemistries. *Science* **2015**, *350* (6263), 938–943.
- (226) Borodin, O.; Self, J.; Persson, K. A.; Wang, C.; Xu, K. Uncharted Waters: Super-Concentrated Electrolytes. *Joule* **2020**, *4* (1), 69–100.
- (227) Schwaab, G.; Sebastiani, F.; Havenith, M. Ion Hydration and Ion Pairing as Probed by THz Spectroscopy. *Angew. Chem., Int. Ed.* **2019**, *58* (10), 3000–3013.
- (228) Borodin, O.; Ren, X.; Vatamanu, J.; von Wald Cresce, A.; Knap, J.; Xu, K. Modeling Insight into Battery Electrolyte Electrochemical Stability and Interfacial Structure. *Acc. Chem. Res.* **2017**, *50* (12), 2886–2894.
- (229) Borodin, O.; Suo, L.; Gobet, M.; Ren, X.; Wang, F.; Faraone, A.; Peng, J.; Olguin, M.; Schroeder, M.; Ding, M. S.; Gobrogue, E.; von Wald Cresce, A.; Munoz, S.; Dura, J. A.; Greenbaum, S.; Wang, C.; Xu, K. Liquid Structure with Nano-Heterogeneity Promotes Cationic Transport in Concentrated Electrolytes. *ACS Nano* **2017**, *11* (10), 10462–10471.
- (230) Suo, L.; Borodin, O.; Wang, Y.; Rong, X.; Sun, W.; Fan, X.; Xu, S.; Schroeder, M. A.; Cresce, A. V.; Wang, F.; Yang, C.; Hu, Y.; Xu, K.; Wang, C. Water-in-Salt” Electrolyte Makes Aqueous Sodium-Ion Battery Safe, Green, and Long-Lasting. *Adv. Energy Mater.* **2017**, *7* (21), 1701189.
- (231) Ko, S.; Yamada, Y.; Yamada, A. A 62 m K-Ion Aqueous Electrolyte. *Electrochim. Commun.* **2020**, *116*, 106764.
- (232) Wang, F.; Borodin, O.; Gao, T.; Fan, X.; Sun, W.; Han, F.; Faraone, A.; Dura, J. A.; Xu, K.; Wang, C. Highly Reversible Zinc Metal Anode for Aqueous Batteries. *Nat. Mater.* **2018**, *17* (6), 543–549.
- (233) Zhou, A.; Jiang, L.; Yue, J.; Tong, Y.; Zhang, Q.; Lin, Z.; Liu, B.; Wu, C.; Suo, L.; Hu, Y.-S.; Li, H.; Chen, L. Water-in-Salt Electrolyte Promotes High-Capacity FeFe(CN)₆ Cathode for Aqueous Al-Ion Battery. *ACS Appl. Mater. Interfaces* **2019**, *11* (44), 41356–41362.
- (234) Auer, B. M.; Skinner, J. L. IR and Raman Spectra of Liquid Water: Theory and Interpretation. *J. Chem. Phys.* **2008**, *128* (22), 224511.
- (235) Ko, S.; Yamada, Y.; Yamada, A. Formation of a Solid Electrolyte Interphase in Hydrate-Melt Electrolytes. *ACS Appl. Mater. Interfaces* **2019**, *11* (49), 45554–45560.
- (236) Ko, S.; Yamada, Y.; Miyazaki, K.; Shimada, T.; Watanabe, E.; Tateyama, Y.; Kamiya, T.; Honda, T.; Akikusa, J.; Yamada, A. Lithium-Salt Monohydrate Melt: A Stable Electrolyte for Aqueous Lithium-Ion Batteries. *Electrochim. Commun.* **2019**, *104*, 106488.
- (237) Yoshida, K.; Nakamura, M.; Kazue, Y.; Tachikawa, N.; Tsuzuki, S.; Seki, S.; Dokko, K.; Watanabe, M. Oxidative-Stability Enhancement and Charge Transport Mechanism in Glyme-Lithium Salt Equimolar Complexes. *J. Am. Chem. Soc.* **2011**, *133* (33), 13121–13129.
- (238) Santos, E.; Lundin, A.; Pötting, K.; Quaino, P.; Schmickler, W. Model for the Electrocatalysis of Hydrogen Evolution. *Phys. Rev. B* **2009**, *79* (23), 235436.
- (239) Agmon, N. The Grotthuss Mechanism. *Chem. Phys. Lett.* **1995**, *244* (5–6), 456–462.
- (240) Wolke, C. T.; Fournier, J. A.; Dzugan, L. C.; Fagiani, M. R.; Odbadrakh, T. T.; Knorke, H.; Jordan, K. D.; McCoy, A. B.; Asmis, K. R.; Johnson, M. A. Spectroscopic Snapshots of the Proton-Transfer Mechanism in Water. *Science* **2016**, *354* (6316), 1131–1135.
- (241) Jiang, J.-C.; Wang, Y.-S.; Chang, H.-C.; Lin, S. H.; Lee, Y. T.; Niedner-Schatzberg, G.; Chang, H.-C. Infrared Spectra of $\text{H}^+(\text{H}_2\text{O})_{5\text{--}8}$ Clusters: Evidence for Symmetric Proton Hydration. *J. Am. Chem. Soc.* **2000**, *122* (7), 1398–1410.
- (242) Miyazaki, M.; Fujii, A.; Ebata, T.; Mikami, N. Infrared Spectroscopic Evidence for Protonated Water Clusters Forming Nanoscale Cages. *Science* **2004**, *304* (5674), 1134–1137.
- (243) Headrick, J. M.; Diken, E. G.; Walters, R. S.; Hammer, N. I.; Christie, R. A.; Cui, J.; Myshakin, E. M.; Duncan, M. A.; Johnson, M. A.; Jordan, K. D. Spectral Signatures of Hydrated Proton Vibrations in Water Clusters. *Science* **2005**, *308* (5729), 1765–1769.
- (244) Shin, J.-W.; Hammer, N. I.; Diken, E. G.; Johnson, M. A.; Walters, R. S.; Jaeger, T. D.; Duncan, M. A.; Christie, R. A.; Jordan, K. D. Infrared Signature of Structures Associated with the $\text{H}^+(\text{H}_2\text{O})_n$ ($n = 6$ to 27) Clusters. *Science* **2004**, *304* (5674), 1137–1140 DOI: [10.1126/science.1096466](https://doi.org/10.1126/science.1096466).
- (245) Tuckerman, M.; Laasonen, K.; Sprik, M.; Parrinello, M. Ab Initio Molecular Dynamics Simulation of the Solvation and Transport of Hydronium and Hydroxyl Ions in Water. *J. Chem. Phys.* **1995**, *103*, 150–161.
- (246) Marx, D.; Tuckerman, M. E.; Hutter, J.; Parrinello, M. The Nature of the Hydrated Excess Proton in Water. *Nature* **1999**, *397* (6720), 601–604.
- (247) Tuckerman, M. E.; Marx, D.; Klein, M. L.; Parrinello, M. On the Quantum Nature of the Shared Proton in Hydrogen Bonds. *Science* **1997**, *275* (5301), 817–820.
- (248) Lobaugh, J.; Voth, G. A. The Quantum Dynamics of an Excess Proton in Water. *J. Chem. Phys.* **1996**, *104* (5), 2056–2069.
- (249) Zhao, Q.; Majsztrik, P.; Benziger, J. Diffusion and Interfacial Transport of Water in Nafion. *J. Phys. Chem. B* **2011**, *115* (12), 2717–2727.
- (250) Hammer, R.; Schönhoff, M.; Hansen, M. R. Comprehensive Picture of Water Dynamics in Nafion Membranes at Different Levels of Hydration. *J. Phys. Chem. B* **2019**, *123* (39), 8313–8324.
- (251) Galitskaya, E.; Privalov, A. F.; Weigler, M.; Vogel, M.; Kashin, A.; Ryzhkin, M.; Sinitsyn, V. NMR Diffusion Studies of Proton-Exchange Membranes in Wide Temperature Range. *J. Membr. Sci.* **2020**, *596*, 117691.
- (252) Nicotera, I.; Coppola, L.; Rossi, C. O.; Youssry, M.; Ranieri, G. A. NMR Investigation of the Dynamics of Confined Water in Nafion-Based Electrolyte Membranes at Subfreezing Temperatures. *J. Phys. Chem. B* **2009**, *113* (42), 13935–13941.
- (253) Sacchetti, F.; Orecchini, A.; Cunsolo, A.; Formisano, F.; Petrillo, C. Coherent Neutron Scattering Study of Confined Water in Nafion. *Phys. Rev. B* **2009**, *80* (2), 024306.
- (254) Lange, K. M.; Hodeck, K. F.; Schade, U.; Aziz, E. F. Nature of the Hydrogen Bond of Water in Solvents of Different Polarities. *J. Phys. Chem. B* **2010**, *114* (50), 16997–17001.
- (255) Smith, J. W.; Saykally, R. J. Soft X-Ray Absorption Spectroscopy of Liquids and Solutions. *Chem. Rev.* **2017**, *117* (23), 13909–13934.
- (256) Meibohm, J.; Schreck, S.; Wernet, P. Temperature Dependent Soft X-Ray Absorption Spectroscopy of Liquids. *Rev. Sci. Instrum.* **2014**, *85* (10), DOI: [10.1063/1.4896977](https://doi.org/10.1063/1.4896977).
- (257) Dubouis, N.; Serva, A.; Berthoin, R.; Jeanmairet, G.; Porcheron, B.; Salager, E.; Salanne, M.; Grimaud, A. Tuning Water Reduction

- through Controlled Nanoconfinement within an Organic Liquid Matrix. *Nat. Catal.* **2020**, *3* (8), 656–663.
- (258) Dubouis, N.; Serva, A.; Salager, E.; Deschamps, M.; Salanne, M.; Grimaud, A. The Fate of Water at the Electrochemical Interfaces: Electrochemical Behavior of Free Water Versus Coordinating Water. *J. Phys. Chem. Lett.* **2018**, *9* (23), 6683–6688.
- (259) Narangoda, P.; Spanos, I.; Masa, J.; Schlägl, R.; Zeradjanin, A. R. Electrocatalysis Beyond 2020: How to Tune the Preexponential Frequency Factor. *ChemElectroChem.* **2022**, *9* (4), DOI: 10.1002/celc.202101278.
- (260) Stamenkovic, V. R.; Fowler, B.; Mun, B. S.; Wang, G.; Ross, P. N.; Lucas, C. A.; Markovic, N. M. Improved Oxygen Reduction Activity on Pt₃Ni(111) via Increased Surface Site Availability. *Science* **2007**, *315* (5811), 493.
- (261) Zeradjanin, A. R. Is a Major Breakthrough in the Oxygen Electrocatalysis Possible? *Curr. Opin. Electrochem.* **2018**, *9*, 214–223.
- (262) Hammes-Schiffer, S.; Soudakov, A. V. Proton-Coupled Electron Transfer in Solution, Proteins, and Electrochemistry. *J. Phys. Chem. B* **2008**, *112* (45), 14108–14123.
- (263) Koper, M. T. M. Thermodynamic Theory of Multi-Electron Transfer Reactions: Implications for Electrocatalysis. *J. Electroanal. Chem.* **2011**, *660* (2), 254.
- (264) Jencks, W. P. Binding Energy, Specificity, and Enzymic Catalysis: The Circe Effect. In: *Adv. Enzymol. Relat. Areas Mol. Biol.* **1975**, *43*, 219–410.
- (265) Stühmeier, B. M.; Pietsch, M. R.; Schwämmlein, J. N.; Gasteiger, H. A. Pressure and Temperature Dependence of the Hydrogen Oxidation and Evolution Reaction Kinetics on Pt Electrocatalysts via PEMFC-Based Hydrogen-Pump Measurements. *J. Electrochem. Soc.* **2021**, *168* (6), 064516.
- (266) Neyerlin, K. C.; Gu, W.; Jorne, J.; Gasteiger, H. A. Study of the Exchange Current Density for the Hydrogen Oxidation and Evolution Reactions. *J. Electrochem. Soc.* **2007**, *154* (7), B631.
- (267) Sheng, W.; Gasteiger, H. A.; Shao-Horn, Y. Hydrogen Oxidation and Evolution Reaction Kinetics on Platinum: Acid vs Alkaline Electrolytes. *J. Electrochem. Soc.* **2010**, *157* (11), B1529.
- (268) Ledezma-Yanez, I.; Wallace, W. D. Z.; Sebastián-Pascual, P.; Climent, V.; Feliu, J. M.; Koper, M. T. M. Interfacial Water Reorganization as a pH-Dependent Descriptor of the Hydrogen Evolution Rate on Platinum Electrodes. *Nat. Energy* **2017**, *2* (4), 17031.
- (269) Yu, S.; Yamauchi, H.; Wang, S.; Aggarwal, A.; Kim, J.; Gordiz, K.; Huang, B.; Xu, H.; Zheng, D. J.; Wang, X.; Iriawan, H.; Menga, D.; Shao-Horn, Y. CO₂-to-Methanol Electroconversion on a Molecular Cobalt Catalyst Facilitated by Acidic Cations. *Nat. Catal.* **2024**, *7* (9), 1000–1009.
- (270) Conway, B. E.; Wilkinson, D. F. Entropic and Enthalpic Components of the Symmetry Factor for Electrochemical Proton Transfer from Various Proton Donors over a Wide Temperature Range. *J. Electroanal. Chem.* **1986**, *214* (1–2), 633.
- (271) Conway, B. E.; Tessier, D. F.; Wilkinson, D. P. Experimental Evidence for the Potential-Dependence of Entropy of Activation in Electrochemical Reactions in Relations to the Temperature-Dependence of Tafel Slopes. *J. Electroanal. Chem.* **1986**, *199* (2), 249.
- (272) Bender, J. T.; Petersen, A. S.; Østergaard, F. C.; Wood, M. A.; Heffernan, S. M. J.; Milliron, D. J.; Rossmeisl, J.; Resasco, J. Understanding Cation Effects on the Hydrogen Evolution Reaction. *ACS Energy Lett.* **2023**, *8* (1), 657.
- (273) Parsons, R. Charge Transfer Reactions in Electrochemical and Chemical Processes. *J. Electroanal. Chem. Interfacial Electrochem.* **1987**, *230* (1–2), 290.
- (274) Krishtalik, L. I. The Hydrogen Overpotential—Hydrogen Adsorption Energy Relationship. A New Approach to the Problem. *Electrochim. Acta* **2016**, *218*, 125.
- (275) Zeradjanin, A. R.; Narangoda, P.; Masa, J.; Schlägl, R. What Controls Activity Trends of Electrocatalytic Hydrogen Evolution Reaction? Activation Energy Versus Frequency Factor. *ACS Catal.* **2022**, *12* (19), 11597.
- (276) Ringe, S.; Clark, E. L.; Resasco, J.; Walton, A.; Seger, B.; Bell, A. T.; Chan, K. Understanding Cation Effects in Electrochemical CO₂ Reduction. *Energy Environ. Sci.* **2019**, *12* (10), 3001.
- (277) Sorenson, S. A.; Patrow, J. G.; Dawlaty, J. M. Solvation Reaction Field at the Interface Measured by Vibrational Sum Frequency Generation Spectroscopy. *J. Am. Chem. Soc.* **2017**, *139* (6), 2369.
- (278) Zhu, Q.; Wallentine, S. K.; Deng, G. H.; Rebstock, J. A.; Baker, L. R. The Solvation-Induced Onsager Reaction Field Rather than the Double-Layer Field Controls CO₂ Reduction on Gold. *JACS Au* **2022**, *2* (2), 472–482.
- (279) Bard, A. J.; Faulkner, L. R. *Electrochemical Methods: Fundamentals and Applications*, 2nd ed.; 2000.
- (280) Sarkar, S.; Maitra, A.; Banerjee, S.; Thoi, V. S.; Dawlaty, J. M. Electric Fields at Metal-Surfactant Interfaces: A Combined Vibrational Spectroscopy and Capacitance Study. *J. Phys. Chem. B* **2020**, *124* (7), 1311–1321.
- (281) Huang, X.; Tang, C.; Li, J.; Chen, L. C.; Zheng, J.; Zhang, P.; Le, J.; Li, R.; Li, X.; Liu, J.; Yang, Y.; Shi, J.; Chen, Z.; Bai, M.; Zhang, H. L.; Xia, H.; Cheng, J.; Tian, Z. Q.; Hong, W. Electric Field-Induced Selective Catalysis of Single-Molecule Reaction. *Sci. Adv.* **2019**, *5* (6), DOI: 10.1126/sciadv.aaw3072.
- (282) Li, J.; Li, X.; Gunathunge, C. M.; Waegele, M. M. Hydrogen Bonding Steers the Product Selectivity of Electrocatalytic CO Reduction. *Proc. Natl. Acad. Sci. U. S. A.* **2019**, *116* (19), 9220–9229.
- (283) Banerjee, S.; Zhang, Z. Q.; Hall, A. S.; Thoi, V. S. Surfactant Perturbation of Cation Interactions at the Electrode-Electrolyte Interface in Carbon Dioxide Reduction. *ACS Catal.* **2020**, *10* (17), 9907–9914.
- (284) Zeradjanin, A. R. Understanding Entropic Barriers. *Nat. Energy* **2024**, *9* (5), 514–515.
- (285) Rodellar, C. G.; Gisbert-Gonzalez, J. M.; Saravia, F.; Roldan Cuena, B.; Oener, S. Z. Ion Solvation Kinetics in Bipolar Membranes and at Electrolyte-Metal Interfaces. *Nat. Energy* **2024**, *9* (5), 548.
- (286) Noh, S.; Cho, Y. J.; Zhang, G.; Schreier, M. Insight into the Role of Entropy in Promoting Electrochemical CO₂ Reduction by Imidazolium Cations. *J. Am. Chem. Soc.* **2023**, *145* (50), 27657.
- (287) Strmcnik, D.; Kodama, K.; Van Der Vliet, D.; Greeley, J.; Stamenkovic, V. R.; Marković, N. M. The Role of Non-Covalent Interactions in Electrocatalytic Fuel-Cell Reactions on Platinum. *Nat. Chem.* **2009**, *1* (6), 466–472.
- (288) Kristoffersen, H. H.; Chan, K.; Vegge, T.; Hansen, H. A. Energy-Entropy Competition in Cation-Hydroxyl Interactions at the Liquid Water-Pt(111) Interface. *Chem. Commun.* **2020**, *56* (3), 427–430.
- (289) Orr-Ewing, A. J. Taking the Plunge: Chemical Reaction Dynamics in Liquids. *Chem. Soc. Rev.* **2017**, *46* (24), 7597–7614.
- (290) Orr-Ewing, A. J. Dynamics of Bimolecular Reactions in Solution. *Annu. Rev. Phys. Chem.* **2015**, *66* (1), 119–141.
- (291) Crim, F. F. Molecular Reaction Dynamics across the Phases: Similarities and Differences. *Faraday Discuss.* **2012**, *157*, 9.
- (292) Bergsma, J. P.; Gertner, B. J.; Wilson, K. R.; Hynes, J. T. Molecular Dynamics of a Model S N 2 Reaction in Water. *J. Chem. Phys.* **1987**, *86* (3), 1356–1376.
- (293) Boyle, D. T.; Kong, X.; Pei, A.; Rudnicki, P. E.; Shi, F.; Huang, W.; Bao, Z.; Qin, J.; Cui, Y. Transient Voltammetry with Ultramicroelectrodes Reveals the Electron Transfer Kinetics of Lithium Metal Anodes. *ACS Energy Lett.* **2020**, *5* (3), 701–709.
- (294) Bai, P.; Bazant, M. Z. Charge Transfer Kinetics at the Solid-Solid Interface in Porous Electrodes. *Nat. Commun.* **2014**, *5*, 3585.
- (295) Fragedakis, D.; McEldrew, M.; Smith, R. B.; Krishnan, Y.; Zhang, Y.; Bai, P.; Chueh, W. C.; Shao-Horn, Y.; Bazant, M. Z. Theory of Coupled Ion-Electron Transfer Kinetics. *Electrochim. Acta* **2021**, *367*, 137432.
- (296) Horvath, S.; Fernandez, L. E.; Soudakov, A. V.; Hammes-Schiffer, S. Insights into Proton-Coupled Electron Transfer Mechanisms of Electrocatalytic H₂ Oxidation and Production. *Proc. Natl. Acad. Sci. U. S. A.* **2012**, *109* (39), 15663–15668.

- (297) Costentin, C.; Evans, D. H.; Robert, M.; Savéant, J.-M.; Singh, P. S. Electrochemical Approach to Concerted Proton and Electron Transfers. Reduction of the Water-Superoxide Ion Complex. *J. Am. Chem. Soc.* **2005**, *127* (36), 12490–12491.
- (298) Carter, E. A.; Hynes, J. T. Solute-Dependent Solvent Force Constants for Ion Pairs and Neutral Pairs in a Polar Solvent. *J. Phys. Chem.* **1989**, *93* (6), 2184–2187.
- (299) He, Z.; Chen, Y.; Santos, E.; Schmickler, W. The Pre-exponential Factor in Electrochemistry. *Angew. Chem., Int. Ed.* **2018**, *57* (27), 7948–7956.
- (300) Reorganization Energy. In *The IUPAC Compendium of Chemical Terminology*; International Union of Pure and Applied Chemistry (IUPAC): Research Triangle Park, NC, 2014. DOI: [10.1351/goldbook.R05292](https://doi.org/10.1351/goldbook.R05292).
- (301) Rice, S. A. Chapter 2 Diffusion-Controlled Reactions in Solution. *Diffusion-Limited Reactions. Comprehensive Chemical Kinetics* **1985**, *25*, 3–46.
- (302) Tachiya, M. Theory of Diffusion-Controlled Reactions: Formulation of the Bulk Reaction Rate in Terms of the Pair Probability. *Radiat. Phys. Chem.* **1983**, *21* (1–2), 167.
- (303) Voth, G. A.; Hochstrasser, R. M. Transition State Dynamics and Relaxation Processes in Solutions: A Frontier of Physical Chemistry. *J. Phys. Chem.* **1996**, *100* (31), 13034–13049.
- (304) Owrtsky, J. C.; Raftery, D.; Hochstrasser, R. M. Vibrational Relaxation Dynamics in Solutions. *Annu. Rev. Phys. Chem.* **1994**, *45*, 519–555.
- (305) Benjamin, I.; Gertner, B. J.; Tang, N. J.; Wilson, K. R. Energy Flow in an Atom Exchange Chemical Reaction in Solution. *J. Am. Chem. Soc.* **1990**, *112* (2), 524–530.
- (306) Garcia-Meseguer, R.; Carpenter, B. K. Re-Evaluating the Transition State for Reactions in Solution. *Eur. J. Org. Chem.* **2019**, *2019* (2–3), 254–266.
- (307) Pollak, E.; Pechukas, P. Transition States, Trapped Trajectories, and Classical Bound States Embedded in the Continuum. *J. Chem. Phys.* **1978**, *69* (3), 1218–1226.
- (308) Pollak, E.; Talkner, P. Reaction Rate Theory: What It Was, Where Is It Today, and Where Is It Going? *Chaos: An Interdisciplinary Journal of Nonlinear Science* **2005**, *15* (2), 026116.
- (309) Pechukas, P.; Pollak, E. Classical Transition State Theory Is Exact If the Transition State Is Unique. *J. Chem. Phys.* **1979**, *71* (5), 2062–2068.
- (310) Pechukas, P.; Pollak, E. Trapped Trajectories at the Boundary of Reactivity Bands in Molecular Collisions. *J. Chem. Phys.* **1977**, *67* (12), 5976–5977.
- (311) Bergsma, J. P.; Edelsten, P. M.; Gertner, B. J.; Huber, K. R.; Reimers, J. R.; Wilson, K. R.; Wu, S. M.; Hynes, J. T. Dynamics of the A + BC Reaction in Solution. *Chem. Phys. Lett.* **1986**, *123* (5), 394–398.
- (312) Bergsma, J. P.; Reimers, J. R.; Wilson, K. R.; Hynes, J. T. Molecular Dynamics of the A+BC Reaction in Rare Gas Solution. *J. Chem. Phys.* **1986**, *85* (10), 5625–5643.
- (313) Silverstein, K. A. T.; Haymet, A. D. J.; Dill, K. A. A Simple Model of Water and the Hydrophobic Effect. *J. Am. Chem. Soc.* **1998**, *120* (13), 3166–3175.
- (314) Hribar, B.; Southall, N. T.; Vlachy, V.; Dill, K. A. How Ions Affect the Structure of Water. *J. Am. Chem. Soc.* **2002**, *124* (41), 12302–12311.
- (315) Dill, K. A.; Truskett, T. M.; Vlachy, V.; Hribar-Lee, B. Modeling Water, the Hydrophobic Effect, and Ion Solvation. *Annu. Rev. Biophys. Biomol. Struct.* **2005**, *34*, 173–199.
- (316) Lenhard, J.; Stephan, S.; Hasse, H. A Child of Prediction. On the History, Ontology, and Computation of the Lennard-Jonesium. *Stud Hist Philos. Sci.* **2024**, *103*, 105–113.
- (317) Fischer, J.; Wendland, M. On the History of Key Empirical Intermolecular Potentials. *Fluid Phase Equilib.* **2023**, *573*, 113876.
- (318) Jones, J. E. On the Determination of Molecular Fields. —II. From the Equation of State of a Gas. *Proceedings of the Royal Society of London. Series A, Containing Papers of a Mathematical and Physical Character* **1924**, *106* (738), 463–477.
- (319) Jones, J. E. On the Determination of Molecular Fields.—I. From the Variation of the Viscosity of a Gas with Temperature. *Proceedings of the Royal Society of London. Series A, Containing Papers of a Mathematical and Physical Character* **1924**, *106* (738), 441–462.
- (320) Lennard-Jones, J. E. Cohesion. *Proceedings of the Physical Society* **1931**, *43* (S), 461–482.
- (321) Banerjee, S.; Singh, R. S.; Bagchi, B. Orientational Order as the Origin of the Long-Range Hydrophobic Effect. *J. Chem. Phys.* **2015**, *142* (13), 134505.
- (322) Laage, D.; Stirnemann, G.; Sterpone, F.; Rey, R.; Hynes, J. T. Reorientation and Allied Dynamics in Water and Aqueous Solutions. *Annu. Rev. Phys. Chem.* **2011**, *62*, 395–416.
- (323) Laage, D.; Hynes, J. T. A Molecular Jump Mechanism of Water Reorientation. *Science* **2006**, *311* (5762), 832–835.
- (324) Woutersen, S.; Emmerichs, U.; Bakker, H. J. Femtosecond Mid-IR Pump-Probe Spectroscopy of Liquid Water: Evidence for a Two-Component Structure. *Science* **1997**, *278* (5338), 658–660.
- (325) Nienhuys, H.-K.; van Santen, R. A.; Bakker, H. J. Orientational Relaxation of Liquid Water Molecules as an Activated Process. *J. Chem. Phys.* **2000**, *112* (19), 8487–8494.
- (326) Gallot, G.; Bratos, S.; Pommeret, S.; Lascoux, N.; Leicknam, J.-Cl.; Koziński, M.; Amir, W.; Gale, G. M. Coupling between Molecular Rotations and OH...O Motions in Liquid Water: Theory and Experiment. *J. Chem. Phys.* **2002**, *117* (24), 11301–11309.
- (327) Steinel, T.; Asbury, J. B.; Zheng, J.; Fayer, M. D. Watching Hydrogen Bonds Break: A Transient Absorption Study of Water. *J. Phys. Chem. A* **2004**, *108* (50), 10957–10964.
- (328) Fecko, C. J.; Loparo, J. J.; Roberts, S. T.; Tokmakoff, A. Local Hydrogen Bonding Dynamics and Collective Reorganization in Water: Ultrafast Infrared Spectroscopy of HOD/D₂O. *J. Chem. Phys.* **2005**, *122* (5), 054506.
- (329) Moilanen, D. E.; Fenn, E. E.; Lin, Y.-S.; Skinner, J. L.; Bagchi, B.; Fayer, M. D. Water Inertial Reorientation: Hydrogen Bond Strength and the Angular Potential. *Proc. Natl. Acad. Sci. U. S. A.* **2008**, *105* (14), 5295–5300.
- (330) Bakker, H. J.; Rezus, Y. L. A.; Timmer, R. L. A. Molecular Reorientation of Liquid Water Studied with Femtosecond Mid-infrared Spectroscopy. *J. Phys. Chem. A* **2008**, *112* (46), 11523–11534.
- (331) Abragam, A.; Hebel, L. C. The Principles of Nuclear Magnetism. *Am. J. Phys.* **1961**, *29* (12), 860–861.
- (332) Jonas, J.; DeFries, T.; Wilbur, D. J. Molecular Motions in Compressed Liquid Water. *J. Chem. Phys.* **1976**, *65* (2), 582–588.
- (333) Lang, E.; Lüdemann, H.-D. Pressure and Temperature Dependence of the Longitudinal Proton Relaxation Times in Supercooled Water to -87 °C and 2500 bar. *J. Chem. Phys.* **1977**, *67* (2), 718–723.
- (334) Qvist, J.; Halle, B. Thermal Signature of Hydrophobic Hydration Dynamics. *J. Am. Chem. Soc.* **2008**, *130* (31), 10345–10353.
- (335) Ropp, J.; Lawrence, C.; Farrar, T. C.; Skinner, J. L. Rotational Motion in Liquid Water Is Anisotropic: A Nuclear Magnetic Resonance and Molecular Dynamics Simulation Study. *J. Am. Chem. Soc.* **2001**, *123* (33), 8047–8052.
- (336) Lawrence, C. P.; Skinner, J. L. Vibrational Spectroscopy of HOD in Liquid D₂O. III. Spectral Diffusion, and Hydrogen-Bonding and Rotational Dynamics. *J. Chem. Phys.* **2003**, *118*, 264–272.
- (337) Paesani, F.; Voth, G. A. The Properties of Water: Insights from Quantum Simulations. *J. Phys. Chem. B* **2009**, *113* (17), 5702–5719.
- (338) Sprik, M.; Hutter, J.; Parrinello, M. *Ab Initio* Molecular Dynamics Simulation of Liquid Water: Comparison of Three Gradient-Corrected Density Functionals. *J. Chem. Phys.* **1996**, *105* (3), 1142–1152.
- (339) Silvestrelli, P. L. Are There Immobilized Water Molecules around Hydrophobic Groups? Aqueous Solvation of Methanol from First Principles. *J. Phys. Chem. B* **2009**, *113* (31), 10728–10731.

- (340) Laage, D.; Hynes, J. T. Reorientational Dynamics of Water Molecules in Anionic Hydration Shells. *Proc. Natl. Acad. Sci. U. S. A.* **2007**, *104* (27), 11167–11172.
- (341) Laage, D.; Hynes, J. T. On the Molecular Mechanism of Water Reorientation. *J. Phys. Chem. B* **2008**, *112* (45), 14230–14242.
- (342) Cabral, J. T.; Luzar, A.; Teixeira, J.; Bellissent-Funel, M.-C. Single-Particle Dynamics in Dimethyl-Sulfoxide/Water Eutectic Mixture by Neutron Scattering. *J. Chem. Phys.* **2000**, *113* (19), 8736–8745.
- (343) Luzar, A. Resolving the Hydrogen Bond Dynamics Conundrum. *J. Chem. Phys.* **2000**, *113* (23), 10663–10675.
- (344) Huse, N.; Ashihara, S.; Nibbering, E. T. J.; Elsaesser, T. Ultrafast Vibrational Relaxation of O-H Bending and Vibrational Excitations in Liquid H₂O. *Chem. Phys. Lett.* **2005**, *404* (4–6), 389–393.
- (345) Venables, D. S.; Huang, K.; Schmuttenmaer, C. A. Effect of Reverse Micelle Size on the Vibrational Band of Confined Water and Methanol. *J. Phys. Chem. B* **2001**, *105* (38), 9132–9138.
- (346) Laage, D.; Stirnemann, G.; Sterpone, F.; Hynes, J. T. Water Jump Reorientation: From Theoretical Prediction to Experimental Observation. *Acc. Chem. Res.* **2012**, *45* (1), 53–62.
- (347) Nandi, N.; Bhattacharyya, K.; Bagchi, B. Dielectric Relaxation and Solvation Dynamics of Water in Complex Chemical and Biological Systems. *Chem. Rev.* **2000**, *100* (6), 2013–2046.
- (348) Barthel, J. M. G.; Buchner, R. High Frequency Permittivity and Its Use in the Investigation of Solution Properties. *Pure Appl. Chem.* **1991**, *63* (10), 1473–1482.
- (349) Maroncelli, M. The Dynamics of Solvation in Polar Liquids. *J. Mol. Liq.* **1993**, *57* (C), 1–37.
- (350) Jimenez, R.; Fleming, G. R.; Kumar, P. V.; Maroncelli, M. Femtosecond Solvation Dynamics of Water. *Nature* **1994**, *369* (6480), 471–473.
- (351) Vijayadamodar, G. V.; Bagchi, B. Molecular Hydrodynamic Theory of Non-Markovian Collective Orientational Relaxation in Dense Dipolar Liquids. *J. Chem. Phys.* **1991**, *95* (7), 5289–5299.
- (352) Roy, S.; Bagchi, B. Ultrafast Underdamped Solvation: Agreement between Computer Simulation and Various Theories of Solvation Dynamics. *J. Chem. Phys.* **1993**, *99* (2), 1310–1319.
- (353) Nandi, N.; Roy, S.; Bagchi, B. Ultrafast Solvation Dynamics in Water: Isotope Effects and Comparison with Experimental Results. *J. Chem. Phys.* **1995**, *102* (3), 1390–1397.
- (354) Stirnemann, G.; Wernersson, E.; Jungwirth, P.; Laage, D. Mechanisms of Acceleration and Retardation of Water Dynamics by Ions. *J. Am. Chem. Soc.* **2013**, *135* (32), 11824–11831.
- (355) Marcus, Y.; Heftet, G. Ion Pairing. *Chem. Rev.* **2006**, *106* (11), 4585–4621.
- (356) Bian, H.; Wen, X.; Li, J.; Chen, H.; Han, S.; Sun, X.; Song, J.; Zhuang, W.; Zheng, J. Ion Clustering in Aqueous Solutions Probed with Vibrational Energy Transfer. *Proc. Natl. Acad. Sci. U. S. A.* **2011**, *108* (12), 4737–4742.
- (357) Zhang, Q.; Wu, T. M.; Chen, C.; Mukamel, S.; Zhuang, W. Molecular Mechanism of Water Reorientational Slowing down in Concentrated Ionic Solutions. *Proc. Natl. Acad. Sci. U. S. A.* **2017**, *114* (38), 10023–10028.
- (358) Shalit, A.; Ahmed, S.; Savolainen, J.; Hamm, P. Terahertz Echoes Reveal the Inhomogeneity of Aqueous Salt Solutions. *Nat. Chem.* **2017**, *9* (3), 273–278.
- (359) Heisler, I. A.; Mazur, K.; Meech, S. R. Low-Frequency Modes of Aqueous Alkali Halide Solutions: An Ultrafast Optical Kerr Effect Study. *J. Phys. Chem. B* **2011**, *115* (8), 1863–1873.
- (360) Pluhařová, E.; Stirnemann, G.; Laage, D. On Water Reorientation Dynamics in Cation Hydration Shells. *J. Mol. Liq.* **2022**, *363*, 119886.
- (361) Piskulich, Z. A.; Laage, D.; Thompson, W. H. A Structure-Dynamics Relationship Enables Prediction of the Water Hydrogen Bond Exchange Activation Energy from Experimental Data. *Chem. Sci.* **2024**, *15* (6), 2197–2204.
- (362) Hansen, J. S.; Kisliuk, A.; Sokolov, A. P.; Gainaru, C. Identification of Structural Relaxation in the Dielectric Response of Water. *Phys. Rev. Lett.* **2016**, *116* (23), 237601.
- (363) Spanoudaki, A.; Albela, B.; Bonneviot, L.; Peyrard, M. The Dynamics of Water in Nanoporous Silica Studied by Dielectric Spectroscopy. *Eur. Phys. J. E* **2005**, *17*, 21–27.
- (364) Moreno, A. J.; Colmenero, J.; Alegria, A.; Alba-Simionescu, C.; Dosseh, G.; Morineau, D.; Frick, B. Methyl Group Dynamics in a Confined Glass. *Eur. Phys. J. E* **2003**, *12* (S1), 43–46.
- (365) Sauer, D.; Schuster, B.; Rosenstiel, M.; Schneider, S.; Talluto, V.; Walther, T.; Blochowicz, T.; Stühn, B.; Vogel, M. Dynamics of Water-Alcohol Mixtures: Insights from Nuclear Magnetic Resonance, Broadband Dielectric Spectroscopy, and Triplet Solvation Dynamics. *J. Chem. Phys.* **2014**, *140* (11), 114503.
- (366) Ando, K.; Hynes, J. T. Acid-Base Proton Transfer and Ion Pair Formation in Solution. *Advances in Chemical Physics* **1999**, *110*, 381–430.
- (367) Ando, K.; Hynes, J. T. HF Acid Ionization in Water: The First Step. *Faraday Discuss.* **1995**, *102*, 435.
- (368) Richardson, J. O.; Pérez, C.; Lobsiger, S.; Reid, A. A.; Temelso, B.; Shields, G. C.; Kisiel, Z.; Wales, D. J.; Pate, B. H.; Althorpe, S. C. Concerted Hydrogen-Bond Breaking by Quantum Tunneling in the Water Hexamer Prism. *Science* **2016**, *351* (6279), 1310–1313.
- (369) Paesani, F.; Yoo, S.; Bakker, H. J.; Xantheas, S. S. Nuclear Quantum Effects in the Reorientation of Water. *J. Phys. Chem. Lett.* **2010**, *1* (15), 2316–2321.
- (370) Wilkins, D. M.; Manolopoulos, D. E.; Pipolo, S.; Laage, D.; Hynes, J. T. Nuclear Quantum Effects in Water Reorientation and Hydrogen-Bond Dynamics. *J. Phys. Chem. Lett.* **2017**, *8* (12), 2602–2607.
- (371) Mitsui, T.; Rose, M. K.; Fomin, E.; Ogletree, D. F.; Salmeron, M. Water Diffusion and Clustering on Pd(111). *Science* **2002**, *297* (5588), 1850–1852.
- (372) Fang, W.; Chen, J.; Pedevilla, P.; Li, X.-Z.; Richardson, J. O.; Michaelides, A. Origins of Fast Diffusion of Water Dimers on Surfaces. *Nat. Commun.* **2020**, *11*, 1689.
- (373) Ranea, V. A.; Michaelides, A.; Ramírez, R.; de Andres, P. L.; Vergés, J. A.; King, D. A. Water Dimer Diffusion on Pd{111} Assisted by an H-Bond Donor-Acceptor Tunneling Exchange. *Phys. Rev. Lett.* **2004**, *92* (13), 136104.
- (374) Laborda, E.; Henstridge, M. C.; Batchelor-McAuley, C.; Compton, R. G. Asymmetric Marcus-Hush Theory for Voltammetry. *Chem. Soc. Rev.* **2013**, *42* (12), 4894.
- (375) Marcus, R. A. Chemical and Electrochemical Electron-Transfer Theory. *Annu. Rev. Phys. Chem.* **1964**, *15* (1), 155–196.
- (376) Albery, W. J. The Application of the Marcus Relation to Reactions in Solution. *Annu. Rev. Phys. Chem.* **1980**, *31*, 227–263.
- (377) Marcus, R. A. Electron Transfer Reactions in Chemistry. Theory and Experiment. *Rev. Mod. Phys.* **1993**, *65* (3), 599–610.
- (378) Ghosh, S.; Soudackov, A. V.; Hammes-Schiffer, S. Electrochemical Electron Transfer and Proton-Coupled Electron Transfer: Effects of Double Layer and Ionic Environment on Solvent Reorganization Energies. *J. Chem. Theory Comput.* **2016**, *12* (6), 2917–2925.
- (379) Smalley, J. F.; Feldberg, S. W.; Chidsey, C. E. D.; Linford, M. R.; Newton, M. D.; Liu, Y.-P. The Kinetics of Electron Transfer Through Ferrocene-Terminated Alkanethiol Monolayers on Gold. *J. Phys. Chem.* **1995**, *99* (35), 13141–13149.
- (380) Liu, Y.-P.; Newton, M. D. Reorganization Energy for Electron Transfer at Film-Modified Electrode Surfaces: A Dielectric Continuum Model. *J. Phys. Chem.* **1994**, *98* (29), 7162–7169.
- (381) Bangle, R. E.; Schneider, J.; Conroy, D. T.; Aramburu-Trošelj, B. M.; Meyer, G. J. Kinetic Evidence That the Solvent Barrier for Electron Transfer Is Absent in the Electric Double Layer. *J. Am. Chem. Soc.* **2020**, *142* (35), 14940–14946.
- (382) Terrettaz, S.; Becka, A. M.; Traub, M. J.; Fettinger, J. C.; Miller, C. J. Omega-Hydroxythiol Monolayers at Au Electrodes. *S.*

- Insulated Electrode Voltammetric Studies of Cyano/Bipyridyl Iron Complexes. *J. Phys. Chem.* **1995**, *99* (28), 11216–11224.
- (383) Smalley, J. F.; Finklea, H. O.; Chidsey, C. E. D.; Linford, M. R.; Creager, S. E.; Ferraris, J. P.; Chalfant, K.; Zawodzinsk, T.; Feldberg, S. W.; Newton, M. D. Heterogeneous Electron-Transfer Kinetics for Ruthenium and Ferrocene Redox Moieties through Alkanethiol Monolayers on Gold. *J. Am. Chem. Soc.* **2003**, *125* (7), 2004–2013.
- (384) Chidsey, C. E. D. Free Energy and Temperature Dependence of Electron Transfer at the Metal-Electrolyte Interface. *Science* **1991**, *251* (4996), 919–922.
- (385) Willard, A. P.; Reed, S. K.; Madden, P. A.; Chandler, D. Water at an Electrochemical Interface—a Simulation Study. *Faraday Discuss.* **2009**, *141*, 423–441.
- (386) Reed, S. K.; Madden, P. A.; Papadopoulos, A. Electrochemical Charge Transfer at a Metallic Electrode: A Simulation Study. *J. Chem. Phys.* **2008**, *128* (12), 124701.
- (387) Limaye, A. M.; Ding, W.; Willard, A. P. Understanding Attenuated Solvent Reorganization Energies near Electrode Interfaces. *J. Chem. Phys.* **2020**, *152* (11), 114706.
- (388) Varghese, S.; Kannam, S. K.; Hansen, J. S.; Sathian, S. P. Effect of Hydrogen Bonds on the Dielectric Properties of Interfacial Water. *Langmuir* **2019**, *35* (24), 8159–8166.
- (389) Schaaf, C.; Gekle, S. Spatially Resolved Dielectric Constant of Confined Water and Its Connection to the Non-Local Nature of Bulk Water. *J. Chem. Phys.* **2016**, *145* (8), 084901.
- (390) Dinpajoh, M.; Matyushov, D. V. Dielectric Constant of Water in the Interface. *J. Chem. Phys.* **2016**, *145*, 014504.
- (391) Caleman, C.; Hub, J. S.; van Maaren, P. J.; van der Spoel, D. Atomistic Simulation of Ion Solvation in Water Explains Surface Preference of Halides. *Proc. Natl. Acad. Sci. U. S. A.* **2011**, *108* (17), 6838–6842.
- (392) Bonthuis, D. J.; Gekle, S.; Netz, R. R. Dielectric Profile of Interfacial Water and Its Effect on Double-Layer Capacitance. *Phys. Rev. Lett.* **2011**, *107* (16), 166102.
- (393) Bonthuis, D. J.; Gekle, S.; Netz, R. R. Profile of the Static Permittivity Tensor of Water at Interfaces: Consequences for Capacitance, Hydration Interaction and Ion Adsorption. *Langmuir* **2012**, *28* (20), 7679–7694.
- (394) Majumdar, J.; Moid, M.; Dasgupta, C.; Maiti, P. K. Dielectric Profile and Electromelting of a Monolayer of Water Confined in Graphene Slit Pore. *J. Phys. Chem. B* **2021**, *125* (24), 6670–6680.
- (395) Olivieri, J.-F.; Hynes, J. T.; Laage, D. Confined Water's Dielectric Constant Reduction Is Due to the Surrounding Low Dielectric Media and Not to Interfacial Molecular Ordering. *J. Phys. Chem. Lett.* **2021**, *12* (17), 4319–4326.
- (396) Rossmeisl, J.; Chan, K.; Skúlasón, E.; Björketun, M. E.; Tripkovic, V. On the PH Dependence of Electrochemical Proton Transfer Barriers. *Catal. Today* **2016**, *262*, 36–40.
- (397) Monteiro, M. C. O.; Dattila, F.; López, N.; Koper, M. T. M. The Role of Cation Acidity on the Competition between Hydrogen Evolution and CO₂ Reduction on Gold Electrodes. *J. Am. Chem. Soc.* **2022**, *144* (4), 1589–1602.
- (398) Qin, X.; Hansen, H. A.; Honkala, K.; Melander, M. M. Cation-Induced Changes in the Inner- and Outer-Sphere Mechanisms of Electrocatalytic CO₂ Reduction. *Nat. Commun.* **2023**, *14* (1), 7607.
- (399) Koper, M. T. M. Theory and Kinetic Modeling of Electrochemical Cation-Coupled Electron Transfer Reactions. *J. Solid State Electrochem.* **2024**, *28* (5), 1601–1606.
- (400) Cukier, R. I.; Nocera, D. G. PROTON-COUPLED ELECTRON TRANSFER. *Annu. Rev. Phys. Chem.* **1998**, *49* (1), 337–369.
- (401) Warburton, R. E.; Soudakov, A. V.; Hammes-Schiffer, S. Theoretical Modeling of Electrochemical Proton-Coupled Electron Transfer. *Chem. Rev.* **2022**, *122* (12), 10599–10650.
- (402) Costentin, C.; Robert, M.; Savéant, J.-M. Adiabatic and Non-Adiabatic Concerted Proton-Electron Transfers. Temperature Effects in the Oxidation of Intramolecularly Hydrogen-Bonded Phenols. *J. Am. Chem. Soc.* **2007**, *129* (32), 9953–9963.
- (403) Lam, Y.-C.; Soudakov, A. V.; Hammes-Schiffer, S. Theory of Electrochemical Proton-Coupled Electron Transfer in Diabatic Vibronic Representation: Application to Proton Discharge on Metal Electrodes in Alkaline Solution. *J. Phys. Chem. C* **2020**, *124* (50), 27309–27322.
- (404) Layfield, J. P.; Hammes-Schiffer, S. Hydrogen Tunneling in Enzymes and Biomimetic Models. *Chem. Rev.* **2014**, *114* (7), 3466–3494.
- (405) Koper, M. T. M. Temperature Dependence of the Transfer Coefficient of Simple Electrochemical Redox Reactions Due to Slow Solvent Dynamics. *J. Phys. Chem. B* **1997**, *101* (16), 3168–3173.
- (406) Conway, B. E.; Bockris, J. O.; Vijh, A. K. Modern Aspects of Electrochemistry. *J. Electrochem. Soc.* **1973**, *120* (4), 148C.
- (407) Krishtalik, L. I. Kinetic Isotope Effect in the Hydrogen Evolution Reaction. *Electrochim. Acta* **2001**, *46* (19), 2949–2960.
- (408) Nazmutdinov, R. R.; Bronshtein, M. D.; Zinkicheva, T. T.; Glukhov, D. V. Modeling of Electron Transfer across Electrochemical Interfaces: State-of-the Art and Challenges for Quantum and Computational Chemistry. *Int. J. Quantum Chem.* **2016**, *116* (3), 189–201.
- (409) Ledezma-Yanez, I.; Wallace, W. D. Z.; Sebastián-Pascual, P.; Climent, V.; Feliu, J. M.; Koper, M. T. M. Interfacial Water Reorganization as a PH-Dependent Descriptor of the Hydrogen Evolution Rate on Platinum Electrodes. *Nat. Energy* **2017**, *2* (4), 17031.
- (410) Huang, J. Mixed Quantum-Classical Treatment of Electron Transfer at Electrocatalytic Interfaces: Theoretical Framework and Conceptual Analysis. *J. Chem. Phys.* **2020**, *153* (16), 164707.
- (411) Huang, J.; Li, P.; Chen, S. Quantitative Understanding of the Sluggish Kinetics of Hydrogen Reactions in Alkaline Media Based on a Microscopic Hamiltonian Model for the Volmer Step. *J. Phys. Chem. C* **2019**, *123* (28), 17325–17334.
- (412) Shen, L.-f.; Lu, B.-a.; Li, Y.-y.; Liu, J.; Huang-fu, Z.-c.; Peng, H.; Ye, J.-y.; Qu, X.-m.; Zhang, J.-m.; Li, G.; Cai, W.-b.; Jiang, Y.-x.; Sun, S.-g. Interfacial Structure of Water as a New Descriptor of the Hydrogen Evolution Reaction. *Angewandte Chemie* **2020**, *132*, 22583–22588.
- (413) Wang, Y. H.; Zheng, S.; Yang, W. M.; Zhou, R. Y.; He, Q. F.; Radjenovic, P.; Dong, J. C.; Li, S.; Zheng, J.; Yang, Z. L.; Attard, G.; Pan, F.; Tian, Z. Q.; Li, J. F. In Situ Raman Spectroscopy Reveals the Structure and Dissociation of Interfacial Water. *Nature* **2021**, *600* (7887), 81–85.
- (414) Li, P.; Jiao, Y.; Ruan, Y.; Fei, H.; Men, Y.; Guo, C.; Wu, Y.; Chen, S. Revealing the Role of Double-Layer Microenvironments in PH-Dependent Oxygen Reduction Activity over Metal-Nitrogen-Carbon Catalysts. *Nat. Commun.* **2023**, *14*, 6936.
- (415) Zhang, Z.-M.; Wang, T.; Cai, Y.-C.; Li, X.-Y.; Ye, J.-Y.; Zhou, Y.; Tian, N.; Zhou, Z.-Y.; Sun, S.-G. Probing Electrolyte Effects on Cation-Enhanced CO₂ Reduction on Copper in Acidic Media. *Nat. Catal.* **2024**, *7* (7), 807–817.
- (416) Li, P.; Jiang, Y.; Hu, Y.; Men, Y.; Liu, Y.; Cai, W.; Chen, S. Hydrogen Bond Network Connectivity in the Electric Double Layer Dominates the Kinetic PH Effect in Hydrogen Electrocatalysis on Pt. *Nat. Catal.* **2022**, *5* (10), 900–911.
- (417) Ramaswamy, N.; Ghoshal, S.; Bates, M. K.; Jia, Q.; Li, J.; Mukerjee, S. Hydrogen Oxidation Reaction in Alkaline Media: Relationship between Electrocatalysis and Electrochemical Double-Layer Structure. *Nano Energy* **2017**, *41*, 765–771.
- (418) Li, X.; Wang, T.; Cai, Y.; Meng, Z.; Nan, J.; Ye, J.; Yi, J.; Zhan, D.; Tian, N.; Zhou, Z.; Sun, S. Mechanism of Cations Suppressing Proton Diffusion Kinetics for Electrocatalysis. *Angew. Chem., Int. Ed.* **2023**, *62* (14), No. e202218669.
- (419) Wu, J.; Gerstandt, K.; Zhang, H.; Liu, J.; Hinds, B. J. Electrophoretically Induced Aqueous Flow through Single-Walled Carbon Nanotube Membranes. *Nat. Nanotechnol.* **2012**, *7* (2), 133–139.
- (420) Cao, Z.; Peng, Y.; Yan, T.; Li, S.; Li, A.; Voth, G. A. Mechanism of Fast Proton Transport along One-Dimensional Water

- Chains Confined in Carbon Nanotubes. *J. Am. Chem. Soc.* **2010**, *132* (33), 11395–11397.
- (421) Markovitch, O.; Chen, H.; Izvekov, S.; Paesani, F.; Voth, G. A.; Agmon, N. Special Pair Dance and Partner Selection: Elementary Steps in Proton Transport in Liquid Water. *J. Phys. Chem. B* **2008**, *112* (31), 9456–9466.
- (422) Moilanen, D. E.; Piletic, I. R.; Fayer, M. D. Water Dynamics in Nafion Fuel Cell Membranes: The Effects of Confinement and Structural Changes on the Hydrogen Bond Network. *J. Phys. Chem. C* **2007**, *111* (25), 8884–8891.
- (423) Kreuer, K.-D.; Paddison, S. J.; Spohr, E.; Schuster, M. Transport in Proton Conductors for Fuel-Cell Applications: Simulations, Elementary Reactions, and Phenomenology. *Chem. Rev.* **2004**, *104* (10), 4637–4678.
- (424) Hickner, M. A. Water-mediated Transport in Ion-containing Polymers. *J. Polym. Sci. B Polym. Phys.* **2012**, *50* (1), 9–20.
- (425) Rahbari, A.; Hartkamp, R.; Moulton, O. A.; Bos, A.; van den Broeke, L. J. P.; Ramdin, M.; Dubbeldam, D.; Lyulin, A. V.; Vlugt, T. J. H. Electro-Osmotic Drag and Thermodynamic Properties of Water in Hydrated Nafion Membranes from Molecular Dynamics. *J. Phys. Chem. C* **2022**, *126* (18), 8121–8133.
- (426) Cui, R.; Li, S.; Yu, C.; Zhou, Y. The Evolution of Hydrogen Bond Network in Nafion via Molecular Dynamics Simulation. *Macromolecules* **2023**, *56* (4), 1688–1703.
- (427) Elliott, J. A.; Paddison, S. J. Modelling of Morphology and Proton Transport in PFSA Membranes. *Phys. Chem. Chem. Phys.* **2007**, *9* (21), 2602.
- (428) Jiao, K.; Li, X. Water Transport in Polymer Electrolyte Membrane Fuel Cells. *Prog. Energy Combust. Sci.* **2011**, *37* (3), 221–291.
- (429) Markovitch, O.; Agmon, N. Structure and Energetics of the Hydronium Hydration Shells. *J. Phys. Chem. A* **2007**, *111* (12), 2253–2256.
- (430) Graham, D. J.; Nocera, D. G. Electrocatalytic H₂ Evolution by Proton-Gated Hangman Iron Porphyrins. *Organometallics* **2014**, *33* (18), 4994–5001.
- (431) Margarit, C. G.; Schnedermann, C.; Asimow, N. G.; Nocera, D. G. Carbon Dioxide Reduction by Iron Hangman Porphyrins. *Organometallics* **2019**, *38* (6), 1219–1223.
- (432) Bhunia, S.; Rana, A.; Dey, S. G.; Ivancich, A.; Dey, A. A Designed Second-Sphere Hydrogen-Bond Interaction That Critically Influences the O–O Bond Activation for Heterolytic Cleavage in Ferric Iron-Porphyrin Complexes. *Chem. Sci.* **2020**, *11* (10), 2681–2695.
- (433) Kretchmer, J. S.; Boekelheide, N.; Warren, J. J.; Winkler, J. R.; Gray, H. B.; Miller, T. F. Fluctuating Hydrogen-Bond Networks Govern Anomalous Electron Transfer Kinetics in a Blue Copper Protein. *Proc. Natl. Acad. Sci. U. S. A.* **2018**, *115* (24), 6129–6134.
- (434) Cantu, D. C.; Padmaperuma, A. B.; Nguyen, M. T.; Akhade, S. A.; Yoon, Y.; Wang, Y. G.; Lee, M. S.; Glezakou, V. A.; Rousseau, R.; Lilga, M. A. A Combined Experimental and Theoretical Study on the Activity and Selectivity of the Electrocatalytic Hydrogenation of Aldehydes. *ACS Catal.* **2018**, *8* (8), 7645–7658.
- (435) Nguyen, M. T.; Akhade, S. A.; Cantu, D. C.; Lee, M. S.; Glezakou, V. A.; Rousseau, R. Electro-Reduction of Organics on Metal Cathodes: A Multiscale-Modeling Study of Benzaldehyde on Au (111). *Catal. Today* **2020**, *350*, 39–46.
- (436) Zhou, W.; Inoue, S.; Iwahashi, T.; Kanai, K.; Seki, K.; Miyamae, T.; Kim, D.; Katayama, Y.; Ouchi, Y. Double Layer Structure and Adsorption/Desorption Hysteresis of Neat Ionic Liquid on Pt Electrode Surface — an in-Situ IR-Visible Sum-Frequency Generation Spectroscopic Study. *Electrochim. commun.* **2010**, *12* (5), 672–675.
- (437) DeWalt-Kerian, E. L.; Kim, S.; Azam, Md. S.; Zeng, H.; Liu, Q.; Gibbs, J. M. PH-Dependent Inversion of Hofmeister Trends in the Water Structure of the Electrical Double Layer. *J. Phys. Chem. Lett.* **2017**, *8* (13), 2855–2861.
- (438) Rehl, B.; Ma, E.; Parshotam, S.; DeWalt-Kerian, E. L.; Liu, T.; Geiger, F. M.; Gibbs, J. M. Water Structure in the Electrical Double Layer and the Contributions to the Total Interfacial Potential at Different Surface Charge Densities. *J. Am. Chem. Soc.* **2022**, *144* (36), 16338–16349.
- (439) Kraack, J. P.; Kaech, A.; Hamm, P. Surface Enhancement in Ultrafast 2D ATR IR Spectroscopy at the Metal-Liquid Interface. *J. Phys. Chem. C* **2016**, *120* (6), 3350–3359.
- (440) Lotti, D.; Hamm, P.; Kraack, J. P. Surface-Sensitive Spectro-Electrochemistry Using Ultrafast 2D ATR IR Spectroscopy. *J. Phys. Chem. C* **2016**, *120* (5), 2883–2892.
- (441) Flanagan, J. C.; Valentine, M. L.; Baiz, C. R. Ultrafast Dynamics at Lipid-Water Interfaces. *Acc. Chem. Res.* **2020**, *53* (9), 1860–1868.
- (442) Nucci, N. V.; Pometun, M. S.; Wand, A. J. Site-Resolved Measurement of Water-Protein Interactions by Solution NMR. *Nat. Struct. Mol. Biol.* **2011**, *18* (2), 245–249.